ROLE OF CALCIUM-BINDING PROTEINS AND VOLTAGE-GATED CALCIUM CHANNELS IN METHYLMERCURY-INDUCED DISRUPTION OF DIVALENT CATION HOMEOSTASIS AND SUBSEQUENT CYTOTOXICITY

By

Joshua R. Edwards

A DISSERTATION

Submitted to
Michigan State University
in partial fulfillment of the requirements
for the degree of

DOCTOR OF PHILOSOPHY

Department of Pharmacology and Toxicology

2004

ABSTRACT

ROLE OF CALCIUM-BINDING PROTEINS AND VOLTAGE-GATED CALCIUM CHANNELS IN METHYLMERCURY-INDUCED DISRUPTION OF DIVALENT CATION HOMEOSTASIS AND SUBSEQUENT CYTOTOXICITY

By

Joshua R. Edwards

Methylmercury (MeHg) is an environmental neurotoxicant that causes selective death of cerebellar granule neurons. In contrast, adjacent cerebellar Purkinje neurons appear to remain unharmed despite being exposed to equal or greater amounts of MeHg. Single-cell microfluorimetry was used to record changes in fluorescence from the Ca^{2+} indicator dye, fura-2, during exposure to MeHg in a variety of cell types including cerebellar Purkinje and granule neurons. Both Purkinje and granule neurons responded to MeHg exposure with a similar biphasic increase in fura-2 fluorescence. Purkinje cells had a significantly delayed time-to-onset of elevations of first and second phase increases of fura-2 fluorescence compared to granule cells in the 0.5 and 1 μM MeHg treatment groups. Furthermore, viability assays of Purkinje and granule cells show that Purkinje cells are more resistant to MeHg-induced neurotoxicity with 97.7% of Purkinje cells remaining viable after exposure to 3 μM MeHg. In contrast, only 40.6 ± 13% of granule cells were viable after exposure to 3 μM MeHg.

Several differences exist between Purkinje and granule cells such as voltage-gated Ca^{2+} channels (VGCCs), Ca^{2+}-binding proteins (CaBPs), glutamate receptors, cell size and metallothionein expression. The expression of VGCCs and the CaBP calbindin-D28k

(CB), were examined as possible factors that might contribute to the differential effects of MeHg-induced neurotoxicity and dysregulation of Ca^{2+} homeostasis. Purkinje cells express CB at very high levels whereas granule cells do not. To determine if the presence of functional VGCCs influenced MeHg-induced dysregulation of Ca^{2+} homeostasis and cytotoxicity, the responses of pheochromocytoma (PC12) and PC18 cells to MeHg were compared. PC18 cells are a sub-clone of PC12 cells that lack functional VGCCs. The time-to-onset of increases of fura-2 fluorescence was delayed significantly in PC18 cells as compared to PC12 cells. When L-type VGCCs were inhibited in PC12 cells there was a resulting delay in MeHg-induced time-to-onset of increases in fura-2 fluorescence and increased cell viability. Multiple approaches were used to determine how the presence of CB would alter MeHg-induced cytotoxicity and dysregulation of Ca^{2+} homeostasis. Myenteric plexus neurons grown in culture represent a cell culture system in which approximately 45% of the neurons present express CB. When exposed to MeHg a greater portion of viable myenteric plexus neurons expressed CB, whereas non-CB immuno-positive cells were preferentially lost. PC12 cells transfected with expression plasmids containing the sequence for CB were more resistant to the neurotoxic effects of MeHg, as measured by lactate dehydrogenase (LDH) release. In addition, CB-transfected PC12 cell mean time-to-onset of increases in fura-2 fluorescence tended to be higher compared to non-transfected PC12 cells. Data presented within this thesis show the differential effects of MeHg in causing dysregulation of Ca^{2+} homeostasis and subsequent cytotoxicity in cerebellar granule and Purkinje neurons grown in culture. Furthermore, the selective expression of CB and VGCCs might be factors that influence the susceptibility of a particular cell type to the neurotoxic effects of MeHg.

ACKNOWLEDGEMENTS

I would like to thank Doug Atchison, Lindsay Stevens, Alnelis Rodriguez, Jean Van Dalen and Jessica Gomulka for their excellent technical assistance in collecting the data presented in this manuscript. In addition I would like to thank Ashley Bauer and Mallory Koglin for their assistance in preparing this thesis.

TABLE OF CONTENTS

LIST OF TABLES

LIST OF FIGURES

LIST OF ABBREVIATIONS

AH	after hyperpolarizing
AMPA	α-amino-3-hydroxy-5-methylisoxazole-4- propionic acid
Ara-C	cytosine-β-arabinofuranoside
CaMkinase	calmodulin-dependent protein kinases
CaBP	calcium binding protein
CB	calbindin-$D28_K$
CMF-HBSS	calcium- magnesium-free Hanks buffered saline solution
CNS	central nervous system
CPA	cyclopiazonic acid
DMEM	Dulbecco's modified eagle medium
DPBS	Dulbecco's phsophate buffered saline
FBS	fetal bovine serum
g	gram
g	force of gravity
GABA	γ-amino butyric acid
GFP	green fluorescence protein
HBS	hepes buffered saline
HEPES	4-(2-hydroxyethyl)piperazine-1-ethanesulfonic acid
hr	hour
IP3	1,4,5 - inositol trisphosphate
K_d	dissociation constant

kg	kilogram
LDH	lactate dehydrogenase
MeHg	methylmercury
MEM	minimum essential medium
min	minutes
MPP^+	1-methyl-4-phenylpyridinium
MPTP	1-methyl-4-phenyl-1,2,3,6-tetrahydropyridine
MTP	mitochondrial transition pore
NADH	nicotinamide adenine dinucleotide
NMDA	n-methyl-d-aspartate
NOS	nitric oxide synthase
SER	smooth endoplasmic reticulum
TPEN	N,N,N',N'-tetrakis (2-pyridylmethyl)ethylenediamine
PC	pheochromocytoma
PI	phosphatidylinositides
VGCC	voltage gated calcium channel

CHAPTER ONE

BACKGROUND

A. General Introduction

MeHg is a ubiquitous environmental contaminant that causes selective neurotoxicity (Chang, 1977; Chang *et al.*, 1977; Leyshon-Sorland *et al.*, 1994; Kobayashi *et al.*, 1998; Takeuchi and Eto, 1999). Recent epidemiological studies have suggested that adverse human health effects are attributable to sustained low-level exposure to MeHg and Hg^{2+} in Canadian Cree Indians (McKeown-Eyssen and Ruedy, 1983), French Guiana Amerindians (Frery *et al.*, 2001) and Faroe Islanders (Meyers and Davidson, 1998). There have also been several well publicized episodes of mass MeHg poisonings in Japan (Takeuchi *et al.*, 1962) and Iraq (Bakir *et al.*, 1973). In both Japan and Iraq, a consistent pathological observation of MeHg intoxication was the global loss of granule neurons from the granule cell layer of the cerebellum (Jacobs *et al.,* 1977; Takeuchi and Eto, 1999). Both animal and human data demonstrate that cerebellar granule cells are one of the most sensitive neuronal types to the neurotoxic effects of MeHg (Hunter and Russell, 1954; Leyshon and Morgan, 1991; Leyshon-Sorland *et al.*, 1994; Kobayashi *et al.*, 1998; Mori *et al.,* 2000). In contrast, adjacent Purkinje cells are relatively unaffected despite accumulating to equal or greater concentrations of MeHg than cerebellar granule cells (Leyshon-Sorland *et al.,* 1994; Mori *et al.*, 2000).

While the pathological consequences of MeHg exposure have been identified, the etiology of MeHg neurotoxicity remains unknown. MeHg causes the disruption of Ca^{2+} homeostasis at low concentrations (sub-μM range), *in vitro* and in a wide variety of cell types or preparations, including cerebellar granule cells (Sarafian, 1993; Marty and

Atchison, 1997; Limke and Atchison, 2002), NG108-15 cells (Hare *et al.,* 1993; Hare and Atchison, 1995a,b), rat brain synaptosomes (Komulainen and Bondy *et al.*, 1987; Levesque *et al.*, 1992; Denny *et al.,* 1993), and Purkinje cells (Edwards and Atchison, 2001). As a result of MeHg exposure, the above cell types or preparations have a multiphasic increase in intracellular Ca^{2+} concentration ($[Ca^{2+}]_i$). The initial increase in Ca^{2+} is in part due to release of Ca^{2+} and other non-Ca^{2+} divalent cations from intracellular sources. This is followed by a second elevation of $[Ca^{2+}]_i$ due to entry of $Ca^{2+}{}_e$ (Marty and Atchison, 1997; Edwards and Atchison, 2001; Limke and Atchison, 2002). In correlation with studies showing that MeHg causes elevations of $[Ca^{2+}]_i$, MeHg also increases the formation of inositol 1,4,5-trisphosphate (IP_3) levels in cerebellar granule cells (Sarafian, 1993). Whole animal studies also support the idea that elevated $[Ca^{2+}]_i$ has a role in organomercurial-mediated cell death. Mori *et al.* (2000) used the Ca^{2+}-sensitive dye, alizarin red to detect Ca^{2+} deposits in cerebellar slices of rats that were treated by injection of dimethylmercury. Gross atrophy and accumulations of Ca^{2+} within granule cells in the granule layer of the cerebellum were evident as early as 19 days after initial treatment. Adjacent Purkinje cells did not show any sign of cell loss or death, nor did Purkinje cells accumulate $Ca^{2+}{}_i$ as indicated by a lack of staining for Ca^{2+} deposits (Mori *et al.*, 2000). Thus, the presence or absence of Ca^{2+} deposits within the cerebellum is directly correlated with sensitivity or resistance to MeHg neurotoxicity, respectively.

The reason for the apparent differential MeHg-induced neurotoxicity of cerebellar granule and Purkinje cells is currently unknown. One potential factor is the selective expression

of the calcium-binding protein (CaBP), calbindinD-28_K (CB). CB is a CaBP associated with increased resistance to Ca^{2+}-mediated cell death (Mattson *et al.*, 1991; McMahon *et al.*, 1998). Purkinje cells express CB at very high levels (0.1-0.2 mM), whereas cerebellar granule cells do not (Celio, 1990). As such, the focus of my dissertation will be to determine the relative effectiveness of MeHg to alter Ca^{2+} homeostasis and subsequent cell death in cerebellar Purkinje and granule neurons. Another specific aim of my dissertation will be to elucidate the potential role of proteins, such as CB and voltage-gated calcium channels (VGCCs), that may be contributing factors in MeHg-induced dysregulation of Ca^{2+} homeostasis and cytotoxicity.

B. MeHg as a Public Health Concern

It is relevant to review the global cycle of the different forms of mercury before considering sources and the toxicological significance of MeHg present within the environment. Several forms of mercury persist in the environment. Each species of mercury varies in toxicity, biological effects, and physical properties such as; charge, size, lipophilicity, volatility and solid state at room temperature. Hg^0 is described as mercurous, metallic or elemental mercury. Hg^0 is the only metal that is liquid at room temperature, has little tendency to dissolve in water and is volatile. Hg^{2+}, or mercuric mercury, is the oxidized form of Hg^0. Approximately 95% of all mercury in the atmosphere is in the form of Hg^0 where it can remain for up to a year where it becomes slowly oxidized to Hg^{2+} primarily through the action of ozone (Morel *et al.*, 1998). Mercury present in the atmosphere returns to the Earth's surface in the form of Hg^{2+}

dissolved in rain water. This oxidation of Hg^0 occurs very slowly, and Hg^0 can remain in the atmosphere for up to a year, all the while being distributed globally. Once in the aquatic environment, mercury is often deposited in aquatic sediments where Hg^{2+}, and to a lesser extent Hg^0, can become methylated into a more insidious form, MeHg, through the action of aquatic bacteria and other microbes (Siciliano and Lean, 2002). It is generally accepted that sulfate-reducing bacteria located in anoxic waters and aquatic sediment are the primary converters of Hg^0 or Hg^{2+} to MeHg, however methylation of either form of mercury occurs to a lesser extent within oxygenated surface waters as well (Siciliano and Lean, 2002).

Sources of environmental mercury include: venting of the earth's crust, industrial waste effluent and anthropogenic activities such as, gold mining, burning of fossil fuels and paper production (World Health Organization (WHO), 1989). Natural sources of environmental mercury may be significant. An estimated 25,000 to 125,000 tons of mercury is released per year due to degassing of the earth's crust (WHO, 1989). World production of Hg^0 through mining and smelting was approximately 10,000 tons per year in 1973 and has increased by 2% every year thereafter (WHO, 1990). Compared to Hg^0 or Hg^{2+}, MeHg has greater lipophilicity. As a result, MeHg bioaccumulates within the food chain as evidenced by the direct correlation between human consumption of piscivorous fish species and high mercury concentrations found in hair samples (Frery *et al.*, 2001). However MeHg is still water soluble. The most common route of exposure to MeHg is the consumption of MeHg-contaminated fish or seafood products (Sherlock *et*

al., 1982; Takeuchi and Eto, 1999; Frery *et al.*, 2001). Approximately 130 tons of Hg^0 is used per year in French Guiana in the extraction of gold from river sediments, soils or ground water rocks. Predatory fish species downstream of a gold mining facility located in French Guiana were found to have significantly elevated tissue mercury levels, with approximately 95 ± 5% of the total mercury in the form of MeHg (Frery *et al.*, 2001). Furthermore, individuals who consumed proportionally more predatory fish species had significantly higher concentrations of mercury within hair samples when compared to individuals who consumed predominantly herbivorous or non-predatory fish species (Frery *et al.*, 2001).

The adverse health effects of excessive MeHg exposure have been known for decades. The first large-scale poisoning due to MeHg was in Minamata Bay, Japan where the Minamata plant of Chisso Co. Ltd. used mercury sulfate in the production of acetaldehyde during the mid-1950's (Takeuchi and Eto, 1999). One by-product of the Chisso factory was the production of organomercurials, predominately MeHg. The adverse health effects of MeHg were unknown at the time and the organomercurial by-products were released into adjacent Minamata Bay. Residents of Minamata Bay were exposed to MeHg through the consumption of contaminated fish and other seafood products (Takeuchi *et al.*, 1962). During the entire period of operation of the plant (1932-1968) the Chisso factory released approximately 500 kg of mercury-containing waste into the bay (Takeuchi and Eto, 1999). As a result of this mercury discharge, autopsies of 201 people who had lived in MeHg-contaminated areas were confirmed to have pathological

lesions in the cerebellum as a result of excessive MeHg exposure. By 1996, 2,262 patients in the Minamata Bay area were found to have neurological defects due to exposure to MeHg (Takeuchi and Eto, 1999).

Another well-known mass MeHg poisoning episode occurred in the early 1970's in Iraq. In this episode, organomercurials were used to cover grain as a fungicide, and were not washed off prior to the processing of the grain (Bakir *et al.*, 1973). The contaminated grain was ground up into flour for the making of bread. During this period, several hundred Iraqi people suffered acute MeHg toxicity. Based on epidemiological data obtained from the Iraq outbreak, the current Environmental Protection Agency (EPA) reference dose for MeHg is 0.1 μg/kg/day (Goyer *et al.*, 2000). The reference dose is the maximum daily consumption of a substance for a lifetime without any adverse health effects as a consequence of that exposure. Recent epidemiological studies in the Faroe Islands and New Zealand where large amounts of predatory fish species are consumed (Meyers and Davidson, 1998) indicate that the developing nervous system of the fetus is highly susceptible to even relatively low amounts of maternal MeHg exposure. In the New Zealand and Faroe Island studies, a direct correlation existed between the MeHg concentration found in maternal hair samples and lack of cognitive function in their children (Meyers and Davidson, 1998). Cree Indians located in Northern Quebec, another population that consumes large amounts of fish, showed a significant correlation between delayed or abnormal tendon reflex response in children of mothers who were exposed to MeHg (McKeown-Eyssen and Ruedy, 1983). Furthermore, a study performed on full-

term two week old infants born in the Faroe Islands showed an inverse relationship between an infant's functional abilities, reflexes and stability and the cord-whole-blood mercury concentrations. Cord-whole blood mercury concentrations over 40 μg/L (159 nM) was associated with diminished infant neuronal function (Stewerwald *et al.*, 2000). The current reference dose for MeHg that is derived from the Iraqi outbreak and may be lowered based on these recent epidemiological studies that specifically address the ability of MeHg to disrupt neuronal development.

MeHg readily crosses the blood-brain barrier (Vahter *et al.*, 1994) and other cell membranes. Most signs and symptoms of MeHg exposure are neurological in origin and include sensory deficits, affective disorder and an increasingly dysfunctional gait eventually leading to ataxia (total loss of coordination in gait) (Takeuchi *et al.*, 1962; Bakir *et al.*, 1973; Chang, 1977; Gerstner and Huff, 1977). One of the first signs of MeHg neurotoxicity is a slight disturbance in gait and lower limb weakness. Patients with MeHg poisoning are unable to walk in a coordinated manner and are prone to frequently stumble and fall (Takeuchi *et al.,* 1979; Takeuchi and Eto, 1999). With time and additional MeHg exposure, this condition worsens and patients typically become ataxic. The progression of ataxia is due to worsening damage to the motor pathways, specifically involving the cerebellum. The time-course for the appearance of ataxia in MeHg patients is tightly correlated with the loss/dysfunction of granule cells within the cerebellum (Takeuchi and Eto, 1999). In the Iraqi MeHg outbreak, a total of 17 patients had blood mercury concentrations of 3 - 4 mg/ml (11.9 - 15.9 μM) all 17 patients were

ataxic prior to death (Bakir *et al.*, 1973). Visual and hearing defects were not reported in all patients that had blood mercury concentrations of 3 - 4 mg/ml, indicating that loss of coordination in gait is a more sensitive indicator to the neurotoxic effects of MeHg. The half time for clearance of MeHg was assumed to be 70 days in the Bakir *et al.* (1973) study; however, other reports have noted a shorter average half time for clearance of 52 days (Sherlock *et al.*, 1984). It should be noted that blood mercury samples from the Bakir *et al.* (1973) report were taken an average of 65 days after cessation of MeHg exposure. Therefore actual peak blood mercury levels would have been higher at the onset of signs of neurological dysfunction. During acute exposure to MeHg, approximately 95% of hospitalized patients with signs of ataxia had an estimated body burden of 200 mg of MeHg (Bakir *et al.*, 1973).

C. Biology of the Cerebellum

The cerebellum is a region of the brain that influences the motor systems by adjusting the functioning of motor centers in the brain stem and cortex. Five neuronal cell types make up the cerebellum. There are four inhibitory neuronal cell types, the Purkinje, stellate, Golgi and basket cells, and one excitatory type, the granule cell. Of all the neurons in the human central nervous system (CNS), the cerebellar granule cell is the most abundant with 1×10^{11} cells. In addition, the granule cell is one of the smallest neurons in size with a soma only 9-10 μm wide. By contrast, the cerebellar Purkinje cell is the one of the least abundant cell types and is one of the largest in size with a soma 25-30 μm wide (Ito, 1984). There are two excitatory inputs into the cerebellum. One excitatory input is the

Figure 1.1 Drawing showing the cytoarchitecture of the cerebellum. The excitatory mossy fibers that synapse onto granule cells as well as climbing fibers that synapse onto Purkinje cells in the cerebellum are shown. Note the many parallel fibers that are granule cell axons form excitatory synapses onto vast Purkinje cell dendrites. Also notice the apparent size difference between Purkinje and granule cells. Figure 1.1, modified from Kandel *et al.*, (2000).

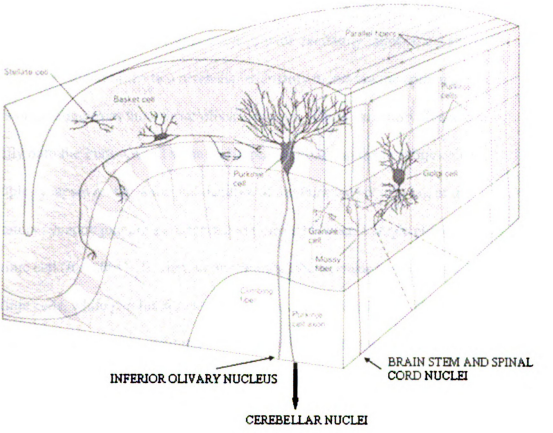
Parallel fibers
Stellate cell
Basket cell
Purkinje cell
Golgi cell
Granule cell
Mossy fiber
Climbing fiber
Purkinje cell axon
INFERIOR OLIVARY NUCLEUS
BRAIN STEM AND SPINAL CORD NUCLEI
CEREBELLAR NUCLEI

FIGURE 1.1

mossy fibers that originate in spinal cord and brain stem nuclei, which synapse directly onto granule cell dendrites. The axons of granule cells bifurcate to form parallel fibers and synapse directly onto multiple Purkinje and Golgi cell dendrites (Kandel *et al.*, 2000). Approximately one million parallel fibers provide excitatory input onto a single Purkinje neuron. The second of the two cerebellar excitatory inputs are the aptly named climbing fibers originating from the inferior olivary nucleus. These excitatory fibers, synapse directly onto the Purkinje cell soma and appear to climb up the Purkinje cell and make multiple synapses on the soma and dendrite of the Purkinje cell. In rat, as many as 26,000 excitatory synaptic junctions are estimated to form between a single climbing fiber and a Purkinje cell (Ito, 2001). Excitation of climbing fibers causes complex spike formation in Purkinje cells, while parallel fibers cause simple spikes (Ito, 1984). The sole output of the cerebellar cortex is the inhibitory Purkinje cell axon that penetrates the white matter and subsequently acts on the deep nuclei and vestibular nuclei (Kandel *et al.*, 2000). As a consequence, normal cerebellar function ultimately depends upon Purkinje cell output.

In comparing Purkinje cells to cerebellar granule cells, several differences become apparent that might contribute to the overall sensitivity to MeHg neurotoxicity. Purkinje neurons express P-, N- and L-type VGCCs with approximately 90% of Ca^{2+} current due to the P-type channel during depolarization (Mintz, 1992). In contrast, cerebellar granule cells grown in culture express L-, N-, P-/Q- and R-type VGCCs (Randall and Tsien, 1995). Purkinje and granule cells express both ryanodine and IP_3 receptors. In Purkinje cells, IP_3 receptors are localized primarily in the dendrites and ryanodine

Table 1.1 Comparison of cerebellar Purkinje and granule cell biology.

Footnotes

A mGluR1 subunits included in type I metabotrophic receptors with 4 splice variants (a-d).

Purkinje neurons express mGluR1 at very high levels compared to other CNS neurons.

B Purkinje cells predominately express α_{1C} with some immunoreactivity for α_{1D} in adult rats. n 2.5 yr old aged rats this distribution changes such that α_{1D} becomes more evident.

C Purkinje cells predominately express type I IP_3 receptors at a concentration several fold higher than total IP_3 receptors in granule cells.

D RyRβ is present in 1 week old chick Purkinje neurons, then gradually disappears.

E α_3 $GABA_A$ receptor subunit is expressed in immature Purkinje cells and α_2 subunit is expressed in immature granule cells during development.

Property	Purkinje Cell	Granule Cell	Reference
Soma size	25-30[1], 50-80 μm^2	5-8 μm[1]	[1]Ito, 1984 [2]Kandel *et al.*, 2000
Density (human)	$1.5x10^7$	$1x10^{11}$ cells	Ito, 1984
Type of neurotransmitter released	GABA	glutamate, nitric oxide	Kandel *et al.*, 2000 Ito, 2001
AMPA/kainate receptors	GluR1, GluR2, GluR3	GluR2	Keinanen *et al.*, 1990
Metabotropic glutamate receptor subytpes	mGluR1[A]	mGluR4	Berthele, 1998
NMDA receptors	Not functional	NR2A, NR2C and NR2B subunits	Didier *et al.*, 1997
VGCCs (subunits)	P-, L- and N-type[1 (B)] $\beta 2$, $\gamma 2$, $\gamma 4$	P-/Q-, R-, L- and N-type[2]	1) Mintz *et al.*, 1992 2) Randall and Tsien, 1995
IP_3 receptors	IP_3R1, IP_3R3[C]	IP_3R1, IP_3R3	Sharp *et al.*, 1999
Ryanodine receptors	RyRα, RyRβ[D]	RyRβ	Kuwajima *et al.*, 1992
Phospholipase C	PLC-β_3, PLC-β_4, PLC-γ_2	PLCβ_3, PLC-$_\gamma$	Tanaka and Kondo, 1994
Muscarinic receptor subtypes	M1, M2, M4	M2, M3	Tayebati *et al.*, 2001
$GABA_A$ receptor subunits	α_1[E]	α_6, α_1	Takayama and Inoue, 2004
Protein kinase G	Present	Not present	Feil, 2003
Excitatory amino acid transporters (EAAT)	EAAT-1	EAAT-3	Danbolt, 2001
Calmodulin-dependent protein kinase (CaMK)	CaMKIIα	CaMKIIβ	Wallaas *et al.*, 1988
Guanylyl cyclase	Present	Not present	Wassef and Sotelo, 1984
CaBPs	Parvalbumin, CB[1]	Calretinin[2]	1) Celio, 1990 2) Bastianelli, 2003

receptors within the soma (Khodakhah and Armstrong, 1997). IP_3 and ryanodine receptors share a common, functional Ca^{2+} pool in both cell types. Purkinje cells express the CaBPs, CB and parvalbumin (Gruol, 1983; Furuya *et al.*, 1998; Kobayashi *et al.*, 1998). In contrast, granule cells lack these CaBPs, but express calretinin (Bastianelli, 2003).

D. Ca^{2+} Mediated Cell Death

Ca^{2+} is an important second messenger molecule that is essential for normal cell function; however, prolonged elevations of $[Ca^{2+}]_i$ can lead to cell injury and/or cell death. The following are general events that can result from prolonged and elevated $[Ca^{2+}]_i$ that can ultimately lead to cell death 1) disruption of cell membrane integrity 2) depletion of ATP 3) activation of catabolic enzymes 4) promotion of free radical formation. These Ca^{2+}-mediated events may act synergistically to cause cell death.

Elevated $[Ca^{2+}]_i$ promotes the dissociation of the microfilament, actin from the plasma membrane anchoring proteins, α-actinin and fodrin. This represents a mechanism by which the cell membrane may become compromised as a result of high $[Ca^{2+}]_i$. With an approximately 10,000 fold difference in free cytosolic $[Ca^{2+}]$ and $[Ca^{2+}]_e$, about 25% of all ATP production in a neuron is devoted to maintaining that ion gradient. Elevated and prolonged $[Ca^{2+}]_i$ activates Ca^{2+}-ATPases located in the SER and outer cell membranes and eventually can deplete energy stores. Furthermore, ATP producing mitochondria can act as a buffer for Ca^{2+}_i but at the cost of the mitochondrial membrane potential. The ion

gradients found within the mitochondria are necessary for the generation of ATP through the oxidative phsophorylation process. Therefore, when Ca^{2+} enters the mitochondria oxidative phosphorylation and ultimately ATP generation is compromised (Nicotera *et al.*, 1992).

There are three major groups of catabolic enzymes that are activated by Ca^{2+} that are involved in cell death; these are: proteases, phospholipases and endonucleases. Calpains are a type of Ca^{2+}-activated cysteine protease that are nonlysosomal, located within the cytosol and likely degrade cytoskeletal elements (Orrenius *et al.*, 2003). Phospholipase C and phospholipase A_2 are examples of Ca^{2+}-activated enzymes, however Ca^{2+} may also indirectly activate these proteins in a calmodulin-dependent manner. Prolonged activation of phospholipase A_2 can lead to cell membrane breakdown. Ca^{2+} activated endonuclease acts to cleave deoxyribonucleic acid (DNA) at internucleosomal linker regions in fragments of multiples of approximately 200 base pairs (Nicotera *et al.*, 1992). This would lead to irreversible damage as a result of Ca^{2+} overload. In addition, topoisomerase II may become locked in a form that cleaves but does not relegate DNA. Dehydrogenase enzymes located in the citric acid cycle are also activated by Ca^{2+}, causing increased hydrogen output to the electron transport chain (Orrenius *et al.*, 2003). As a consequence to the compromised mitochondrial membrane potential described above, and greater flux of electrons along the electron transport chain, there is greater production of the oxygen free radical, superoxide $O_2^{\cdot}$. Furthermore, the proteins responsible for scavenging free radicals, such as glutathione reductase, may be degraded by the activity

of Ca^{2+}-dependent proteases. Therefore, the cell would have an impaired ability to defend against free radical damage.

Ca^{2+}-mediated cell death has been best studied following glutamate excitotoxicity. There is a direct correlation with increasing concentrations of $^{45}Ca^{2+}$ uptake after glutamate exposure and cell death in cerebellar granule cells in culture (Eimerl and Schramm, 1994). After 15 min exposure to 300 μM NMDA, approximately 50% of granule cells died. Furthermore, if $[Ca^{2+}]_i$ is buffered with the cell permeant Ca^{2+} chelator BAPTA-AM, there is a significant decrease in $[Ca^{2+}]_i$ after glutamate (1 mM) exposure in the neuroblastoma cell line CHP 100 (Clementi *et al.* 1996). Therefore, it appears the enhanced ability of a cell to buffer excess $[Ca^{2+}]_i$ leaves the cell less vulnerable to the cytotoxic effects of elevations of $[Ca^{2+}]_i$.

E. Ca^{2+} Binding Proteins

CaBPs belong to the EF-hand family of proteins and contain multiple, highly conserved EF-hand structural motifs. Each motif binds one Ca^{2+} with high affinity ($K_d = 10^{-8}$-10^{-10} M) and consists of two α helices separated by 12 amino acids containing side chain oxygens that are necessary for orienting Ca^{2+} (Christakos *et al.*, 2000). Examples of proteins belonging to the EF-hand family of CaBPs include the following: calmodulin, parvalbumin, troponin C, calretinin, calcineurin, calpain, myosin light chain kinase, CB and calbindin-$D9_K$. Calbindin-$D9_K$ is localized primarily in epithelial cells located in mammalian intestine while CB is more ubiquitous. Within the CNS several neuronal cell

types express CB. CB is also found in non-neuronal tissue such as: intestine (Arnold *et al.*, 1976; Feher, 1983; Shimura and Wasserman, 1984; Christakos *et al.*, 1989; Zhou and Galligan, 2000), kidney (Delrome *et al.*, 1983; Rhoten *et al.*, 1985) and bone (Balmain *et al.*, 1986). CB has also been found in neurons innervating cerebral blood vessels (Shimizu *et al.*, 2000). The expression of CB in cells outside the central nervous system is highly induced by the hormonally active form of vitamin D, 1,25 dihydroxyvitamin D_3 (Norman *et al.*, 1982; Theofan *et al.*, 1987). CB expression within rat CNS was not induced by 1,25 dihydroxyvitamin D_3 as measured by Northern blot analysis (Christakos *et al.*, 1989). The difference between vitamin D expression of CB in neuronal and non-neuronal tissue is presumably due to the inability of 1,25 dihydroxyvitamin D_3 to cross the blood brain barrier.

CB, and other CaBPs, are selectively expressed in specific neurons within the CNS such as cerebellar Purkinje, hippocampal CA1 pyramidal and dentate gyrus neurons (Celio, 1990). As such, CaBPs have proven to be useful tools as neuroanatomical markers. Structurally, CB is composed of 261 amino acid residues and has a molecular weight of approximately 28,000 daltons (based on migration on sodium dodecyl sulfate polyacrylamide gels) (Minghetti *et al.*, 1988). CB has six EF-hand domains; however only four are functional and bind Ca^{2+}. In cerebellar Purkinje neurons, expression of CB is high at 0.1 - 0.2 mM (Celio 1990). Purkinje cells express CB when they first appear during development at embryonic days 14-16 in rats. In contrast, cerebellar granule cells do not express CB. In adults, Purkinje cell function, as indicated by [^{3}H]-GABA uptake

assay, is disrupted when CB levels are decreased after CB anti-sense treatment (Vig *et al.*, 1999). These data suggest that CB serves a vital role in cerebellar Purkinje neurons. Unlike calmodulin, the specific function of CaBPs, such as CB and parvalbumin, is unknown. However, there is some evidence which suggests that CB alters VGCC functioning. In the GH_3 cell line, CB-transfected cells have reduced Ca^{2+} current density while Na^+ and K^+ current density were unchanged (Lledo *et al.*, 1992). In addition, GH_3 cells transfected with CB had greater Ca^{2+} current decay as measured by comparing peak Ca^{2+} current minus end current during a 500 ms voltage step from -40 mV to +10 mV. This would indicate a greater degree of inactivation of VGCC in CB containing cells compared to non-transfected cells (Lledo *et al.*, 1992). Parvalbumin and CB do not undergo conformational changes when Ca^{2+} is bound. However, based on the Ca^{2+} binding ability of these proteins alone, CB can potentially alter or influence Ca^{2+}-mediated cell signals.

CB might function as a neuroprotectant. In patients with Parkinson's Disease there was no significant loss of neurons in the *substantia nigra pars compacta* which stain positive for CB. However there was a significant loss of melanin-containing, non-CB immuno-positive cells in Parkinson's Disease patients compared to control patients (Yamada *et al.*,1990). Similar findings of enhanced neuron viability from Parkinson's Disease patients and 1-methyl-4-phenyl-1,2,3,6-tetrahydropyridine (MPTP)-treated monkeys correlated with positive CB immuno-reactivity (German *et al.*, 1993). *In vivo* studies involving other neurodegenerative disorders, such as Alzheimer's disease and

Amyotrophic Lateral Sclerosis (Shaw and Eggett, 2000), have also shown that neurons immunopositive for CB are less susceptible to neurodegeneration. The etiology of these neurological disorders is unknown, however dysregulation of Ca^{2+} homeostasis has been implicated in Amyotrophic Lateral Sclerosis (Shaw and Eggett 2000).

CB expression may be up-regulated during prolonged elevations of $[Ca^{2+}]_i$. Presumably this occurs as a compensatory mechanism in response to elevations of $[Ca^{2+}]_i$. CB was up-regulated in the hippocampus after focal stimulation of the perforant pathway (Lowenstein *et al.* 1991). After three and six hours of stimulation, both Northern blot analysis as well as *in situ* hybridization revealed significant increases in CB expression in the hippocampus. In addition, when isolated rat cerebellar slices were perifused with the selective glutamate agonist kainic acid, CB immunoreactivity increased (Batini *et al.* 1993). These data support the notion that one function of CB is to buffer excess $[Ca^{2+}]_i$.

Mattson *et al.* (1991) reported that hippocampal neurons which express CB in culture were less susceptible to glutamate (500 μM) excitotoxicity and exposure to the Ca^{2+} ionophore A23187 (1 μM). In comparison, neurons immuno-negative for CB did not buffer the increased $[Ca^{2+}]_i$. In PC12 cells, 1 μM A23187 has been shown to increase $[Ca^{2+}]_i$ five to ten times more than baseline, (Vyas *et al.* 1994). The most convincing data that CB acts to buffer cytotoxic $[Ca^{2+}]_i$ comes from the transfection of CB into naive cells. PC12 cells transfected with CB had a significantly greater cell viability (as measured by LDH release) 6, 9 and 24 hr after glutamate (10 mM) exposure (McMahon

et al. 1998). Furthermore, CB-transfected PC12 cells were more resistant to 1-methyl-4-phenylpyridinium (MPP^+) and serum withdrawal, processes that elevate $[Ca^{2+}]_i$. Similar observations have been made in the human embryonic kidney cell line (HEK293) co-transfected with NMDA (NR1 and NR2 subunits) receptors and CB (Rintoul *et al.*, 2001). CB-transfected HEK293 cells had decreased amplitude of fura-2 fluorescence during application of 2.5 μM A23187 compared to control cells.

F. Ca^{2+} Homeostasis and Neurons

Maintaining Ca^{2+} homeostasis is essential to all cells, especially to neurons, due to the dependence on Ca^{2+}_e entry in action potential formation and release of synaptic vesicles at axon terminals. Free, unbound $[Ca^{2+}]_i$ is maintained at approximately 100-200 nM despite $[Ca^{2+}_e]$ of approximately 1-2 mM (Kass and Orrenius, 1999). This difference in intracellular and extracellular Ca^{2+} concentrations creates a large chemical driving force. In addition, an inward electrical driving force for Ca^{2+} is present due to the relatively negative intracellular environment in comparison to the extracellular fluid. Taken together, there exists a very strong electro-chemical driving force for Ca^{2+} to enter cells. Cells have evolved multiple systems to buffer excess $[Ca^{2+}]_i$ and regulate tightly the entry of Ca^{2+}_e as a consequence of the need to maintain Ca^{2+} homeostasis in the face of such a large electro-chemical driving force.

There are a variety of cellular processes that mediate Ca^{2+} entry into neurons including: VGCCs, Ca^{2+} induced Ca^{2+} entry (CICE), Na^+ - Ca^{2+} exchanger, Ca^{2+} ATPases and pump

and receptors for neurotransmitters such as glutamate, seretonin, adenosine and acetylcholine. Glutamate is a ubiquitous neurotransmitter acting on three types of glutamate receptors that are classified according to their selective agonists and mechanism of action (Ozawa *et al.*, 1998). N-methyl-D-aspartate (NMDA) receptors bind the selective glutamate agonist NMDA with high affinity. NMDA receptors are ionotrophic receptors that allow Ca^{2+} and Na^{+} direct entry into the cell when the receptor is activated. In a resting state NMDA receptors have Mg^{2+} present in the pore of the receptor causing block of cation current. Only once there is binding of glutamate and a depolarization to remove the Mg^{2+} block, do Ca^{2+} and Na^{+} enter the cell through the NMDA receptor operated channel. Amino-3-hydroxy-5-isoxazole-4-propionic acid (AMPA) and kainate receptors selectively bind AMPA and kainate, respectively to cause Na^{+} entry and consequent membrane depolarization and activation of nearby VGCCs (Lerma *et al.*, 2001). This process allows for the indirect entry of $Ca^{2+}{}_{e}$. However, direct entry of $Ca^{2+}{}_{e}$ may occur through AMPA receptors if the GluR2 subunit is not present (Brorson *et al.*, 1999).

In electrically excitable cells such as neurons, $Ca^{2+}{}_{e}$ entry into cells occurs primarily, although not exclusively, through VGCCs. Therefore VGCCs are essential to normal neuronal functioning. Disruption of their function by neurotoxicants can have severe consequences for neurons. There are currently six known types of VGCCs: T-, L-, P-, Q-, N- and R-. Each channel type is unique in its gating kinetics, Ca^{2+} conductance, voltage threshold for activation and pharmacology. VGCCs are comprised of the pore-forming α_1

subunit, as well as α_2, δ, β and γ subunits (Catterall, 1991). The α_1 subunit contains four transmembrane domains. Each domain has six α-helical transmembrane segments (S1 - S6). VGCC type is dictated by the subtype of the α_1 (175 kD) subunit; for example, R-, P-/Q- and N-type VGCCs have α-$_{1E}$, α-$_{1A}$ and α-$_{1B}$ subunits, respectively (Carerall, 1991). Since the current classification scheme is considerably more complex today, an alternative nomenclature has been proposed. L-type VGCC family includes four members $Ca_V1.1$, $Ca_V1.2$, $Ca_V1.3$ and $Ca_V1.4$ corresponding to α-$_{1S}$, α-$_{1C}$, α-$_{1D}$ and α-$_{1F}$, respectively. Each VGCC subtype has differential rates of inactivation, binding affinity for specific VGCC antagonists and localization within specific types of tissue (Klugbauer *et al.*, 2002). Specifically, $Ca_V1.1$ is expressed primarily in striated skeletal muscle tissue $Ca_V1.2$ is present in cardiac and smooth muscle, pancreas, adrenal gland and brain tissue. $Ca_V1.3$ is present primarily in the brain, but also in pancreas, kidney, ovary and cochlea. In accordance with the new L-type VGCC nomenclature, N-, P/Q- and R-type VGCC are named $Ca_V2.2$, $Ca_V2.1$ and $Ca_V2.3$, respectively (Doering and Zamponi, 2003). Lastly, the T-subtype VGCCs which contain α-$_{1G}$, α-$_{1F}$ and α-$_{1I}$ subunits have been replaced by $Ca_V3.1$, $Ca_V3.2$ and $Ca_V3.3$, respectively. The α_2 and δ VGCC subunits are linked together by a disulfide bond to form a transmembrane glycoprotein complex. The hydrophilic β subunit is disposed intracellularly and binds to the intracellular loop connecting the I and II domains of the α_1 subunit. Furthermore, the β subunit is important in transport of newly formed VGCCs to the outer cellular membrane and may influence VGCC kinetics of $Ca_V2.2$ (Dolphin, 2003). Presently, there are 4 known subtypes of β subunit, with splice variants for some types. Immunocytochemistry as well

as *in situ* hybridization studies, demonstrate β_2 protein and mRNA levels are low in all areas of the brain with the exception of cerebellar Purkinje cells, where it is highly expressed. In contrast, β_4 is expressed in both cerebellar Purkinje and granule neurons (Ludwig *et al.*, 1997). The significance of the differential expression of β subunits in Purkinje neurons is as yet unknown. The α_2 and δ subunits are encoded by the same gene. There are 8 putative members of the transmembrane protein VGCC γ subunit family (Black, 2003). The 2γ, 3γ and 4γ subunits are associated with $\alpha\text{-}_{1A}$ and $\alpha\text{-}_{1B}$ VGCC subunits as well as the GluR1 subunit of the AMPA receptor (Black, 2003). The γ subunit may function to alter the activity of VGCCs. For example, when the 2γ subunit was co-expressed with $\alpha\text{-}_{1A}\beta_{1a}\alpha_2$ VGCC subunits in HEK293 cells there was a significant negative shift in the steady-state inactivation curve in the presence of Ca^{2+}. The effect was opposite with a positive shift in the steady-state inactivation curve when Ba^{2+} was the charge carrier (Klugbauer *et al.*, 2000). Thus, the 2γ subunit may be involved in Ca^{2+}-induced inactivation of VGCCs.

An example of L-type VGCC antagonists are the dihydropyridines, which selectively bind to the α_1 subunit and alter the gating kinetics of L-type channels (Doering and Zamponi, 2003). Dihydropyridines bind to two separate regions located in the S5 and S6 regions of the transmembrane domains III and IV of α_{1S} ($Ca_V1.1$) subunit. However, certain dihydropyridines irreversibly blocked Ca^{2+} current in α_{1G} ($Ca_V3.1$) transiently transfected HEK293 cells (Kumar *et al.*, 2002). The funnel web spider (*Agelenopsis aptera*) toxin, Aga IVA, and marine cone snail (*Conus geographus*), ω-Conotoxin GVIA, inhibit the

functioning of P- and N-type VGCCs, respectively. It is currently thought that Aga IVA binds to the α-$_{1A}$ subunit to alter the gating kinetics of the channel such that a larger change in membrane potential is required for channel activation.

Other regulators of $[Ca^{2+}]_i$ are mitochondria and the smooth endoplasmic reticulum (SER). Receptors for IP_3 and ryanodine are located on the surface of the SER. There are three different types of IP_3 receptors and each has various numbers of distinct splice variants. Most cells express all three types of IP_3 receptors, with the exception of cerebellar Purkinje cells which express type I almost exclusively (Patel *et al.*, 1999). The IP_3 receptor is made up of three domains which include an IP_3 binding domain, a regulatory domain that can be phosphorylated, and a pore-forming domain through which Ca^{2+} passes (Patel *et al.*, 1999). The SER is a high-affinity, low-capacity Ca^{2+} buffering system, while the mitochondria represent a low-affinity, high-capacity Ca^{2+} buffering system. The SER is a dynamic organelle in terms of Ca^{2+} homeostasis; the SER has the ability to buffer excess elevations of $[Ca^{2+}]_i$ via a Ca^{2+} ATPase as well as release $Ca^{2+}{}_i$ into the cytosol from IP_3 and ryanodine receptors. In contrast, the mitochondria are primarily a Ca^{2+} sink and do not release cytotoxic concentrations of Ca^{2+} into the cytosol under normal conditions. During adverse conditions, such as anoxia or excess Ca^{2+} accumulation within the mitochondrial matrix, release of mitochondrial Ca^{2+} may occur via an opening of the mitochondrial permeability transition pore (MTP) (Dubinsky and Rothman, 1991). Opening of the MTP and subsequent elevation of $[Ca^{2+}]_i$ is associated with cell death (Schinder *et al.* 1996).

G. Cellular Aspects of MeHg Neurotoxicity

While the pathological consequences of MeHg exposure have been identified, the cellular mechanism(s) of MeHg neurotoxicity remains unknown. It is likely that multiple mechanisms are involved in MeHg cytotoxicity, due in part to the fact that MeHg has high affinity for –SH groups and to the ubiquitous nature of –SH groups present within cells (Hughes, 1957). MeHg has been shown to alter many neuronal processes including: protein phosphorylation (Verity *et al.*,1977), neurotransmitter release (Juang, 1976; Atchison and Narahashi, 1982; Atchison, 1986; Atchison, 1987; Yuan and Atchison, 1999), dysregulation of divalent cation homeostasis (Komulainen and Bondy, 1987; Hare *et al.*, 1993; Hare and Atchison 1995a, b; Sarafian, 1993; Atchison and Marty, 1997; Limke and Atchison, 2002; Limke *et al.*, 2004), glutamate transport in glial cells (Aschner *et al.*, 1993), neuron migration during development (Kunimoto and Suzuki, 1997), neurite outgrowth (Heidemann *et al.* 2001), oxygen consumption in isolated brain slice (Fox et al., 1975), uptake of both GABA and choline (Kusky and McGeer, 1989; Levesque *et al.*, 1992) and neuronal excitability (Yuan and Atchison, 1999).

Although MeHg causes multiple cellular effects, the focus of my thesis will be on the ability of MeHg to disrupt divalent cation homeostasis. Early studies demonstrated that MeHg altered Ca^{2+} homeostasis monitored miniature end plate potential (MEPP) frequency from isolated neuromuscular junctions. MeHg caused an increase in MEPP frequency then a decrease in MEPP frequency in a concentration, and time-dependent manner. However mean peak frequency was not dependent upon the concentration of

MeHg (Atchison and Narahashi, 1982). These effects were not reversed with wash of non-MeHg buffer. Only high concentrations of Ca^{2+}_e (4 mM) and 4-aminopyridine reversed the MeHg-induced effects of MEPP frequency at the neuromuscular junction (Traxinger and Atchison, 1987). MEPP frequency increased when MeHg was present in a Ca^{2+}-free buffer. Furthermore, activation of VGCCs with either Bay K 8644 (Atchison, 1987) or depolarizing KCl solutions (Atchison, 1986) hastened time-to-onset of increases in MEPP frequency in Ca^{2+}-free buffer. Because MEPP frequency is a Ca^{2+}_i-dependent process this indicated that MeHg caused release of Ca^{2+} from intracellular stores. Both the SER (Hare and Atchison, 1995a) and mitochondria (Levesque and Atchison, 1991; Levesque *et al.*, 1992; Limke and Atchison 2002) have been identified as potential sources of Ca^{2+}_i release during MeHg exposure.

There is much evidence that MeHg interacts with mitochondria to disrupt Ca^{2+} homeostasis. In rat brain synaptosomes, the presence of ruthenium red, an inhibitor of the mitochondrial Ca^{2+} influx uniporter, decreased MeHg-mediated release of [^{3}H]acetylcholine. However MeHg did not appear to bind to the same target within the mitochondria as did ruthenium red (Leveseque and Atchison, 1991; Leveseque *et al.*, 1992). Furthermore, MeHg decreased the respiratory rates and $^{45}Ca^{2+}$ uptake of isolated mitochondria in a process that was influenced by the presence of ATP (Levesque and Atchison, 1991). MeHg had differential effects in the presence of specific inhibitors of mitochondrial function. Specifically, the MeHg-induced elevation of MEPP frequency was not attenuated when mitochondrial proton ionophores or K^+ ionophores were present,

but pretreatment with ruthenium red did attenuate MeHg-mediated elevations of MEPP frequency at the rat neuromuscular junction (Levesque and Atchison, 1987). Thus, MeHg disrupts mitochondrial function in a process related to the mitochondrial Ca^{2+} uniporter, but MeHg does not act on the same target as that of ruthenium red.

The MTP is a mega pore that opens in the inner membrane of mitochondria to allow Ca^{2+} release and dissipation of the proton gradient (Dubinsky and Rothman, 1991). When the MTP was inhibited by cyclosporin A, there was a delay in the time-to-onset of MeHg-induced elevation of fura-2 fluorescence and elevated cell viability from exposure to 0.2 μM MeHg in cerebellar granule cells (Limke and Atchsion, 2002). This would further add to the argument that MeHg acts to disrupt Ca^{2+} homeostasis by causing mitochondrial dysfunction.

While considerable evidence indicates that mitochondria may contribute to the release of Ca^{2+}, MeHg may also cause the release of Ca^{2+}_i from other intracellular sources. MeHg may act to release Ca^{2+} from intracellular sources such as the SER. In the NG108-15 cell line, the application of bradykinin results in the elevation of IP_3 and subsequent elevation of $[Ca^{2+}]_i$ (Hare and Atchison, 1995b). When MeHg was applied to NG108-15 cells in a Ca^{2+}-free extracellular buffer, following acute exposure to bradykinin, there was no additional increase in fura-2 fluorescence. Furthermore, application of bradykinin after MeHg exposure had no effect on fura-2 fluorescence in NG108-15 cells (Hare and Atchison, 1995b). Thus, MeHg apparently causes the release of Ca^{2+}_i from similar

intracellular sources of Ca^{2+} that are sensitive to bradykinin in NG108-15 cells. In cerebellar granule cells, inhibition of muscarinic receptors with atropine, or desensitization of muscarinic receptors with chronic application of the muscarinic receptor agonist, bethanecol resulted in a delay in the time-to-onset of MeHg-induced dysregulation of Ca^{2+} homeostasis (Limke *et al.*, 2004). Furthermore, down regulation or inhibition of muscarinic receptors resulted in greater cerebellar granule cell viability after MeHg exposure (Limke *et al.*, 2004). Granule cells express types II and III muscarinic receptors. The type III muscarinic receptor is coupled to phospholipase C, an enzyme that generates IP_3. The M3 specific antagonist, DAMP, delayed MeHg-induced dysregulation of Ca^{2+} homeostasis. In correlation with this, MeHg caused elevated levels of IP_3 in cerebellar granule cells (Sarafian, 1992). Thus, MeHg appears to act on intracellular sources of Ca^{2+} that are sensitive to IP_3 to cause the release of Ca^{2+}. In studies using the Ca^{2+} indicator, fura-2 an initial elevation of $[Ca^{2+}]_i$ due to release of $Ca^{2+}{}_i$ that was followed by a second elevation of $[Ca^{2+}]_i$ due to entry of $Ca^{2+}{}_e$ (Marty and Atchison, 1997; Edwards and Atchison, 2001; Limke and Atchison, 2002). The pathway in which entry of $Ca^{2+}{}_e$ occurs after exposure to MeHg is unknown. However it is likely that MeHg-mediated entry of $Ca^{2+}{}_e$ is not due to the loss of cell membrane integrity (Denny *et al.*, 1993).

MeHg interacts with VGCCs in a non-competitive and irreversible manner to inhibit Ca^{2+} (Shafer, 1998, Peng *et al.*, 2002; Hajela *et al.*, 2003) as well as Ba^{2+} (Sirois and Atchison, 2000) current in a variety of cell types and experimental preparations. The apparent

affinity of MeHg for VGCCs is high as shown by the observation that MeHg causes disruption of VGCC functioning at very low MeHg concentrations. For example, a 24 hr exposure to 30 nM MeHg caused a significant decrease in whole cell Ca^{2+} current in PC12 cells (Shafer *et al.*, 2002). Furthermore, inhibition of VGCCs causes enhanced resistance to MeHg-mediated dysregulation of Ca^{2+} homeostasis in NG108-15 cells (Hare and Atchison, 1995a) and cerebellar granule cells (Marty and Atchison, 1997) as well as, enhanced the resistance to MeHg-induced cerebellar granule cell cytotoxicity (Marty and Atchison, 1998). MeHg may share the same binding site on VGCCs as do the dihydropyridines. In rat forebrain synaptosomes, MeHg decreases the affinity of binding of [^{3}H] nitrendipine (Shafer *et al.*, 1990). When MeHg was applied intracellularly or extracellularly, there was a similar decrease in Ca^{2+} current density in PC12 cells (Shafer, 1998), indicating that inhibition of VGCCs by MeHg may occur through binding of MeHg to either intracellular or extracellular targets. Alternatively, intracellularly applied MeHg may traverse the VGCC pore to bind to the dihydropyridine binding site or diffuse passively through the lipid membrane to gain access to the same dihydropyridine binding site. Although MeHg may bind to a similar binding site of dihydropyridines on L-type VGCCs, recombinant L-type Ca^{2+} channels containing the α_{1C} type subunit expressed in HEK293 cells were incompletely blocked by MeHg (Peng *et al.*, 2002). Complete block of L-type VGCC function required the use of the dihydropyridine, nifedipine.

Several *in vivo* studies have compared the ability of MeHg to disrupt normal cell function and cause cell death in cerebellar granule and Purkinje neurons. In a study by Leyshon

and Morgan (1991), morphological changes in the cerebellum of adult male rats were quantified after exposure to MeHg by gastric gavage for 15 days. At 43 days after initial treatment, rats demonstrated signs of irreversible MeHg poisoning, including, hind limb crossing reflex and flailing reflex. These two reflexes are early indicators in the rodent model of MeHg intoxication (Magos *et al.*, 1978). Electron photomicrographs exhibited a propensity of pyknotic nuclei in cerebellar granule cells with dark granular cytoplasm, indicating cell death and/or dysfunction. In stark contrast, adjacent Purkinje cells in the MeHg-treated rats did not show any significant change in morphology compared to saline-treated control animals. Thus, there is a direct correlation between cerebellar granule cell loss during MeHg exposure and the signs and symptoms of cerebellar ataxia. Mori *et al.* (2000) used a Ca^{2+} sensitive dye, alizarin red S, to visualize intracellular and extracellular Ca^{2+} deposits in cerebellar slices of female rats treated with dimethylmercury by injection. As early as 19 days after the initial treatment, cerebellar granule cells started to show accumulations of Ca^{2+}, with correspondingly increasing Ca^{2+} accumulations at 100 days post-injection. Gross atrophy of the granule cell layer was evident at later time points. Adjacent Purkinje cells did not show any signs of cell loss or death, nor did Purkinje cells accumulate Ca^{2+}_i as indicated by a lack of staining for Ca^{2+} deposits at any of the time points tested. Mori *et al.* (2000) also quantified the degree of neurodegeneration and Ca^{2+} deposits in the cerebral cortex, thalamus, dorsal fascicle and dorsal root ganglia. Of all these regions studied, the granule cell layer of the cerebellar cortex had the greatest degree of neurodegeneration at the earliest time points, along with the greatest intensity of staining for Ca^{2+} accumulation. Thus the presence or absence of

Ca^{2+} deposits within the cerebellum is directly correlated with enhanced sensitivity or resistance to alkyl-mercury neurotoxicity, respectively. In the isolated brain slice preparation, MeHg disrupted inhibitory and excitatory synaptic transmission in a time- and concentration-dependent manner (Yuan and Atchison, 1997; Yuan and Atchison, 1999). Furthermore MeHg differentially affected cerebellar Purkinje and granule cells in a time- and concentration-dependent manner by first increasing then decreasing both amplitude and frequency of spontaneous inhibitory post synaptic currents (Yuan and Atchison, 2003). Specifically, time-to-onset of block of spontaneous inhibitory post synaptic currents was significantly delayed in Purkinje cells compared to granule cells during exposure to 10, 20 and 100 μM MeHg in cerebellar slice preparations. Thus, *in vivo* and *in vitro* experiments, there is a clear demonstration of the differential effects of MeHg on cerebellar granule and Purkinje cells.

Significant increases in cerebellar granule cell viability were observed 3.5 hr post-MeHg exposure when cells were pre-treated with the intracellular Ca^{2+} chelator, BAPTA-AM, however this effect was not observed 24.5 hr post- MeHg exposure (Marty and Atchison, 1998). In addition to causing cytotoxicity, nonlethal concentrations of MeHg disrupt neurite outgrowth in chick forebrain neurons (Heidemann *et al.* 2001). The addition of BAPTA-AM decreased the MeHg-induced disruption of axonal morphogenesis when measured after MeHg exposure (Heidemann *et al.*, 2001). These data suggest that altered Ca^{2+} homeostasis is a possible contributor to MeHg-induced disruption of cell functioning and subsequent cytotoxicity.

In addition to Ca^{2+} homeostasis at least one other divalent cation also is disrupted following MeHg exposure. When granule and Purkinje cells were treated with TPEN, a membrane permeable heavy-metal chelator, the MeHg-induced first-phase increase in fura-2 fluorescence was attenuated, indicating the presence of a non-Ca^{2+} divalent cation (Marty and Atchison, 1997). One of the non-Ca^{2+} divalent cations released during exposure to MeHg has been identified in rat cortical synaptosomes as Zn^{2+} using ^{19}F-NMR (Denny and Atchison, 1994). The source of Zn^{2+} was determined to be the soluble fraction of the synaptosomes (Denny *et al.*, 1994). Zn^{2+} modulates the function of many different cell surface proteins including glutamate, $GABA_A$ and glycine receptors as well as VGCCs (Choi and Koh, 1998). Furthermore, cerebellar granule cells exposed to Zn^{2+} undergo concentration-dependent cell death (Manev *et al.*, 1997). Thus, the release of Zn^{2+}_i could be a contributing factor in MeHg-induced neurotoxicity.

In summary, cerebellar Purkinje and granule cells show a differential response to MeHg neurotoxicity *in vivo*. Furthermore, MeHg causes elevations of $[Ca^{2+}]_i$ through the release of Ca^{2+} from intracellular sources followed by entry of Ca^{2+}_e though an as yet unidentified pathway. The prolonged elevation of $[Ca^{2+}]_i$ resulting from MeHg exposure may be an important factor in the etiology of MeHg-mediated cell death. As such, the focus of my thesis is to compare the ability of cerebellar Purkinje and granule cells to undergo MeHg-induced dysregulation of Ca^{2+} homeostasis and to ascertain what significance VGCCs and CB which both act to regulate Ca^{2+} homeostasis, have in MeHg-mediated dysregulation of

cell death and subsequent cytotoxicity.

CHAPTER TWO

COMPARATIVE SENSITIVITY OF RAT CEREBELLAR NEURONS TO DYSREGULATION OF DIVALENT CATION HOMEOSTASIS AND CYTOTOXICITY CAUSED BY METHYLMERCURY

ABSTRACT

The objective of the present study was to determine the relative effectiveness of MeHg to alter divalent cation homeostasis and cause cell death in cerebellar Purkinje and granule neurons. Application of 0.5-5 μM MeHg to Purkinje (21-24 days in culture) and granule (7-10 days in culture) cells grown in culture caused a concentration- and time-dependent biphasic increase in fura-2 fluorescence. At 0.5 and 1 μM MeHg, the elevation of fura-2 fluorescence induced by MeHg was significantly delayed in Purkinje as compared to granule cells. Application of the heavy-metal chelator, TPEN, to Purkinje cells caused a precipitous decline in a proportion of the fura-2 fluorescence signal, indicating that MeHg causes release of Ca^{2+} and non-Ca^{2+} divalent cations. Purkinje cells were also more resistant than granule cells to the neurotoxic effects of MeHg. At 24.5 hr after-application of 5 μM MeHg, 97.7% of Purkinje cells were viable. At 3 μM MeHg there was no detectable loss of Purkinje cell viability. In contrast, only 40.6 ± 13% of cerebellar granule cells were alive 24.5 hr after application of 3 μM MeHg. When acutely dissociated Purkinje cells were exposed to (0.5-5 μM) MeHg there was a resulting single-phase and abrupt increase in fura-2 fluorescence; this response differed from the biphasic response induced by MeHg in Purkinje cells grown in culture. In conclusion, Purkinje neurons (both in primary cultures and acutely dissociated) appear to be more resistant to MeHg-induced dysregulation of divalent cation homeostasis and subsequent cell death when compared to cerebellar granule cells. Moreover, the response to MeHg of acutely dissociated Purkinje neurons differed from that of Purkinje cells maintained in primary culture conditions.

INTRODUCTION

MeHg is a potent environmental neurotoxicant that causes selective cell death in certain populations of neurons. In both animals and humans, postnatal exposure to MeHg causes preferential effects on cerebellar granule cells while the adjacent Purkinje cells apparently remain, at least initially, unharmed (Hunter, 1954; Leyshon and Morgan, 1991; Leyshon-Sorland *et al.*, 1994; Mori *et al.*, 2000). The cellular or molecular mechanisms which contribute to the differential neurotoxic effects of MeHg within the cerebellum are, as yet, unknown. Because Purkinje cells are one of the largest neurons in the CNS and cerebellar granule cells are one of the smallest, Clarkson (1972) suggested that cell size may be a contributing factor in the differential neurotoxic effects of MeHg. Other factors have been suggested to explain why Purkinje cells are relatively more resistant to the neurotoxic effects of MeHg including: ability to chelate metals (Leyshon-Sorland *et al.*, 1994), synaptic transmission (Yuan and Atchison, 2003), glutamate receptor subtype expression and production of nitric oxide (Himi *et al.*, 1996). Because MeHg disrupts a wide variety of cellular processes, it is difficult to pinpoint individual, specific factors that may contribute to the differential neurotoxicity of MeHg observed in cerebellar granule and Purkinje neuronal cell types.

There are no studies comparing directly the cellular effects of MeHg on cerebellar Purkinje and granule cells. Because MeHg has high affinity for -SH groups and the ubiquitous nature of -SH groups present within cells, MeHg has been found to disrupt or alter a variety of cell processes such as: astrocyte function (Aschner, 1993), myelin

formation (Chang *et al.*, 1977), serotonin concentrations (Taylor and DiStefano, 1976) and re-uptake of neurotransmitters (O'Kusky and McGeer, 1989). Experiments utilizing a variety of *in vitro* preparations have shown one of the earliest effects of MeHg is to disrupt homeostasis of Ca^{2+} as well as non-Ca^{2+} divalent cation homeostasis (Komulainen and Bondy, 1987; Sarafian, 1993; Denny *et al.*, 1993; Hare and Atchison, 1995; Marty and Atchison, 1997; Limke and Atchison, 2002). These effects occur at MeHg concentrations in the low-micromolar range in a variety of cell types (Hare *et al.*, 1993) but can occur at sub-micromolar concentrations of MeHg in cerebellar granule cells (Marty and Atchison, 1997; Limke and Atchison, 2002). Furthermore, elevations of $[Ca^{2+}]_i$ appears to be linked to cytotoxicity in cerebellar granule neurons in primary culture. When granule cells are pre-treated with a cell-permeable form of the Ca^{2+} chelator BAPTA, MeHg cytotoxicity was attenuated 3.5 hr after MeHg exposure (Marty and Atchison, 1998). Studies in whole animals also support the idea that elevated $[Ca^{2+}]_i$ has a role in MeHg-mediated cell death. Mori *et al.* (2000) used a Ca^{2+}-sensitive dye, alizarin red S to detect Ca^{2+} deposits in cerebellar slices of rats that were treated by injection of dimethylmercury. As early as 19 days after exposure to dimethylmercury, cerebellar granule cells started to show accumulations of Ca^{2+}, which increased after further exposure to dimethylmercury. Gross atrophy of the granule cell layer was evident at later time points. Adjacent Purkinje cells did not show any sign of cell loss or death, nor did Purkinje cells accumulate $Ca^{2+}{}_i$ as indicated by a lack of staining for Ca^{2+} deposits (Mori *et al.*, 2000). Thus, the presence or absence of Ca^{2+} deposits within the cerebellum is directly correlated with sensitivity or resistance to MeHg neurotoxicity, respectively.

Based on these *in vitro* and *in vivo* observations, alterations in $[Ca^{2+}]_i$ appear to be a contributory factor to MeHg-induced neurotoxicity.

The purpose of this study was to compare the ability of MeHg to disrupt divalent cation homeostasis, as measured by changes in fura-2 fluorescence, and induce cytotoxicity in cerebellar Purkinje and granule neurons. Purkinje cells grown in culture may have a reduced or impaired ability to release Ca^{2+} from intracellular stores when compared to acutely dissociated Purkinje cells (Womack *et al.*, 2000). Therefore, additional experiments were performed to assess the effects of MeHg on release of Ca^{2+}_i from acutely dissociated Purkinje cells as well as from cells grown in culture. The heavy-metal chelator, TPEN, was used to assess the effectiveness of MeHg to disrupt non-Ca^{2+} divalent cation homeostasis in Purkinje neurons.

METHODS

Materials. Methylmercuric chloride (MeHg) was purchased from ICN Biochemicals Inc. (Aurora, OH). Tetrakis-(2pyridylmethyl)ethylenediamine (TPEN), fura-2 acetoxymethyl ester (fura-2 AM) and pluronic acid were purchased from Molecular Probes Inc. (Eugene, OR). 4-(2-Hydroxyethyl)piperazine-1-ethanesulfonic acid (HEPES), Poly-L-ornithine (P-4638), anti-Calbindin D-28K (C-9848), cytosine-β-arabinofuranoside (Ara-C) (C-1768) and sodium selenite (S-1382) were purchased from Sigma Chemical Co. (St. Louis, MO). Goat anti-mouse IgG conjugated to tetramethyl rhodamine (TRITC) (715-025-150) was purchased from Jackson ImmunoResearch Laboratories. Inc. (West Grove, PA). Trypsin (LS003707) and deoxyribonuclease (LS002139) were purchased from Worthington Biochemical Corp. (Freehold, NJ). Fetal bovine serum (FBS) and Dulbecco's Modified Eagle Medium with F12 supplement (cat. # 12400-016) were purchased from Gibco (Grand Island, NY).

Isolation of Purkinje cells for cell cultures (intracellular cation measurements and viability experiments). Two methods were used to isolate Purkinje cells for cell cultures depending on the specific experimental procedure. The rationale for this was as follows, the Purkinje cell isolation protocol for the Ca^{2+} imaging experiments included medium that was found to contain sodium selenite (40 nM). Selenium is protective against many of the toxic effects of MeHg (Watanabe, 2002), although it would likely not affect very rapidly-occurring, acute effects of MeHg such alterations in $[Ca^{2+}]_i$. Furthermore, there was no significant difference in first or second phase time-to-onset of elevations of fura-2

fluorescence caused by 0.5 μM MeHg from granule cells in the presence or absence of 30 nM selenium (ANOVA, $P > 0.05$) (Fig. 2.6). However, selenium could affect subsequent, more delayed effects of MeHg such as cytotoxicity. Therefore, in order to examine cell viability after MeHg exposure an alternative Purkinje cell isolation protocol was utilized in which the medium did not contain selenium.

The Purkinje cell isolation protocol that yielded cells for Ca^{2+} imaging experiments was adapted and modified from that described by Furuya *et al.*, (1998). Cells were isolated from fetal (gestation day 18) rat pups (Harlan, Indianapolis, IN). Cerebellar cortices from pups were dissected and stored in ice-cold Ca^{2+} and Mg^{2+} -free Hanks Balanced Saline Solution (CMF-HBSS) which contained (mM): 5.4 KCl, 0.4 KH_2PO_4, 136.9 NaCl, 0.3 Na_2PO_4, 20 HEPES, 0.6 EDTA, 5.6 d-glucose and 4.2 $NaHCO_3$ (pH 7.3 at 23°C). Isolated cortices were minced and then treated with trypsin (2% w/v) for 5-7 min at 23°C; tissue was then rinsed three times with CMF-HBSS. DNase (0.03% w/v) was applied in CF-HBSS ($MgSO_4$ added to CMF-HBSS, 12 mM final concentration of $MgSO_4$); cells were then gently and slowly triturated with a fire polished glass pipette. After trituration, the tissue homogenate was incubated for 4 min on ice in a polypropylene 15 ml culture tube to allow undigested tissue to settle to the bottom of tube. Dissociated cells were collected from the top layer and stored on ice in a separate container. Undigested tissue underwent further DNase digestions as described above until almost all tissue was dissociated (approx. 4-5 DNase treatments). Dissociated cells were then centrifuged for 5 min at 920*g*, then buffer was removed and the pellet resuspended in CF-HBSS and

centrifuged again to remove completely any trace of DNase. The pellet was then resuspended in DMEM/F12 supplemented with 10% FBS. Cells in suspension were plated on 10 μg/ml poly-L-ornithine coated petri dishes and were allowed to settle for 20 min in a humidified incubator. This step was done to separate the quickly adhering glial cells which contaminated the Purkinje cell isolate. After 20 min the top layer of medium containing non-adhering neurons was collected for plating on coverslips. Cells were plated on coverslips coated with poly-L-ornithine (40 μg/ml) and then placed in a humidified cell culture incubator (5% CO_2 and 37°C) for 1-2 days. After 2 days, coverslips were transferred to a bi-laminar culture system with Purkinje cell plated coverslips on top and a bottom feeder layer consisting of cerebellar granule and glial cells isolated from 7 day old rat pups. A bent, glass capillary tube (approximately 3 mm outer diameter) was used as a spacer between the top and bottom layers so glial cells did not physically contact the coverslip. AraC (10 μM) was added to Purkinje cell cultures approximately 3 days after plating to inhibit proliferating, non-neuronal cells. Purkinje cell culture medium was changed every 3-4 days. The second Purkinje cell isolation procedure, which was used to obtain cell cultures for viability assays, was a modified organo-typic Purkinje cell culture system based on the protocol described by Gruol (1983). In both types of isolations, all experiments were conducted on Purkinje cells at 21-24 DIV to allow the cells in culture to mature and achieve adult morphology and biochemical patterns.

Isolation of acutely dissociated Purkinje cells (intracellular Ca^{2+} measurements).

Briefly, 7-14 day old rat pups were decapitated and then cerebella dissected out and placed in oxygenated Ca^{2+}-free HEPES buffered saline solution (CF-HBS). This contained (mM): 150 NaCl, 5.4 KCl, 0.8 $MgSO_4$, 0.02 EGTA, 20 d-glucose and 20 HEPES (free acid) (pH 7.3 at room temperature). The tissue was then minced, and 3 ml of a 1.6 mg/ml solution of trypsin was added for 5 min at room temperature. After trypsin incubation, the tissue was transferred to a 15 ml polypropylene culture tube and rinsed 3 times with CF-HBS. Then 1.5 ml of a 0.2 mg/ml solution of DNase was added, and the tissue was triturated with a fire-polished glass pipette and set aside. After 4 min, the undissociated tissue settled to the bottom of the culture tube, and dissociated cells remained in the top half of the solution of DNase. Dissociated cells were transferred to another 15 ml cell culture tube, and treatment with DNase was repeated with the undissociated tissue. It was then centrifuged at 920*g* for 5 min. The supernatant was subsequently removed, and the cell pellet resuspended in 2 ml of HBS which contained (mM): 150 NaCl, 5.4 KCl, 1.8 $CaCl_2$, 0.8 $MgSO_4$, 20 d-glucose and 20 HEPES (free acid) (pH 7.3). Cells suspended in HBS were then plated on poly-D-lysine coated glass coverslips and immediately incubated with fura-2AM (see below). Cells maintained for longer than four hours *in vitro* were not used in any of the acutely dissociated Purkinje cell experiments.

Protocol for isolation of cerebellar granule cells protocol. Cerebellar granule cells were isolated and grown according to conditions previously described in Marty and Atchison (1997).

Measurement of changes in fura-2 fluorescence. The ratiometric fluorophore fura-2 was used in all experiments to record changes in divalent cation concentrations induced during continuous perifusion with MeHg in HBS. Purkinje and granule neurons grown in culture were loaded with fura-2 AM (3 - 4 μM) for one hr in the presence of pluronic acid (3 - 4 μM), then were rinsed in perfusing HBS for 30 min at 37°C. The fura-2 AM loading protocol for the acutely dissociated Purkinje cells was the same as that for cells grown in culture, with the exception that acutely dissociated cells were incubated with fura-2AM for 30 min, then perifused for only 15 min prior to the start of the experiment. For each experiment, cells were initially perifused for 2 min with HBS containing 40 mM KCl to depolarize the cell and thus assure cell viability and the ability to buffer Ca^{2+}_i. The KCl depolarizing buffer contained (mM): 105.4 NaCl, 40 KCl, 1.8 $CaCl_2$, 0.8 $MgSO_4$, 20 d-glucose and 20 HEPES (free acid) (pH 7.3). For Purkinje cells grown in culture, data were obtained simultaneously from cell soma and the corresponding dendritic field on the same coverslip. Fura-2 fluorescence data were only obtained from the soma of granule cells and acutely dissociated Purkinje cells. Digital fluorescent images were obtained using an IonOptix cation fluorescence imaging system (Milton, MA) and an MTI charge coupled device (DAGE-MTI Inc., Michigan City, IN) camera to record images. Fura-2 fluorescence changes were monitored simultaneously in the soma of multiple cells within the same microscopic field to minimize cell selection bias. Data from these cells were averaged to provide a mean time-to-onset of increases of fur-2 fluorescence for that dish. None of the agents used in this study, including MeHg (Hare *et al.* 1993), caused a noticeable shift in fura-2 spectra at the concentrations used (results not shown).

Viability assay of cultured Purkinje and granule neurons. Purkinje (21-24 DIV) and granule cells (6-8 DIV) were rinsed three times with warmed HBS. HBS solutions containing (0.5-5 μM)MeHg were then added. Cells were placed in a humidified cell culture incubator (5% CO_2 and 37°C) for 1 hr, after which MeHg was removed and cell culture medium was replaced. The 1 hr MeHg-treatment time was selected because almost all Purkinje or granule cells exhibited an elevation of $[Ca^{2+}]_i$ at all the MeHg concentrations tested after 1 hr of MeHg exposure. Cell viability was assayed 24.5 hr later with the calcein-AM/ethidium homodimer method, using the protocol of Marty and Atchison (1998). Briefly, MeHg exposed cells were rinsed three times with warmed HBS, after which a solution containing calcein-AM (2 μM) and ethidium homodimer (4 μM) was applied for 0.5 hr. Cells were subsequently rinsed three times with warmed HBS and their viability assayed. Healthy cells incorporated calcein-AM and fluoresced green, whereas ethidium homodimer marked cell death by binding to exposed DNA within the nucleus and causing a red fluorescence. For Purkinje cells, three separate cell isolates were used in the viability assay, with each treatment group (HBS control, 3,5 and 7 μM MeHg) being present in each islolate. Based on the distinct adult Purkinje cell morphology, probable Purkinje cells were located on the cell culture dish and the dish bottom was then marked with a Nikon marking objective (2 mm in diameter). This was done so Purkinje cells could be located following immunostaining for CB, which as noted in Chapter One is a CaBP specific to Purkinje neurons within the cerebellum (Gruol and Crimi, 1988, Furuya *et al.*, 1998). Photomicrographs of Purkinje cells within marked areas were taken prior to MeHg exposure, during the viability assay and after

immunotstaining for CB. Probable Purkinje cells were determined to be non-viable by comparing the photomicrographs of the cells prior to and following MeHg exposure. Purkinje cell density varied from 5 to 25 per marked area (3.14 mm^2) on a dish. For granule cells, one isolate was used for all viability assays with four replicates of each treatment group. For granule cells, an arbitrary location on the cell culture dish was chosen and marked with the same Nikon marking objective as used in the Purkinje cell viability assay studies. Granule cell density was much higher as compared to Purkinje cells with approximately 50 cells per marked area (3.14 mm^2). Cell viability was determined manually using a Nikon Diaphot epifluorescence microscope (Nikon Instruments, Tokyo, Japan).

Immunocytochemistry. Other neuronal and non-neuronal cell types were present in the Purkinje cell cultures. To ensure that recordings were made from Purkinje cells, the area from which cells were recorded was located on the coverslip and marked with a Nikon marking objective after the Ca^{2+} imaging experiments. Coverslips were placed in 100% acetone at -20°C, for 10 min to permeabilize and fix the cells. They were next rinsed three times in Dulbecco's Buffered Phosphate Solution (DBPS) which contained: (mM) 140 NaCl, 8.1 NaH_2PO_4, 0.49 $MgCl_2$, 1.47 KH_2PO_4, 2.68 KCl and 0.9 $CaCl_2$ (pH 7.3). Mouse anti-CB antibody (Ab) (1:2000) was applied with 10% FBS as a blocking agent and the cells were incubated overnight. The next day cells were rinsed again with DBPS. Goat anti-mouse TRITC conjugated secondary Ab (1:100) in 3% (w/v) bovine serum albumin (fraction IV) was then applied and cells were incubated for 0.5 hr. After

secondary antibody incubation, cells were rinsed three times with DBPS. Cells located within the marked are of the coverslip were evaluated for CB antibody labeling and photomicrographs were taken of CB-positive cells.

Statistics. For data on the time-to-onset of $[Ca^{2+}]_i$ increases, one *n* value represents the average responses from 2 to 3 cells recorded simultaneously on a single coverslip. Data were analyzed using the GraphPad Instat statistical program (GraphPad Software Inc., San Diego, CA). Comparisons for cell viability for each exposure group were made using a one-way or two-way analysis of variance (ANOVA) and/or students t-test. Percent data were square root transformed prior to statistical analysis. When multiple cell type and MeHg concentration were compared, a two-way ANOVA was used; if a single cell type with multiple MeHg concentrations was compared, a one-way ANOVA was used. If significant differences between sample means were detected, a *post-hoc* Tukey-Kramer test was performed to ascertain which mean values were significantly different. Values of $p < 0.05$ were considered to be statistically significant.

RESULTS

Purkinje cells were grown in culture for 21-24 days *in vitro* (DIV). This extended time of growth was needed for the cells to express characteristics of adult Purkinje cells. I did not observe morphologically distinct Purkinje neurons with extensive dendritic arborization until 18 DIV (Fig. 2.1); this observation is in agreement with other reports of Purkinje cells grown in culture (Gruol, 1983; Furuya *et al.*, 1998). To ensure that the Purkinje cells grown in my cell culture system retained the physiological responses observed in Purkinje cells *in vivo* and had the ability to buffer elevated $[Ca^{2+}]_i$, glutamate agonists were applied and resulting increase in fura-2 fluorescence was measured from soma and dendrite regions of Purkinje cells. After glutamate agonist exposure, the area of the coverslip containing the cell that was recorded from was marked and stained for the presence of CB. Verification of the presence of CB was done to verify that I could identify adult Purkinje cells in a mixed cell culture system. Purkinje cells *in vitro* express AMPA/kainate and metabotrophic glutamate receptors, but do not express functional NMDA receptors (Perkel *et al.*, 1990). Accordingly, I found significant differences in the Purkinje cell response to AMPA,- quisqualate-, and NMDA-evoked elevations of $[Ca^{2+}]_i$. NMDA (Fig. 2.1) produced a significantly lower amplitude fura-2 fluorescence response as compared to kainate or quisqualate (two-way ANOVA, $P \leq 0.05$). No significant differences between soma or dendrite were detected (two-way ANOVA, $P > 0.05$) in any of the glutamate agonist-evoked fura-2 fluorescence responses. These results

Figure 2.1 Photomicrographs of cerebellar Purkinje neurons 23 DIV. Figure 1A is a bright-contrast image of two Purkinje cells. Figure 1B is an image of the same Purkinje cells stained for presence of CB. The unique pear-shaped soma and extensive dendritic arborization were used to identify probable Purkinje neurons before each experiment. Figure 1C is a histogram showing different glutamate agonists causing increases in fura-2 fluorescence, $F_{(340/380)}$, in Purkinje cells. Data are agonist-induced increase in amplitude of $F_{(340/380)}$ normalized to an initial 40 mM KCl-induced depolarization, and are expressed as mean ± SE, for every group (N = 4). Significant differences (two-way ANOVA, Tukey's test; $P \leq 0.05$), in both soma (dark) and dendritic (diagonal) regions, were detected in $F_{(340/380)}$ amplitude resulting from exposure to: NMDA (50 μM) + glycine (10 μM), kainate (50 μM) and quisqualate (10 μM). Single asterisk (*) indicates significant difference from NMDA treatment group and double asterisk (**) indicates significant difference from kainate (two-way ANOVA, Tukey's test; $P \leq 0.05$). No significant differences were detected in comparing soma or dendrite within any of the agonist treatment groups.

(Images in this dissertation are presented in color)

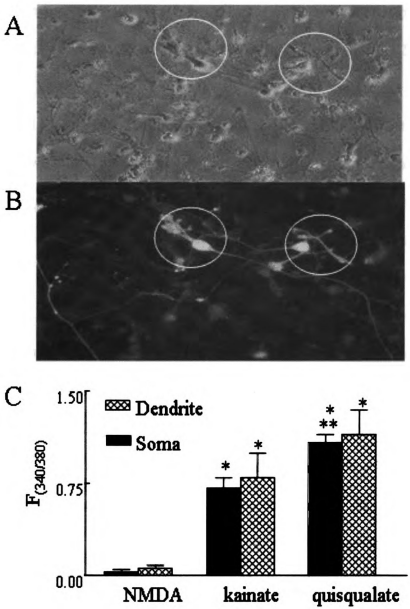
A
B
C
1.50
0.75
0.00
F(340/380)
Dendrite
Soma
*
*
*
**
*
NMDA
kainate
quisqualate

FIGURE 2.1

are in agreement with previous Ca^{2+} imaging and electrophysiology studies of glutamate agonists exposure to Purkinje cells in culture (Yool *et al.*, 1992; Gruol *et al.*, 1996).

In all experiments, Purkinje or granule cells were initially perifused with 40 mM K^+ HBS for two min. This was done to ensure that the cell was viable and maintained the ability to buffer elevations of $[Ca^{2+}]_i$. All Purkinje and granule cells responded to 40 mM K^+ with an elevation of fura-2 fluorescence followed by a return of fura-2 fluorescence to baseline when the 40 mM K^+ perifusion solution was replaced with normal (5.4 mM) K^+ HBS. Cells were exposed to MeHg 6 min after the 40 mM K^+ was withdrawn and the cell had been perifused with normal HBS. All concentrations of MeHg tested (0.5-5 μM) caused a similar biphasic increase in fura-2 fluorescence in Purkinje cells and granule cells (Fig. 2.2) grown in culture. When MeHg was applied in a Ca^{2+}-free HBS solution, there was an absence of any second phase increase in $[Ca^{2+}]$ in both cell types. Therefore, the first phase increase in fura-2 fluorescence was due primarily to release of divalent cations (Ca^{2+} and other non-Ca^{2+}) from intracellular sources, whereas the second phase increase was due primarily to entry of Ca^{2+}_e. While MeHg also caused a biphasic elevation of fura-2 fluorescence in cerebellar granule cells, these elevations occurred on a significantly shorter time scale. Figure 2.3 shows the direct comparison of time-to-onset of first-phase increases of fura-2 fluorescence in Purkinje soma and granule neurons. Qualitatively, both cell types had similar rates of elevation of fura-2 fluorescence. However, Purkinje cells had a significantly delayed time-to-onset at the 0.5 and 1 μM MeHg treatment groups as compared to granule cells (two-way ANOVA, $P > 0.05$).

Figure 2.2 Representative tracings showing changes in fura-2 fluorescence, $F_{(340/380)}$, in a cerebellar granule (A) and a Purkinje (B) neuron grown in culture and exposed to 0.5 μM MeHg. In every experiment, a biphasic increase in $F_{(340/380)}$ was observed in both cell types during continuous perifusion of MeHg. Tracing (A) of the granule cell is representative of 9 cells exposed to 0.5 μM MeHg, and tracing (B) of the Purkinje cell is representative of four cells exposed to 0.5 μM MeHg.

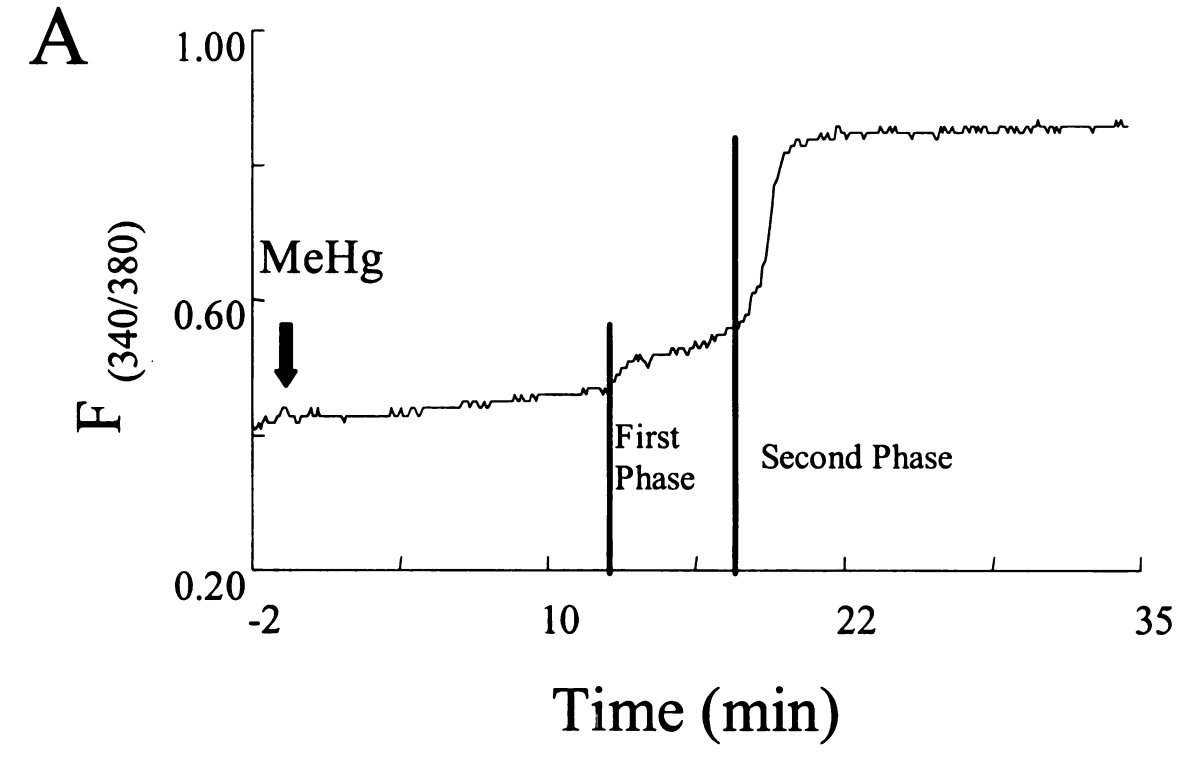
A
1.00
0.60
0.20
F (340/380)
MeHg
First
Phase
Second Phase
-2
10
22
35
Time (min)

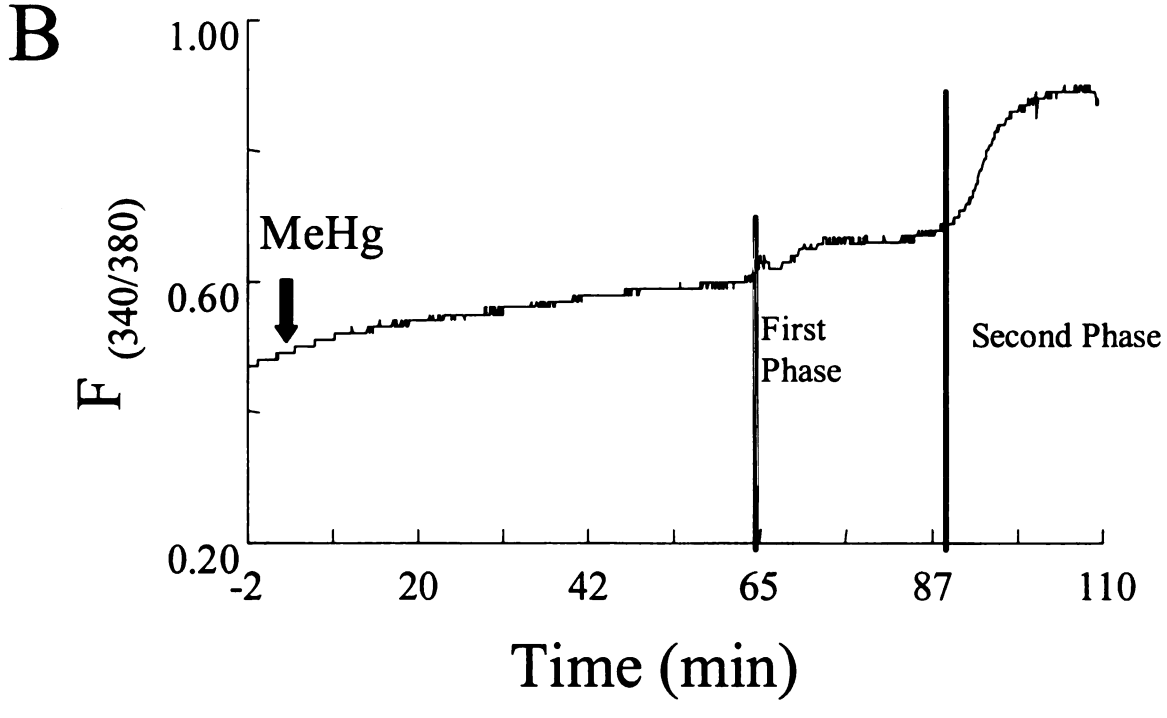
B
1.00
0.60
0.20
F (340/380)
MeHg
First
Phase
Second Phase
-2
20
42
65
87
110
Time (min)

FIGURE 2.2

Figure 2.3 Time-to-onset of first phase increase of fura-2 fluorescence from Purkinje and granule neurons after application of MeHg. Asterisks indicate significant differences in the mean time-to-onset of fura-2 fluorescence changes between Purkinje and granule cells at 0.5 and 1 μM MeHg (two-way ANOVA, Tukey's test; $P < 0.05$). Granule and Purkinje cells exposed to HBS alone maintained stable basal fura-2 fluorescence for > 60 min. Data are represented as mean ± SE, N = 4 for all groups.

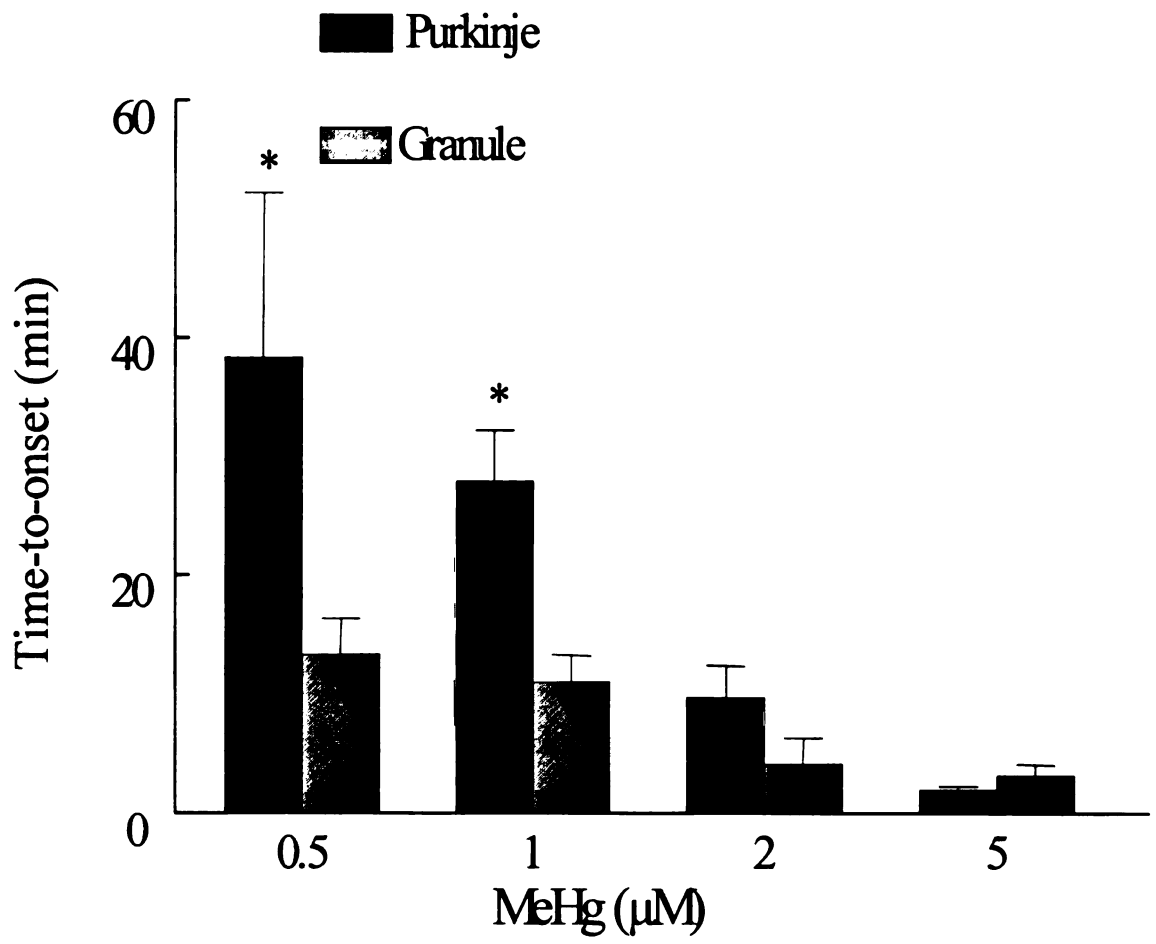

FIGURE 2.3

Figure 2.4 shows the comparative time-to-onset of second phase increases in fura-2 fluorescence induced by MeHg in Purkinje and granule cells. In both cell types, no second phase increase of fura-2 fluorescence was detected unless Ca^{2+} was present in the perifusion buffer. The rate of increase of fura-2 fluorescence and amplitude of fura-2 fluorescence relative to an initial K^+ depolarization were qualitatively similar in both cell types. Purkinje cells had a significantly delayed time-to-onset of second phase fura-2 fluorescence increases at the 0.5, 1 and 2 μM MeHg treatment groups as compared to granule cells (two-way ANOVA $P > 0.05$) (Fig. 2.4). At high concentrations of MeHg, there was no difference between cell types. Experiments using Purkinje cells were conducted to quantify the amplitude of the first phase of fura-2 fluorescence relative to that caused by an initial depolarization resulting from perifusion of 40 mM K^+, data not shown. Amplitude of first phase increase of fura-2 fluorescence was not significantly different at 0.5, 1, 2 or 5 μM MeHg in Purkinje cells (Fig. 2.5, one-way ANOVA $P > 0.05$).

As mentioned previously, a different cell isolation protocol was used for Purkinje cell viability assay experiments (Gruol, 1983) than the protocol used for Ca^{2+} imaging studies (Furuya *et al.*, 1998). Both *in vitro* and *in vivo* studies have shown that selenium can have cytoprotective effects when co-administered with MeHg (Watanabe, 2002). However I found no significant difference between first or second phase time-to-onset of elevations of fura-2 fluorescence when granule cells were exposed to 0.5 μM MeHg in the presence or absence of 30 nM selenium (ANOVA, $P > 0.05$) (Fig. 2.6).

Figure 2.4 Second phase time-to-onset of increases of fura-2 fluorescence from Purkinje and granule neurons after application of MeHg. Asterisks indicate significant differences in the mean time-to-onset of fura-2 fluorescence changes between Purkinje and granule cells at 0.5, 1 and 2 μM MeHg (two-way ANOVA, Tukey's test; $P < 0.05$). Untreated control cells maintained stable basal Ca^{2+} levels for > 60 min. Data are represented as mean ± SE, $n \geq 4$ for all groups.

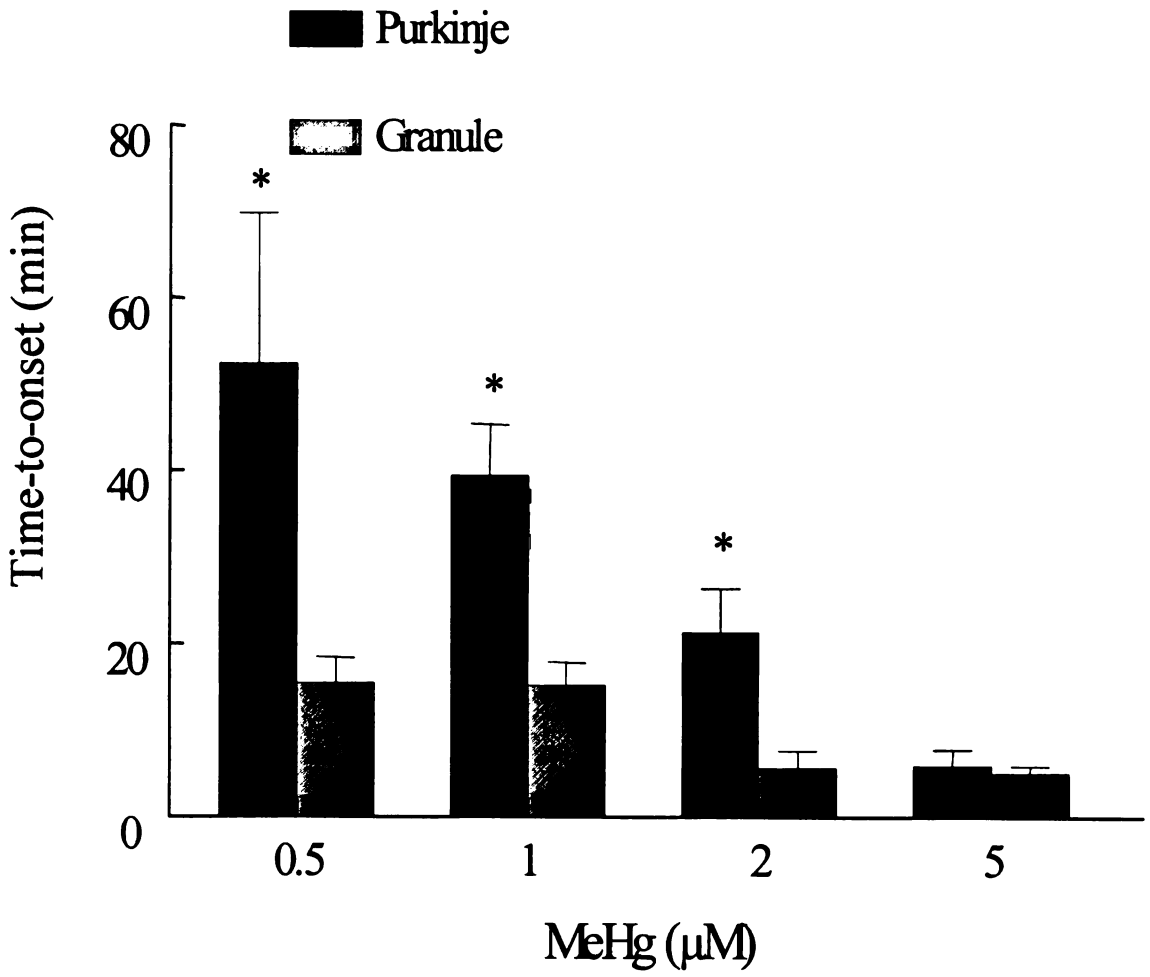

FIGURE 2.4

Figure 2.5 The amplitude of first phase increase of fura-2 fluorescence was not significantly different at 0.5, 1, 2 or 5 μM MeHg in Purkinje cells (Fig. 2.5, one-way ANOVA, $P > 0.05$). Following a 40 mM K^+-induced depolarization, Purkinje cells were perifused in MeHg-containing Ca^{2+}-free (20 μM EGTA) HBS and amplitude of fura-2 fluorescence recorded after MeHg had caused a sustained elevation in fluorescence. N = 2 for the dendrite 2 μM MeHg treatment group.

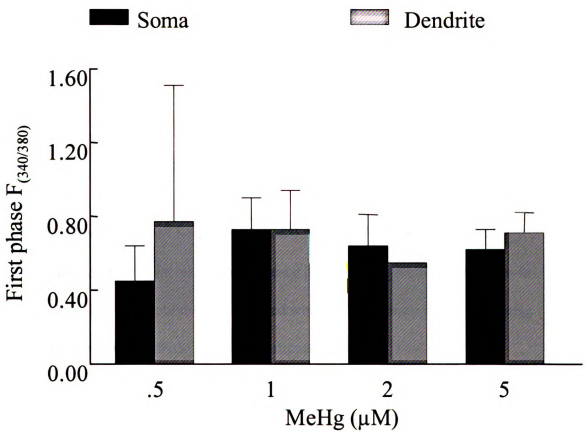
Soma
Dendrite
1.60
1.20
0.80
0.40
0.00
First phase F(340/380)
.5
1
2
5
MeHg (μM)

FIGURE 2.5

Figure 2.6 The effects of 30 nM Selenium (Se) on 0.5 μM MeHg-induced first and second phase time-to-onset of increased fluorescence in cerebellar granule cells grown in culture. Granule cells were continuously perifused with HBS solutions containing MeHg in the presence or absence of 30 nM Se. No significant differences were detected between first or second phase time-to-onset when Se was either present or absent (t-test, $P > 0.05$). Data are represented as mean ± SE; n = 3 for non-Se, MeHg-only, control and n = 4 for Se with MeHg treatment groups.

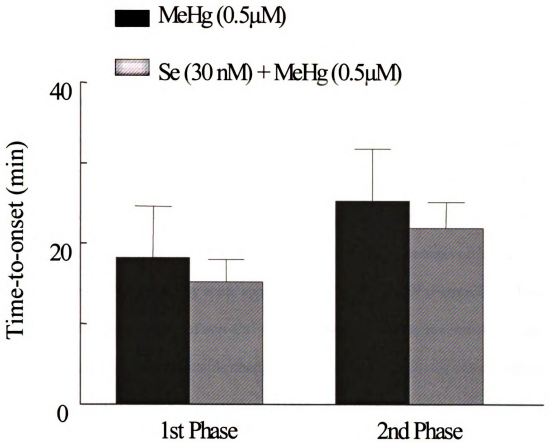
MeHg (0.5μM)
Se (30 nM) + MeHg (0.5μM)
40
20
0
Time-to-onset (min)
1st Phase
2nd Phase

FIGURE 2.6

Fura-2 binds other divalent cations other than Ca^{2+} with high affinity (Grynkiewicz *et al.*, 1985). Non-Ca^{2+} divalent cations are released from intracellular sources when rat cortical synaptosomes or NG108-15 cells are exposed to MeHg (Hare *et al.*, 1993; Denny and Atchison, 1994). Consequently, the heavy-metal, divalent cation chelator, TPEN, was applied during MeHg exposure to unmask any possible contribution of non-Ca^{2+} divalent cations to fura-2 fluorescence in Purkinje cells. TPEN binds with relatively high affinity to Zn^{2+}, Fe^{2+}, and Mn^{2+} (Arslan *et al.*, 1985). TPEN does not bind to any significant extent to Ca^{2+}, MeHg, or fura-2 (Arslan *et al.*, 1985; Komulainen and Bondy, 1987; Hare *et al.*, 1993). The amplitude of the MeHg-induced first phase increase of fura-2 fluorescence was decreased by acute application of 20 μM TPEN (Figure 2.7). Thus there is a substantial release of non-Ca^{2+} divalent cation(s) during the initial increase in fura-2 fluorescence. No detectable change in fura-2 fluorescence was detected when TPEN was applied in the absence of MeHg (Fig. 2.8). The first phase amplitude decrease produced by 20 μM TPEN in the presence of various concentrations of MeHg is illustrated in Figure 2.9. Experiments using TPEN were done on Purkinje cells in the presence of normal (1.8 mM) extracellular calcium (Ca^{2+}_e). Chelation of non-Ca^{2+} divalent cations by TPEN did not alter the time-to-onset of first or second phase increase of fura-2 fluorescence resulting from exposure to 2 μM MeHg in Ca^{2+} (1.8 mM) containing HBS in Purkinje neurons (one-way ANOVA, $P > 0.05$), Figure 2.10.

Using the Purkinje cell isolation protocol of Gruol (1983) allowed us to test the effect of MeHg on viability of adult Purkinje neurons without the presence of selenium in the

Figure 2.7 A representative tracing showing the acute effects of the heavy-metal chelator TPEN (20 μM) on the MeHg-induced (2 μM) first phase increase of fura-2 fluorescence from a cerebellar Purkinje neuron. When TPEN was applied in Ca^{2+} free HBS, there was a resulting rapid drop in fura-2 fluorescence, indicating that non-Ca^{2+} cation(s) contributes to the first phase increase in fura-2 fluorescence. After TPEN addition, the remaining fura-2 fluorescence represents Ca^{2+} increases during the first phase.

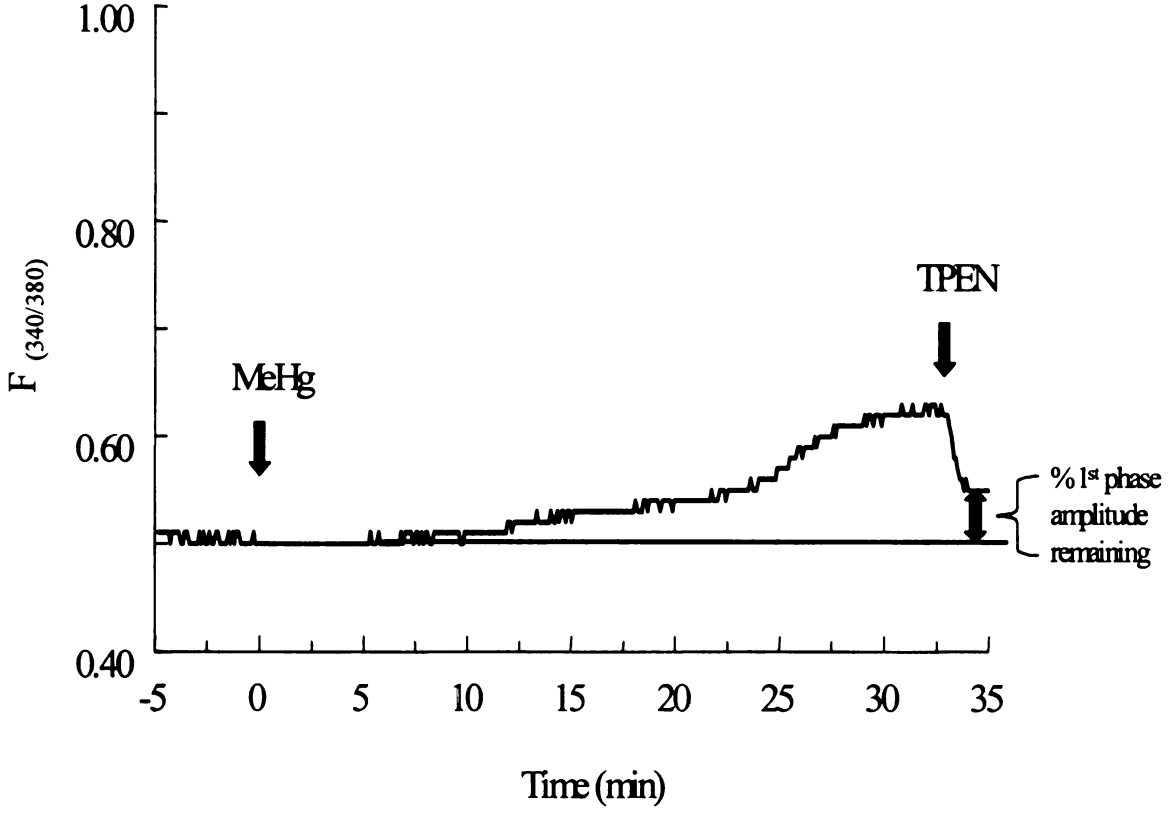
1.00
0.80
0.60
0.40
F (340/380)
MeHg
TPEN
% 1st phase
amplitude
remaining
-5
0
5
10
15
20
25
30
35
Time (min)

FIGURE 2.7

Figure 2.8 Representative tracing showing negligible changes in fura-2 fluorescence (340/380) during acute (2 min) application of the heavy metal chelator, TPEN (20 μM) in the absence of MeHg. The Purkinje cell was exposed to depolarizing 40 mM KCl solutions to ensure cell viability the entire length of the recording.

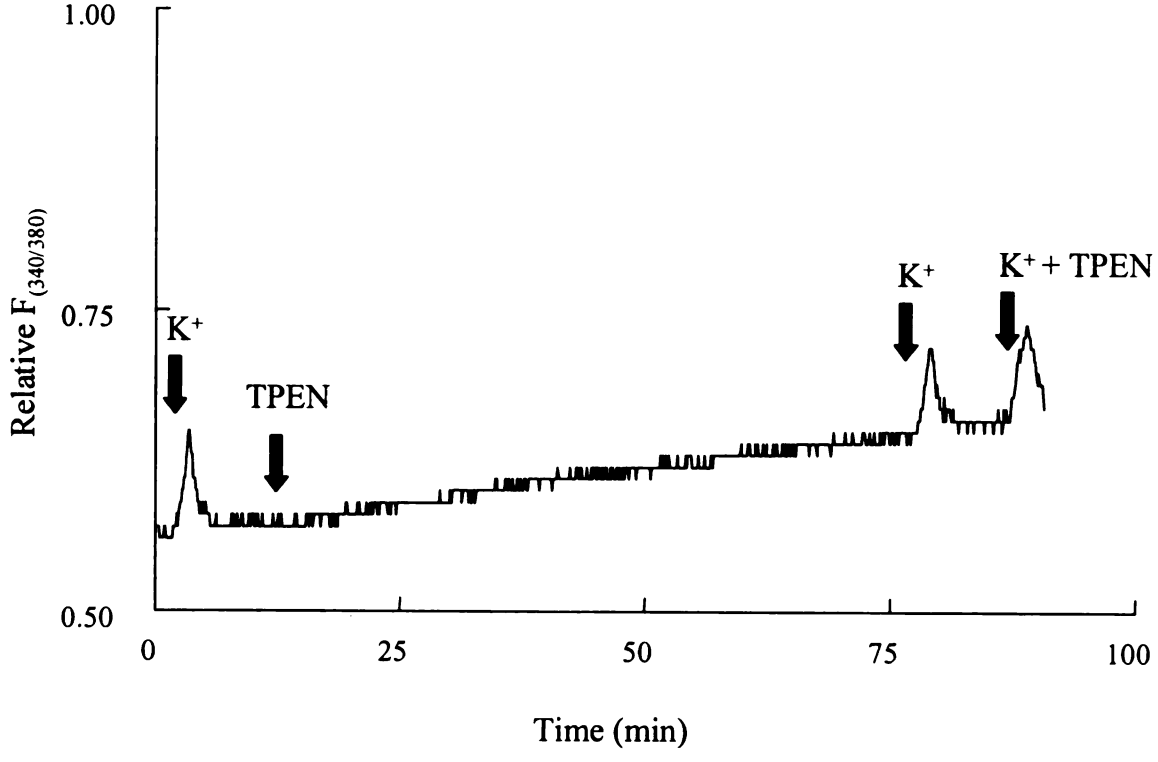
1.00
0.75
0.50
Relative $F_{(340/380)}$
K^+
TPEN
K^+
K^+ + TPEN
0
25
50
75
100
Time (min)

FIGUR E 2.8

Figure 2.9 The cell permeable, heavy-metal chelator, TPEN caused a decrease in MeHg-induced first phase increase in $F_{(340/380)}$ when MeHg was perifused in Ca^{2+}-free, EGTA buffer. Solid and hatched bars represent soma and dendrite, respectively. TPEN caused a significant reduction from soma of 2 μM MeHg-induced elevation of fura-2 fluorescence compared to the 5 μM MeHg treatment group, as indicated by the (*) (two-way ANOVA $P = 0.015$). No significant difference was detected within the dendrites. The first phase amplitude, prior to TPEN addition, was set at 100%. Bars indicate the proportion of this fura-2 fluorescence signal remaining after chelation of non-Ca^{2+} cations with TPEN.

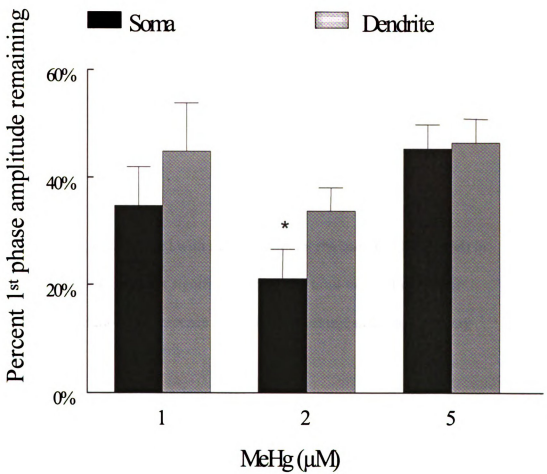
Soma
Dendrite
Percent 1st phase amplitude remaining
60%
40%
20%
0%
*
1
2
5
MeHg (μM)

FIGURE 2.9

Figure 2.10 MeHg (2 μM) co-perifused with the heavy-metal chelator TPEN (20 μM) in Ca^{2+}-containing (1.8 mM) HBS did not significantly alter the time-to-onset of first or second phase increases of fura-2 fluorescence in cerebellar Purkinje neurons (two-way ANOVA, $P > 0.05$).

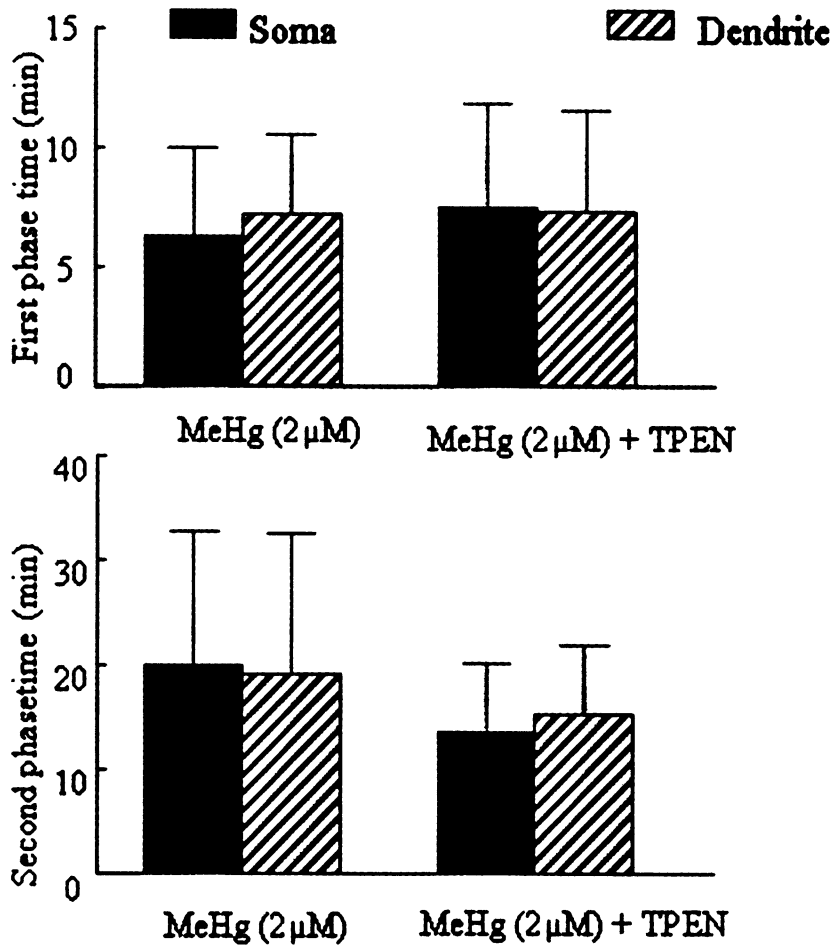
Soma
Dendrite
First phase time (min)
15
10
5
0
MeHg (2μM)
MeHg (2μM) + TPEN
Second phasetime (min)
40
30
20
10
0
MeHg (2μM)
MeHg (2μM) + TPEN

FIGURE 2.10

growth medium as a complicating factor. The medium used for these studies contained only trace amounts of selenium normally found within the horse serum and FBS. Purkinje cells (DIV 21-24) were more resistant to the cytotoxic effects of MeHg than were cerebellar granule neurons (DIV 6-8), as measured by the calcein-AM/ethidium homodimer viability assay method. On average, each tissue culture dish contained between 5-25 Purkinje neurons within the area delineated by the Nikon marking objective (surface area = 3.14 mm^2). Due to the sparse numbers of Purkinje cells present, viability data are presented on a per cell basis (Fig. 2.11). At 7 μM MeHg, Purkinje cell adhesion was affected as Purkinje cells began to lift off the substrate. Minimal effects on Purkinje cell viability were seen at 5 μM MeHg. With granule cells, data were expressed as the percentage of live cells with a minimum of 50 cells examined in each treatment group. In contrast to Purkinje cells, viability of cerebellar granule neurons was significantly decreased in the 5 μM MeHg treatment group as compared to HBS-alone control (Fig. 2.12). Granule cells also lifted off the culture dishes at 5 and 7 μM MeHg treatment groups. Only cells that remained adherent to the cell dish substrate were considered for the viability assay.

Because Purkinje cells grown in long-term cell culture conditions may not be the best representation of Purkinje cell biology *in vivo*, I performed experiments on Purkinje cells using a different type of isolation procedure. Acutely dissociated Purkinje cells taken from rat pups between postnatal days 10 and 14 had a similar fura-2 responses to NMDA, AMPA/kainate and metabotrophic glutamate receptor agonists (Fig. 2.13) as did Purkinje

Figure 2.11 Viability assay of Purkinje neurons (22 DIV) in mixed culture after exposure to 5 μM MeHg for 1 hr; viability was assessed 24 hr after cessation of MeHg exposure. A) Photomicrograph of cells with distinct Purkinje cell morphology before MeHg exposure. B) 24 hr after MeHg exposure, green cells are viable whereas red cells are dead. C) Photomicrograph of the same two Purkinje cells stained for the presence of calbindin-D_{28k}. In panels B and C two surviving Purkinje cells are circled in white. Below, the table shows numbers of viable Purkinje neurons after exposure to 0, 3, 5 and 7 μM MeHg.

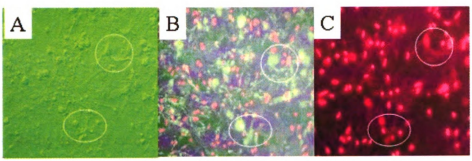

MeHg (μM)	No. of Live PurkinjeCells	Dead	% Live
0	30	0	100
3	17	0	100
5	79	2	97.5
7	3	1	75

FIGURE 2.11

Figure 2.12 Viability assay of cerebellar granule neurons (6-8 DIV) after exposure to 3, 5 or 7 μM MeHg for 1 hr; viability was assessed 24.5 hr after cessation of MeHg exposure. Granule cells underwent a concentration-dependent decrease in cell viability as indicated by ethidium homodimer and calcein-AM viability assay. All data were square root transformed prior to statistical analysis. Significant differences in viability were detected at 5 and 7 μM MeHg treatment groups compared to control values (*) as indicated by one-way ANOVA, (Tukey's test $P < 0.05$). Data are represented as mean ± SE, in each group; N = 4 culture dishes with approximately 50 cells scored for viability on each dish.

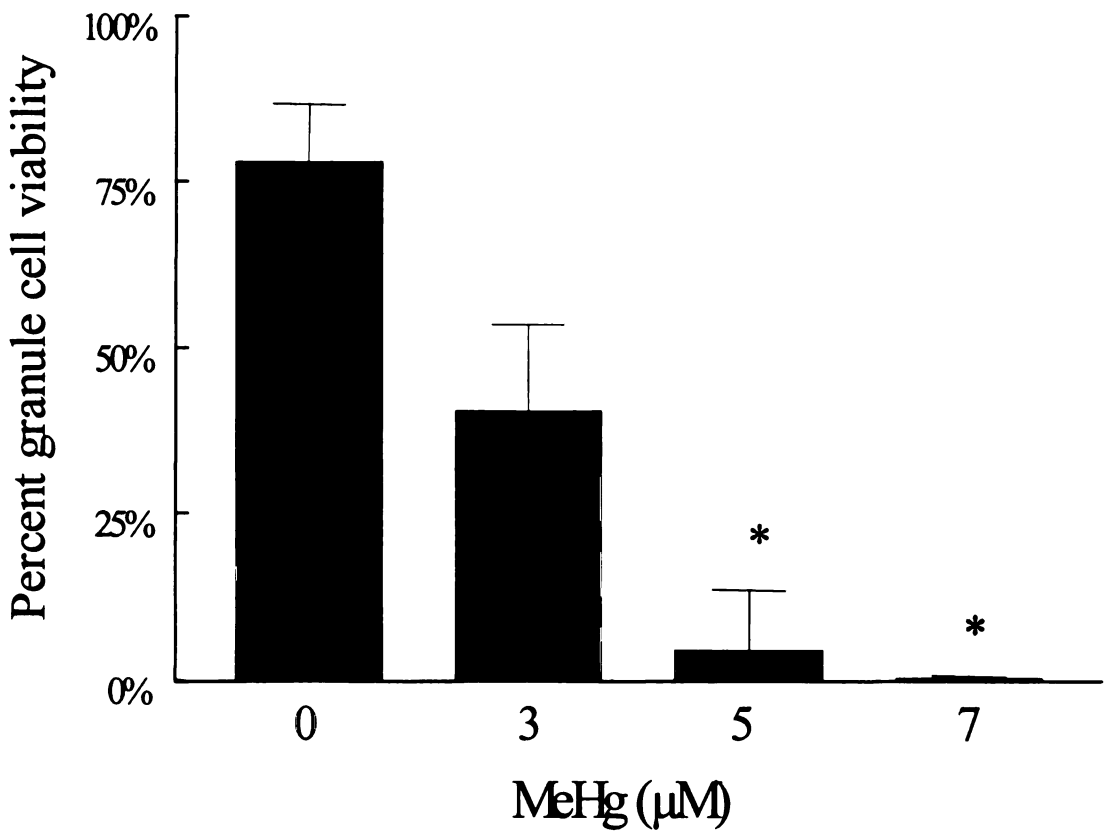

FIGURE 2.12

cells grown in long-term cell culture conditions (Fig. 2.1). Figure 2.14 shows a representative example of the fura-2 fluorescence response of an acutely dissociated Purkinje cell during acute application of 5 μM MeHg in Ca^{2+}-containing HBS. The fura-2 fluorescence response resulting from MeHg exposure from acutely dissociated Purkinje cells appeared somewhat different from that seen in Purkinje cells taken from fetal rats and grown in culture for 21-24 days. In many acutely dissociated Purkinje cells, there was an abrupt, single increase in fura-2 fluorescence with no discernable first phase. This was in contrast to the biphasic increase in fura-2 fluorescence observed in the Purkinje cells grown in long-term culture conditions. Acutely dissociated Purkinje cells responded to MeHg in the same concentration- and time-dependent manner as did Purkinje cells grown in culture (Figure 2.15 compared with Figure 2.3) and both isolates of Purkinje cells were less responsive to MeHg-induced elevations of $[Ca^{2+}]_i$ than were cerebellar granule cells grown in culture. There was little or no increase in fura-2 fluorescence from acutely dissociated Purkinje cells during exposure to a Ca^{2+}-free HBS solution containing 5 μM MeHg (Fig. 2.16). The tracing showing changes in fura-2 fluorescence from acutely dissociated Purkinje cells present in Figure 2.16 shows a second 40 mM KCl-induced depolarization after MeHg exposure. The second depolarization was performed to ensure that the cell remained viable thoughout the entire recording. Consistent with the experiments characterizing the MeHg response in acutely dissociated cells, these data suggest only a small contribution of intracellular stores to first phase fura-2 fluorescence increases. To test for the presence of releasable intracellular Ca^{2+} stores, the inhibitor of SER Ca^{2+} ATPase, cyclopiazonic acid (CPA,

2μM), was applied in a Ca^{2+}-free HBS buffer. A resulting increase in fura-2 fluorescence was recorded after application of CPA in acutely dissociated Purkinje cells (Fig. 2.17). Therefore, a releasable source of Ca^{2+} existed in the acutely dissociated Purkinje cells; however, within the time frame of the experiment, MeHg did not cause release of Ca^{2+} from intracellular Ca^{2+} stores in these cells.

Figure 2.13 Acutely dissociated Purkinje cells responded to the glutamate receptor agonists, NMDA (50 μM) + glycine (10 μM), kainate (50 μM) and quisqualate (10 μM) with increases in fura-2 fluorescence in a manner similar to cerebellar Purkinje cells maintained in long-term culture conditions. Significant differences were detected between treatment groups (one-way ANOVA, $P \leq 0.05$). The(*) indicates significant difference from the NMDA treatment group.

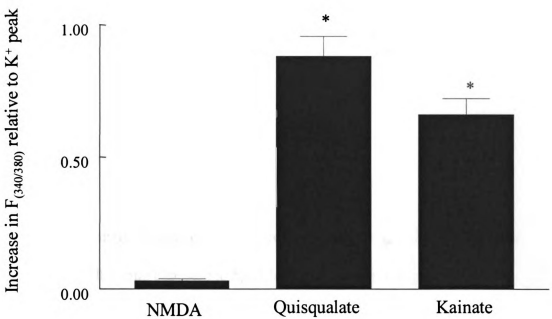
Increase in $F_{(340/380)}$ relative to K^+ peak
1.00
0.50
0.00
*
*
NMDA
Quisqualate
Kainate

FIGURE 2.13

Figure 2.14 A representative tracing of fura-2 fluorescence ratio $F_{(340/380)}$ from an acutely dissociated Purkinje cell during exposure to 5μM MeHg. Purkinje cells were acutely dissociated from 10-14 day old rat pups.

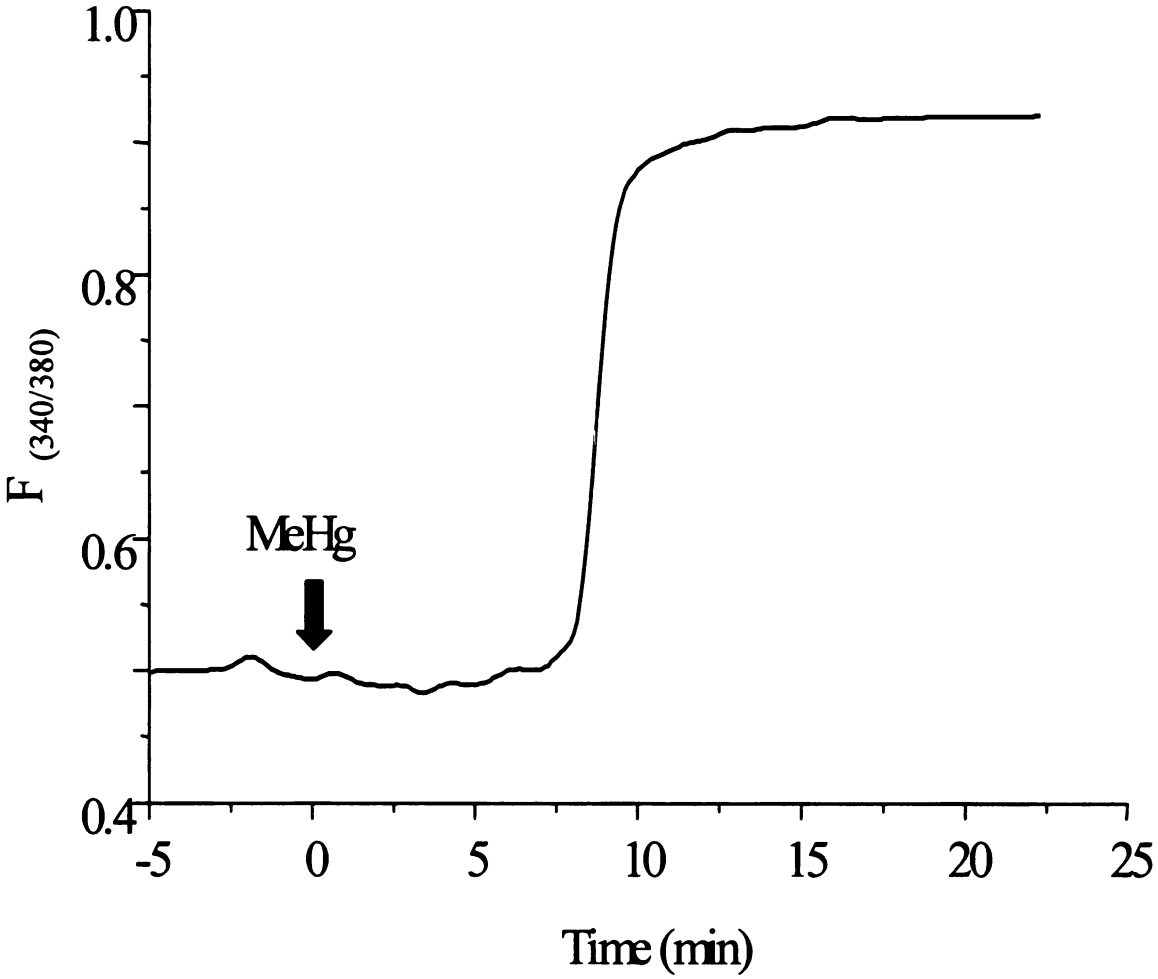

FIGURE 2.14

Figure 2.15 Time-to-onset of elevations of fura-2 fluorescence during perifusion of acutely dissociated Purkinje cells with MeHg (0.5-5 μM) in Ca^{2+}-containing HBS. Untreated control cells maintained stable basal fura-2 fluorescence for > 60 min. The (*) indicates significant differences between the 0.5 and 5 μM MeHg treatment groups. Data are represented as mean ± SE, in each group,N = 3. For each n, value fura-2 fluorescence was recorded from the soma of 1-2 acutely dissociated Purkinje cells per cell culture dish.

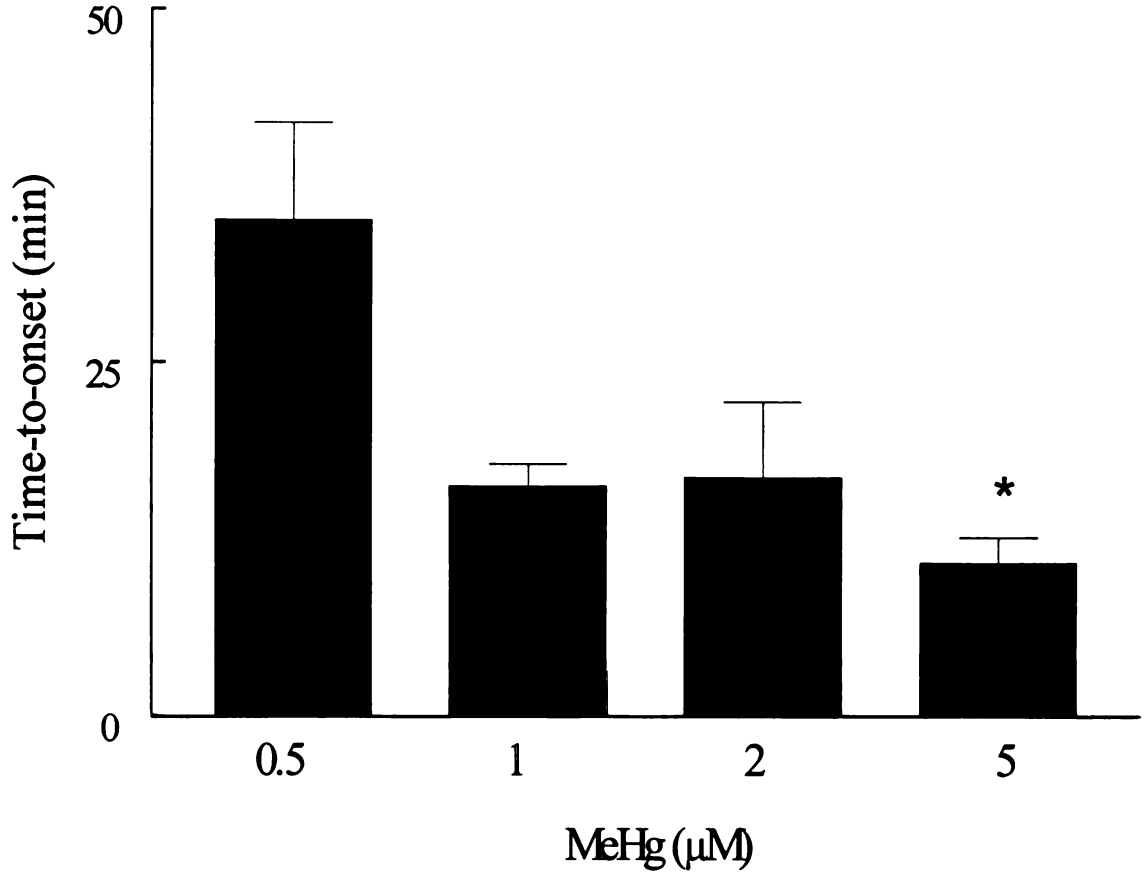

FIGURE 2.15

Figure 2.16 Fura-2 tracing from an acutely dissociated Purkinje neuron showing little or negligible elevation of fura-2 fluorescence during perifusion with 5 μM MeHg in Ca^{2+}-free HBS. A second 40 mM KCl-induced depolarization was performed at the end of the experiment to ensure that the Purkinje cell remained viable during the entire length of the recording. Panels A, B and C shows fura-2 fluorescence emission resulting from the excitation wavelengths of 340 nm, 380 nm and 340/380nm, respectively.

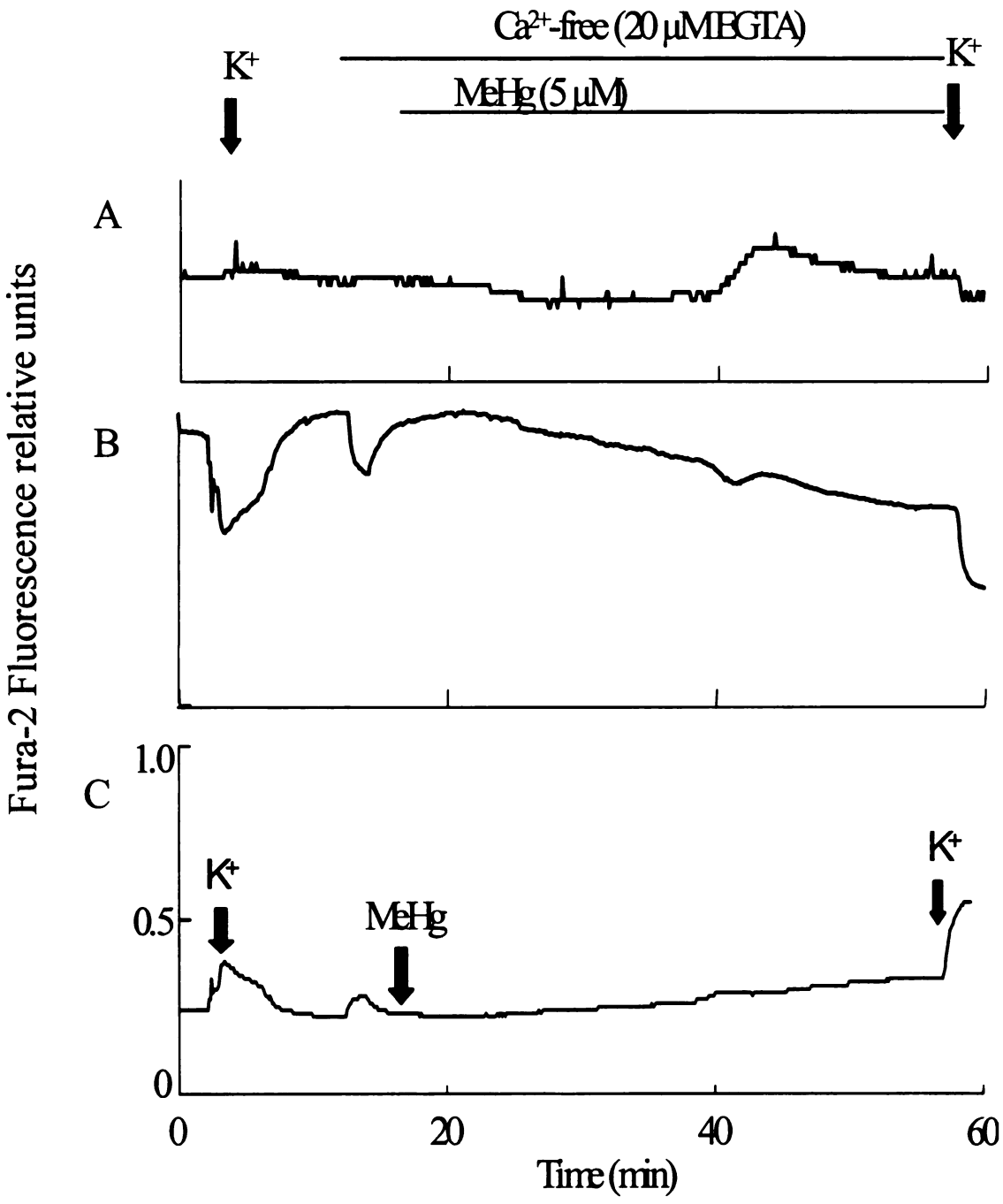
Ca2+-free (20 µM EGTA)
K+
K+
MeHg (5 µM)
A
B
C
Fura-2 Fluorescence relative units
1.0
0.5
0
K+
MeHg
K+
0
20
40
60
Time (min)

FIGURE 2.16

Figure 2.17 The effects of the smooth endoplasmic reticulum Ca^{2+}-ATPase inhibitor, cyclopiazonic acid (CPA), on an acutely dissociated Purkinje neuron. CPA (5 μM) was perifused onto an acutely dissociated Purkinje neuron in Ca^{2+}-free HBS while changes in fura-2 fluorescence were recorded.

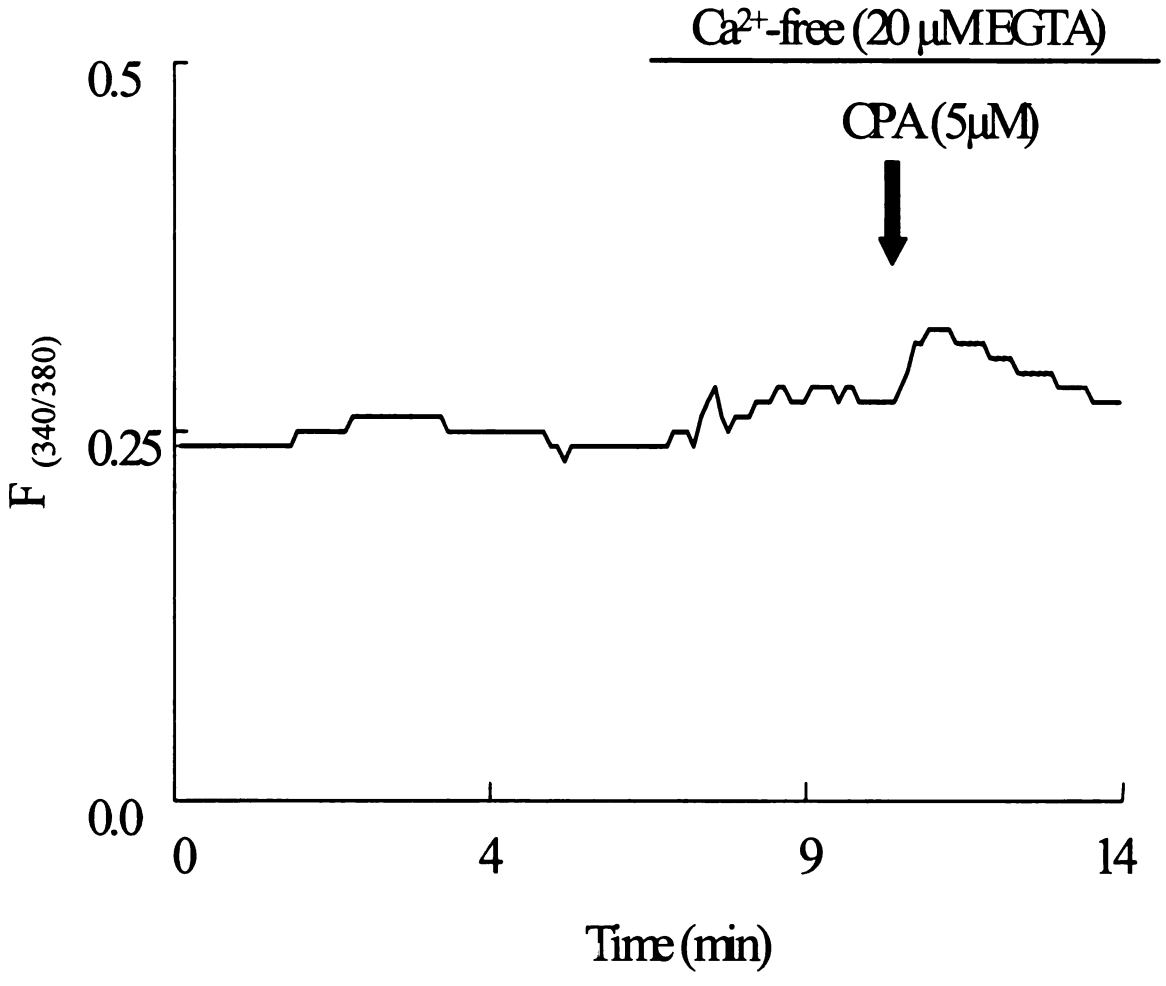

FIGURE 2.17

DISCUSSION

The main goal of this study was to compare the relative effectiveness of MeHg to alter $[Ca^{2+}]_i$ and induce subsequent cytotoxicity in cerebellar granule neurons and Purkinje neurons. The principal findings of this study indicate that both acutely dissociated Purkinje neurons and Purkinje neurons grown in long-term cell culture conditions were more resistant to MeHg-induced dysregulation of Ca^{2+} homeostasis than were cerebellar granule cells grown in culture. Furthermore, when both Purkinje and granule cells were grown in culture and exposed to MeHg, there was a biphasic increase in fura-2 fluorescence which was the result of Ca^{2+} release from intracellular sources followed by entry of Ca^{2+}_e. However, MeHg had a different effect in altering $[Ca^{2+}]_i$ in acutely dissociated Purkinje cells. Acutely dissociated cells had what appeared to be a single phase increase in Ca^{2+}_i due to entry of Ca^{2+}_e as a result of exposure to MeHg. Finally, Purkinje cells grown in culture were more resistant to the cytotoxic effects of MeHg as compared to granule cells. This is in agreement with previous *in vivo* studies concerning the relatively preferential neurotoxic effects of MeHg on cerebellar granule cells as compared with Purkinje neurons (Leyshon-Sorland *et al.*, 1994; Mori *et al.*, 2000).

In this study, I show a correlation between the latency period for alterations in fura-2 fluorescence and the degree of resistance to the neurotoxic effects of MeHg in cerebellar Purkinje and granule neurons. The decreased ability to maintain Ca^{2+} homeostasis may itself be responsible for MeHg-induced cell death. Prolonged elevations of Ca^{2+}_i have well established consequences leading to cell death (Dubinsky, 1993). Several cell types

or preparations have elevated $[Ca^{2+}]_i$ as a result of MeHg exposure. Rat brain synaptosomes (Komulainen and Bondy, 1987; Denny *et al.*, 1993), NG108-15 (Hare *et al.*, 1993; Hare and Atchison, 1995a,b), PC12 cells (Edwards *et al.*, 2002) and cells in primary cultures such as cerebellar granule (Marty and Atchison, 1997, Limke and Atchison, 2002) and myenteric plexus neurons (Edwards and Atchison, 2003) have elevated $[Ca^{2+}]_i$ as a result of MeHg exposure. In each of the above mentioned cell types or preparations, an initial increase in fura-2 fluorescence occurred as a result of release of Ca^{2+} from intracellular sources followed by a second increase due to entry of Ca^{2+}_e through an, as yet, unidentified pathway. One possible determinant for the observed delay in time-to-onset of increases of fura-2 fluorescence is the expression of various sub-types of VGCCs. Purkinje neurons express P-, N - and L-type VGCCs with the P-type having the most Ca^{2+} current during depolarization (Mintz *et al.*, 1992). Approximately 90% of Ca^{2+} current in Purkinje cells occurs through the P - type VGCCs. In contrast, granule cells express five different Ca^{2+} channel types (L-, N-, P-, Q-, and R-), with each sub-type contributing 11-35% as charge carriers (Randall and Tsien 1995). Both the L-type VGCC antagonist, nifedipine, and the N - and Q - type VGCC antagonist ω-CTx - MVIIC significantly delayed the onset of both the first and second phase elevations of fura-2 fluorescence induced by MeHg in cerebellar granule cells (Marty and Atchison, 1997). There was a resulting increase in cerebellar granule cell viability when they were exposed to 0.5 and 1 μM MeHg in the presence of nifedipine and ω-CTx -MVIIC (Marty and Atchison, 1998). Similarly, nifedipine delayed MeHg-induced elevations of $[Ca^{2+}]_i$ in NG-108 cells (Hare and Atchison, 1995a). Although VGCCs play a role in MeHg-

induced alterations in Ca^{2+} homeostasis and neurotoxicity, it is unclear if the sub-type of VGCC is a determining factor. Sirois and Atchison (2000) did not find significant differences in the concentration of MeHg, that blocked current carried through L-, N- and P-/Q- type Ca^{2+} channels in cerebellar granule cells. Hajela *et al.* (2003) reported that recombinant N- and R- type Ca^{2+} channels expressed heterologously in human embryonic kidney (HEK 293) cells were equally sensitive to block by MeHg. However, recombinant L-type Ca^{2+} channels containing the α_{1C} type subunit were incompletely blocked by MeHg (Peng *et al.*, 2002). Complete block of function required the use of the dihydropyridine, L-type VGCC antagonist, nifedipine.

In addition to Ca^{2+} channels, there are other inherent differences between Purkinje and granule cells that may contribute to the selective vulnerability to MeHg neurotoxicity and alterations in $[Ca^{2+}]_i$. Each Purkinje cell receives an estimated one million excitatory glutamatergic synaptic inputs from parallel fibers (granule cell axons) as well as excitatory input from climbing fibers originating from the inferior olive (Ito, 1984). Consequently, Purkinje cells are able to deal adroitly with the excessive and extended elevations of Ca^{2+} due to the activation of AMPA/kainate and metabotrophic glutamate receptors at climbing fiber and parallel fiber synapses. In contrast, each granule cell only receives excitatory input from one mossy fiber (Kendal *et al.*, 2000). Given this, the Purkinje cell may be inherently better at handling extended elevations of $[Ca^{2+}]_i$ as compared to cerebellar granule cells.

Other specific differences between the two cell types include: the expression of type I 1,4,5-inositol triphosphate (IP_3) receptors, N-methyl-D-aspartate (NMDA) receptors, Ca^{2+} binding proteins, and differences in cell soma size. Purkinje cells have the highest density of IP_3 receptors found within the central nervous system (Worley *et al.*, 1989). Activation of IP_3 receptors in Purkinje cells occurs primarily through metabotrophic glutamate receptor activity. MeHg has been shown to cause elevations of IP_3 within cerebellar granule cells (Sarafian 1993). Mundy *et al.* (2000) found that acute application of 10 μM MeHg to rat brain cortical slices caused increased hydrolysis of phosphatidylinositides (PI) to inositol phosphates and diacylglycerol, and also increased PI hydrolysis in cerebellar slices. In addition, MeHg interacts with muscarinic acetylcholine receptors to cause elevation of $[Ca^{2+}]_i$ originating from intracellular sources within cerebellar granule cells (Limke *et al.* 2004). Furthermore, when the muscarinic receptor in cerebellar granule cells was desensitized or inhibited there was a delay in the time-to-onset of alterations of fura-2 fluorescence as well as enhanced cell viability after MeHg exposure (Limke *et al.* 2004). Purkinje cells also express ryanodine receptors, with IP_3 receptors localized primarily in the dendrites and ryanodine receptors within the soma (Khodakhah and Armstrong, 1997). During recordings of fura-2 fluorescence, I detected no difference in the MeHg-induced release of Ca^{2+} from the IP_3 receptor rich dendrites as compared to the ryanodine receptor rich soma. This may be explained by the observation that in Purkinje cells, both receptor types overlap in location and they share a common functional Ca^{2+} pool (Khodakhah and Armstrong, 1997).

Purkinje cells do not express functional NMDA receptors (Gruol, 1983) while granule cells do. Other studies have shown a role for NMDA receptors in MeHg-mediated neurotoxicity in granule cells (Park *et al.*, 1996), however the addition of the NMDA receptor antagonists MK-801 and AP-5, did not significantly delay MeHg-induced time-to-onset of alterations of Ca^{2+} homeostasis in cerebellar granule neurons (Marty and Atchison, 1997).

Another potential difference between Purkinje and granule cells that may contribute to the differential neurotoxic effects of MeHg is the presence or absence of "buffer-type" Ca^{2+} binding proteins, which are thought to have a role in minimizing excessive elevations of free Ca^{2+}_i and in preventing excitotoxicity (Batini *et al.*, 1997; Christakos, *et al.*, 2000). Purkinje cells express both parvalbumin and CB Ca^{2+} binding proteins. Granule cells do not express either protein (Groul and Crimi, 1988), but express an alternate Ca^{2+} binding protein, calretinin. CB expression is associated with enhanced resistance to Ca^{2+}-mediated cell death in a variety of cell types. In Purkinje cells, CB may help to buffer the increases of $[Ca^{2+}]_i$ caused by MeHg.

Lastly, cerebellar granule neurons are one of the smallest (5-6 μm soma diameter) cells in the CNS while Purkinje neurons are one of the largest with somas approximately 20-25 μm wide (Ito, 1984; Gruol and Crimi, 1988). In terms of MeHg neurotoxicity the size difference between these two cell types may be significant because MeHg causes cell swelling and shrinking *in vivo* (Syversen *et al.*, 1981).

In this study, we observed a substantial decrease in fura-2 fluorescence when the heavy-metal chelator, TPEN, was applied acutely during the initial, first phase increase in fura-2 fluorescence induced by MeHg. This suggests that a large percentage of fura-2 fluorescence from Purkinje cells is due to non-Ca^{2+} divalent cations interacting with fura-2. In rat brain synaptosomes, MeHg causes the release of Zn^{2+} (Denny and Atchison, 1994). At least one source of the MeHg-labile Zn^{2+} was from a soluble protein from a synaptosomal homogenate. Cerebellar Purkinje cells express proteins that may account for the release of non-Ca^{2+} divalent cations during MeHg exposure. *In situ* hybridization studies have shown that Purkinje cells express the metal binding protein, metallothionein (Leyshon-Sorland *et al.*, 1994). Purkinje neurons contain a high concentration of thiol groups (Zhang and Ottersen, 1992), presumably due to the presence of metallothionein. Metallothionein is a soluble protein of approximately 60 amino residues, 20 of which are cysteine (Aschner 1997), providing many -SH groups with which MeHg can interact. This is significant because MeHg has been shown to bind with high affinity to -SH groups (Hughes, 1957). Metallothionein binds with high affinity to Zn^{2+}, Fe^{2+}, and Hg^{2+} (for review see; Aschner 1997). Perhaps MeHg displaces Zn^{2+} from metallothionein during the initial increase in fura-2 fluorescence. Leyshon-Sorland *et al.* (1994) found a correlation between the location of metallothionein in Purkinje cells and accumulations of Hg using a modified silver staining technique. Furthermore, MeHg displaces Zn^{2+} from type I recombinant mouse metallothionein and MeHg binds to metallothionein with high affinity (Leiva-Presa *et al.*, 2004). This MeHg-metallothionein interaction may explain partly the greater resistance of Purkinje cells to MeHg. Both Purkinje cells and granule

cells (Marty and Atchison, 1997) release non-Ca^{2+} cations resulting from MeHg response, although metallothionein was not detected in granule cells (Leyshon-Sorland *et al.* 1994). As promising as metallothionein may be as a potential source of MeHg-labile Zn^{2+}, it is not the only source of MeHg-induced release of Zn^{2+}_i in rat brain synaptosomes. Metallothionein has a low molecular weight of 7 - 8 kDa and at least one of the sources of Zn^{2+} in rat brain synaptosomes had a molecular weight of 50 - 55 kDa (Denny *et al.*, 1994).

Release of Ca^{2+} or other divalent cations from intracellular sources was not detected in acutely dissociated Purkinje cells after exposure to 5 μM MeHg. This was surprising because acutely dissociated Purkinje cells have been reported to have an enhanced ability to release Ca^{2+} from intracellular sources as compared to Purkinje cells maintained in long-term culture conditions (Womack *et al.*, 2000). Photo-releaseable IP_3 and caffeine caused a greater increase in amplitude of fura-2 fluorescence in acutely dissociated Purkinje cells as compared to Purkinje cells grown in long-term cultures. If MeHg causes the generation of IP_3 and subsequent elevations of $[Ca^{2+}]_i$, MeHg should have a greater effect on the release of Ca^{2+} from intracellular sources in acutely dissociated Purkinje cells as compared to Purkinje cells maintained in long term culture conditions. This observation is difficult to reconcile. However, the acutely dissociated Purkinje cell isolation and long-term Purkinje cell culture isolation protocols used in the study by Womack *et al.* (2000) were different from those used in this study. Hence, it is possible that the acutely dissociated Purkinje cells used in this study differed in their ability to

release $Ca^{2+}{}_i$ compared to those in the Womack *et al.* (2000) report.

Future studies on the etiology of MeHg-induced elevations of $[Ca^{2+}]_i$ should focus on the specific factors that may contribute to the differential neurotoxic effects of MeHg observed in Purkinje and granule cells. Specifically, further research needs to be done to determine the role of metallothionein and Ca^{2+}-binding proteins such as CB in MeHg-mediated alterations of divalent cation homeostasis. In understanding how cerebellar Purkinje and granule cells differ in their response to MeHg the mechanism(s) by which MeHg causes cell death may be elucidated.

CHAPTER THREE

PRESENCE OF FUNCTIONAL VOLTAGE-GATED CALCIUM CHANNELS ALTERS METHYLMERCURY-INDUCED DYSREGULATION OF $[Ca^{2+}]_i$ AND CYTOTOXICITY IN TWO RAT PHEOCHROMOCYTOMA CELL LINES

ABSTRACT

MeHg is a neurotoxicant that causes elevations of $[Ca^{2+}]_i$. Other heavy metals such as Cd^{2+} and Pb^{2+} enter cells through VGCC. The objective of the present study was to test the hypothesis that MeHg enters cells through VGCCs to cause dysregulation of Ca^{2+} homeostasis. To do this, I measured dysregulation of Ca^{2+} homeostasis and cytotoxicity as a result of exposure to MeHg in two types of differentiated rat pheochromocytoma (PC) cell lines: PC12 cells which express functional VGCCs and PC18 which do not. PC12 cells responded to exposure to depolarizing solutions of KCl (40 mM) with a brief elevation of fura-2 fluorescence which could be blocked by pretreatment with L-type VGCC antagonists. In contrast, the intensity of fura-2 fluorescence from PC18 cells did not change when cells were exposed to solutions containing 40 or 80 mM KCl, even in the presence of the L-type VGCC agonist, BayK 8644. Both PC12 and PC18 cells responded to MeHg exposure with a biphasic increase in fura-2 fluorescence in a time- and concentration-dependent manner (0.5, 1, 2 and 5 μM MeHg). The time-to-onset of the first phase increase in fluorescence was delayed in PC18 compared to PC12 cells, and in PC12 cells when VGCCs were inhibited. The response was reduced to a single phase in each cell type when MeHg was co-applied with EGTA in Ca-free buffer. In addition, 24.5 hrs after cessation of a 2 hr treatment with MeHg, there was a corresponding increase in cell viability after MeHg exposure, under conditions in which VGCCs were either absent in PC18 cells or inhibited in PC12 cells. Thus, lack of expression or inhibition of VGCCs resulted in delayed time-to-onset of MeHg-induced elevation of $[Ca^{2+}]_i$ and diminished cytotoxicity. These data support the hypothesis that VGCCs are

one potential pathway in which MeHg enters cells to cause dysregulation of Ca^{2+} homeostasis. However VGCCs are not needed to induce release of Ca^{2+} from intracellular stores and the subsequent entry of Ca^{2+}_c into cells in response to MeHg.

INTRODUCTION

Several lines of evidence suggest that VGCCs have an important role in MeHg-induced dysregulation of Ca^{2+} homeostasis and cell death. The L-type VGCC antagonist, nifedipine attenuates or delays the disruptive effects of MeHg on Ca^{2+} homeostasis in NG108-15 cells (Hare and Atchison, 1995) and cerebellar granule cells (Marty and Atchison, 1997). Inhibition of N- and P/Q-type-VGCCs with ω-conotoxin MVIIC or L-type VGCCs with nifedipine, causes enhanced resistance to MeHg-induced cytotoxicity in cerebellar granule cells (Marty and Atchison, 1998). Furthermore, VGCC function is highly sensitive to MeHg exposure. Chronic exposure to 30 nM MeHg reduced whole-cell Ca^{2+} currents in PC12 cells 24 hr post-MeHg exposure (Shafer *et al.*, 2002). The effects of MeHg on VGCCs are nearly irreversible and occur in all the major sub-types of high-voltage-activated channels (L-, R-, P/Q- and N-type) at low (0.5 μM) concentrations of MeHg (Sirois and Atchison, 2000). VGCCs have been suggested to act as portals for MeHg entry into cells and cause dysregulation of Ca^{2+} homeostasis (Atchison, 1986; Atchison, 1987). Other heavy metals have been found to enter cells through VGCCs. Using the Ca^{2+} fluorophore, fura-2, as an indicator of heavy metals, entry of Pb^{2+} (Mazzolini *et al.*, 2001) and Cd^{2+} (Hinkle and Osborne, 1994) into cells was dependent upon the presence of functional VGCCs.

The aim of this study was to test the hypothesis that MeHg enters cells through VGCCs to cause dysregulation of Ca^{2+} homeostasis and subsequent cytotoxicity. To test this hypothesis, I used two cell lines, PC12 and PC18. PC12 cells are a rat cell line isolated

from a catecholamine-secreting tumor of the adrenal medulla (Greene and Tischler, 1979). When exposed to neuronal growth factor PC12 cells display neuron-like characteristics, such as: increased expression of voltage-gated Na^+ channels and VGCCs, as well as neurite outgrowth and discontinued replication (Shafer and Atchison, 1992). PC18 cells are a subclone of PC12 cells. Unlike PC12 cells, PC18 cells do not express functional VGCCs (Hinkle and Osborne, 1994). In this study, the PC12 and PC18 cell lines were exposed to MeHg and resulting alterations in Ca^{2+} homeostasis were monitored with the Ca^{2+} indicator, fura-2. The VGCC antagonist, nimodipine was used to examine further the potential role that VGCCs may have in MeHg-induced disruption of Ca^{2+} homeostasis. In addition, viability assays were performed on PC12 and PC18 cells to elucidate the potential role of VGCCs in MeHg-mediated cytotoxicity.

METHODS

Materials. Poly-L lysine (P-2658), nerve growth factor (N-0513), BayK 8644 (B-133), nimodipine (N-149), trypan blue (T-8154) and thapsigargin (T-9033) were purchased from Sigma Chemical Co. (St. Louis, MO). RPMI 1640 medium (31800-014) and heat-inactivated horse serum (26050-088) were purchased from Invitrogen (Carlsbad, CA).

PC12 and PC18 cell culture conditions. PC12 cells were purchased from American Type Culture Collection (ATCC). PC18 cells were a generous gift from Dr. A. William Tank (University of Rochester, Rochester, NY). Both cell types were maintained in RPMI 1640 medium supplemented with 10% heat-inactivated horse serum and 2.5% FBS on poly-L lysine (0.1mg/ml) coated culture flasks in a humidified environment and 5% CO_2. Cells were passaged in culture when they were approximately 80% confluent. PC12 cells were used from relative passage numbers 2 to 15 from the original culture received from ATCC. For experiments, cells were plated on 35mm culture dishes (plating density 2.5 X 10^4 cells per dish) with collagen-coated coverslips for fura-2 fluorescence experiments, and collagen-coated culture dishes, without coverslips, for viability assays. PC12 and PC18 cells in culture dishes were maintained in 3 ml of RPMI serum-supplemented medium with 100 ng/ml nerve growth factor for 7 days prior to experimentation, to allow for neuronal differentiation.

Measurement of fura-2 fluorescence changes. The ratio-metric Ca^{2+} indicator fura-2 was used to record divalent cation flux as described in Chapter Two with the exception

that for PC12 and PC18 cells, fura-2AM (3-4 μM) dissolved in HBS for 30 min at room temperature in the presence of pluronic acid (3-4μM) after this incubation, cells were rinsed free of unincorporated fura-2AM in perfusing HBS for 15 min at 30°C.

Viability assays

Calcein-AM/ethidium homodimer. Prior to MeHg exposure, cells were observed using an inverted microscope and the undersides of the culture dishes were marked with a circular Nikon marking objective (2 mm diameter). Cells located within each marked area were quantified, in terms of viability, after MeHg exposure. PC12 and PC18 cells plated on culture dishes were rinsed 3 times in sterile HBS at 37°C. Cells were exposed to 0.5, 1, 2 and 5 μM MeHg with and without nimodipine (1 μM) as well as HBS alone for 2 hr. After 2 hr, cell culture medium was replaced, cells were returned to the humidified incubation chambers and viability was assessed 24 hr later. The remainder of the PC12 and PC18 cell viability assay protocol mirrors that of cerebellar granule and Purkinje cells described in Chapter Two.

Trypan blue dye exclusion. Following a 2 hr exposure to MeHg, a proportion of cells lifted off the cell culture dish. Trypan blue dye exclusion cell viability assay was performed on PC12 and PC18 cells that lifted off the culture dish 24 hr after MeHg treatment. The 2 hr treatment of cells with MeHg in the trypan blue viability assay, is identical to that given above. Cell culture medium sample volumes of 100 μl from MeHg-treated and HBS-control PC12 and PC18 cell culture dishes were removed 24 hr

after cessation of MeHg exposure and added to 100 µl trypan blue (0.4% v/v, stock solution) in 500 µl HBS. This solution was then mixed and light (live) and dark (dead), cells were then observed using a Nikon Diaphot epifluorescence microscope (Nikon Instruments).

Statistics

For all fura-2 fluorescence data, one *n* value represents the average responses from 4 to 6 PC12 or PC18 cell soma recorded from simultaneously on a single coverslip. Data were analyzed using the Sigma Stat statistical program (Point Richmond, CA). Mean values were compared using a one-way or two-way analysis of variance (ANOVA) or students t-test, as appropriate. Two-way ANOVA was used when comparing multiple cell types and multiple MeHg concentrations. Percent data were first square root transformed prior to statistical analysis. If significant differences between sample means were detected ($P \leq 0.05$), a *post-hoc* Tukey-Kramer test was performed to ascertain which mean values were significantly different.

RESULTS

Both PC12 and PC18 cell types responded to 100 ng/ml NGF with increased neurite outgrowth and slowing of replication rate. However, PC18 cells tended to continue to replicate albeit at a slower rate when grown in the presence of 100 ng/ml NGF. PC12 cells responded to depolarizing solutions of 40 mM KCl with a rapid increase then a return to baseline fura-2 fluorescence. In contrast, the intensity of fura-2 fluorescence from PC18 cells did not change when cells were exposed to 40 or 80 mM KCl-HBS solutions alone or in the presence of the L-type VGCC agonist, (1 μM) BayK 8644 (Fig. 3.1). This is in agreement with previous $^{45}Ca^{2+}$ uptake and fura-2 fluorescence studies comparing PC12 with PC18 cells in the presence of depolarizing agents (Hinkle and Osborne 1994). Although PC18 cells lacked a response to depolarizing solutions, they did have the capacity to buffer elevations of Ca^{2+} induced by exposure to the smooth endoplasmic reticulum ATPase inhibitor, thapsigargin (1 μM) (Fig. 3.1). PC12 (Fig. 3.2 panel A) and PC18 (Fig. 3.2 panel B) cell types had a similar, biphasic increase in fura-2 fluorescence in response to exposure to all MeHg concentrations (0.5-5 μM) tested. Other cell types including: NG108-15 (Hare and Atchison, 1995), cerebellar granule neurons (Marty and Atchison, 1997) and cerebellar Purkinje neurons (Edwards and Atchison, 2001) have shown a similar increases in fura-2 fluorescence resulting from MeHg exposure. When MeHg was applied in Ca^{2+}-free, EGTA-containing (20 μM) HBS solution, the second phase was absent in PC12 and PC18 cell types (Fig. 3.3). Thus, in both PC12 and PC18 cells, there was an initial increase in fura-2 fluorescence that was due to release of Ca^{2+} from intracellular stores followed by a later, second phase, increase

Figure 3.1. Tracing of fura-2 fluorescence taken from a PC18 cell during exposure to depolarizing (40 and 80 mM) KCl solutions in the presence of the L-type VGCC agonist, Bay K 8644 (1 μM) and the smooth endoplasmic reticulum ATPase inhibitor, thapsigargin (1 μM). Solutions were perifused at a rate of 2 ml/min and depolarizing KCl solutions were perifused for a total of 2 minutes for each application. A 2 min pre-treatment of BayK 8644 was performed prior to perifusion of BayK 8644-containing KCl solutions.

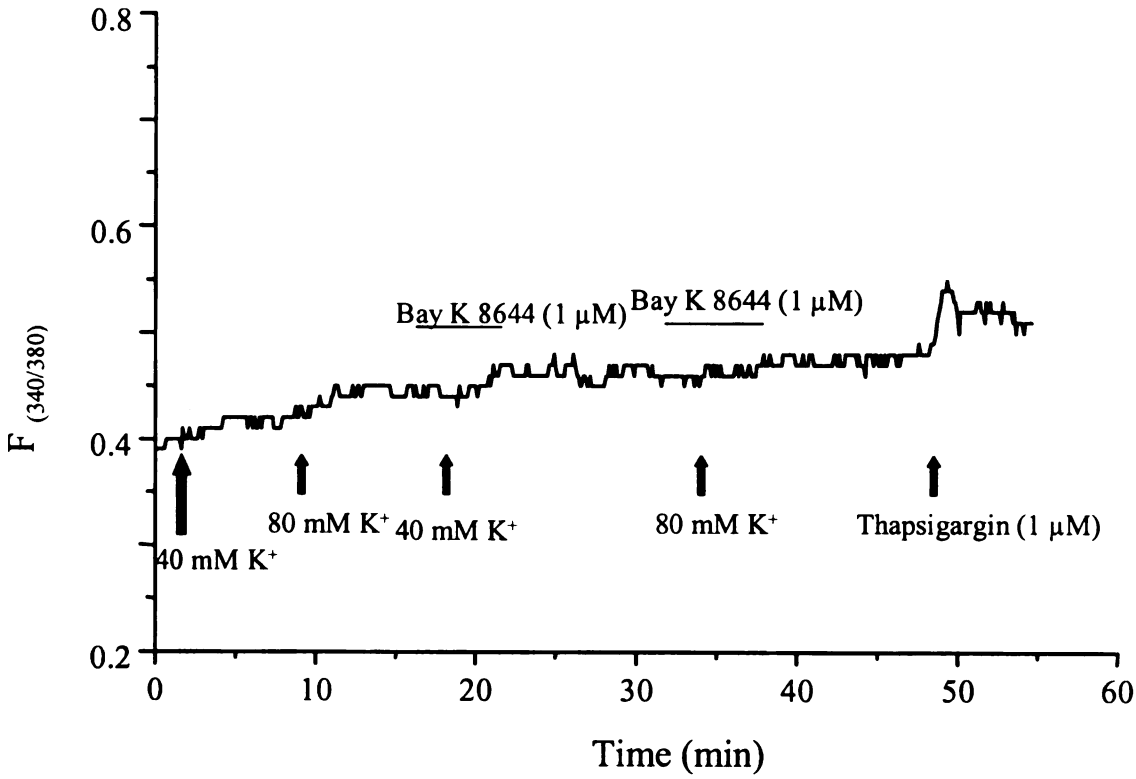
0.8
0.6
0.4
0.2
F (340/380)
Bay K 8644 (1 μM)
Bay K 8644 (1 μM)
40 mM K+
80 mM K+
40 mM K+
80 mM K+
Thapsigargin (1 μM)
0
10
20
30
40
50
60
Time (min)

Figure 3.1

Figure 3.2 Representative tracings showing changes in fura-2 fluorescence from PC12 (A) and PC18 (B) cells during exposure to 2 μM MeHg. In every experiment, a biphasic increase in fura-2 fluorescence was observed during continuous perifusion (2 ml/min) of MeHg-containing HBS in both PC12 and PC18 cell types.

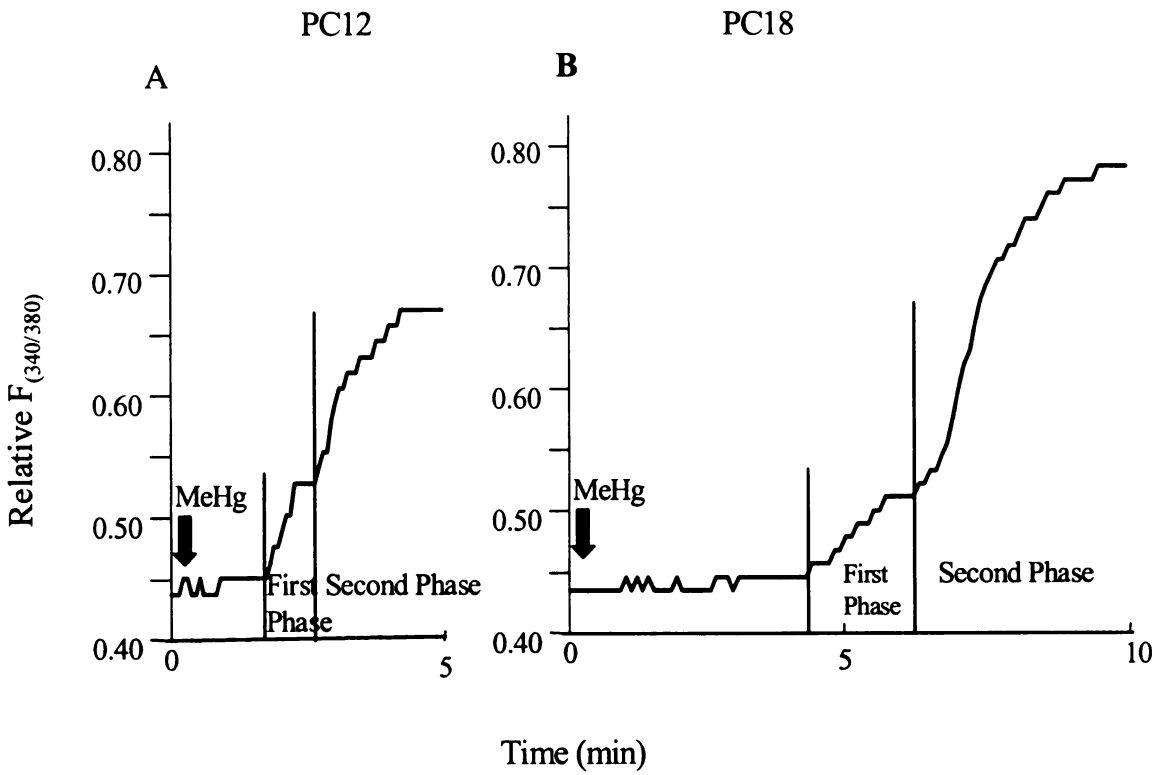
PC12
PC18
A
B
0.80
0.70
0.60
0.50
0.40
Relative F(340/380)
MeHg
First Phase
Second Phase
0
5
10
Time (min)

FIGURE 3.2

Figure 3.3 Tracings showing a single phase increase in fura-2 fluorescence from PC12 (A) and PC18 (B) cells exposed to MeHg in Ca^{2+}-free, 20 μM EGTA-containing HBS. Both cells were perifused with Ca^{2+}-free HBS 2 min prior to application of MeHg. The PC12 cell in panel A was exposed to 1 μM MeHg and the PC18 cell in panel B was exposed to 2 μM MeHg.

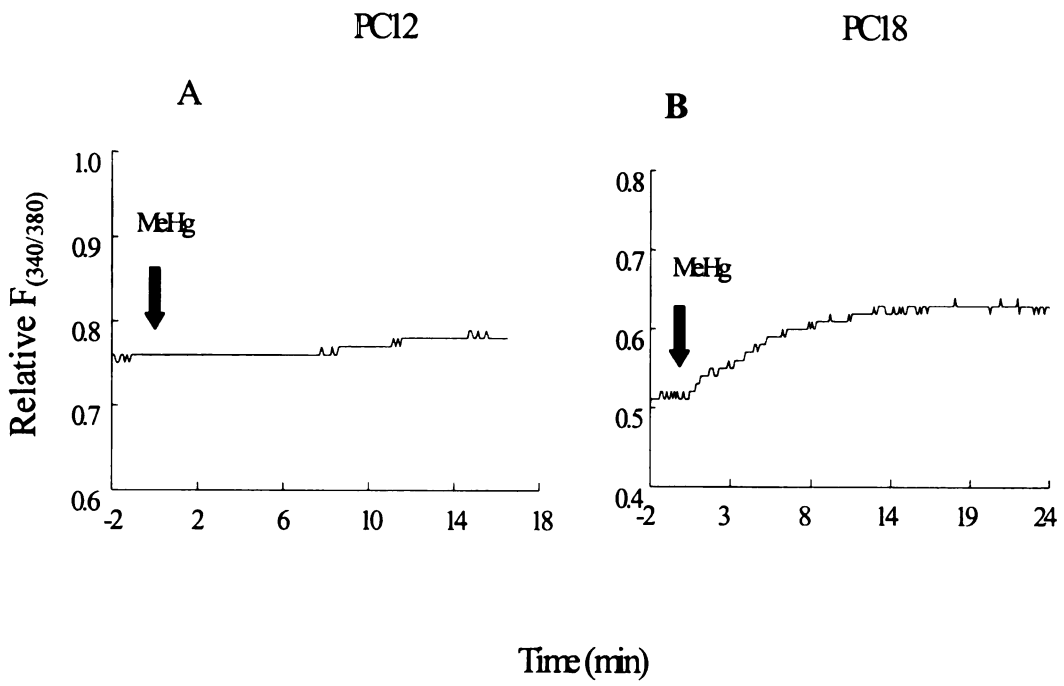
PC12
PC18
A
B
MeHg
MeHg
Relative F(340/380)
1.0
0.9
0.8
0.7
0.6
0.8
0.7
0.6
0.5
0.4
-2
2
6
10
14
18
-2
3
8
14
19
24
Time (min)

FIGURE 3.3

Figure 3.4 The effects of MeHg concentration on the time-to-onset (min) of first and second phase increases in fura-2 fluorescence, $F_{(340/380)}$, in PC12 cells. MeHg was applied continually by perifusion while changes in fluorescence were recorded. Significant differences were detected (two-way ANOVA $P < 0.01$). The (*) indicates significant differences between the time-to-onset compared to that of the 5 μM MeHg treatment group. Values are mean ± SE min, N = 3.

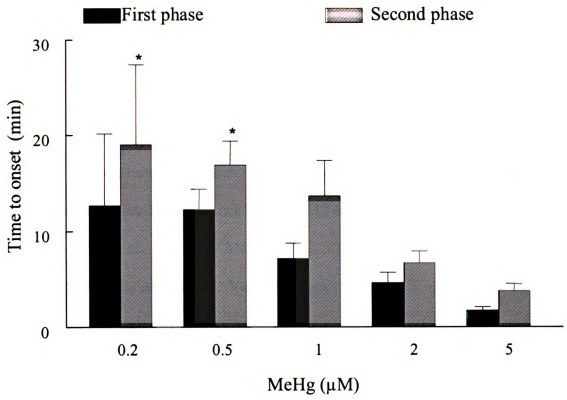
First phase
Second phase
30
20
10
0
Time to onset (min)
*
*
0.2
0.5
1
2
5
MeHg (μM)

FIGURE 3.4

Figure 3.5 MeHg caused a time- and concentration-dependent decrease in time-to-onset of first phase increases in fura-2 fluorescence in both PC12 and PC18 cells. The (*) indicates significant differences (two-way ANOVA, $P < 0.05$) between PC12 and PC18 cells in the 5 μM MeHg treatment groups. Values are mean ± SE min, N = 3 for PC12 and PC18 cells at all μM MeHg treatment groups.

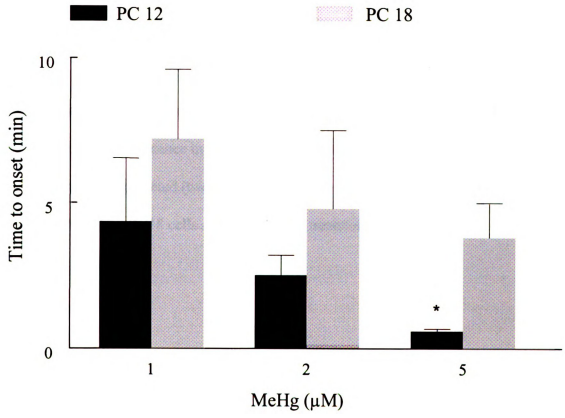

FIGURE 3.5

Figure 3.6 MeHg caused a time-dependent decrease in the time-to-onset of the second phase increases of fura-2 fluorescence in both PC12 and PC18 cells. However, no significant differences were detected (two-way ANOVA, $P > 0.05$). Values are mean ± SE min, N = 3 for PC12 and PC18 cells at all μM MeHg treatment groups.

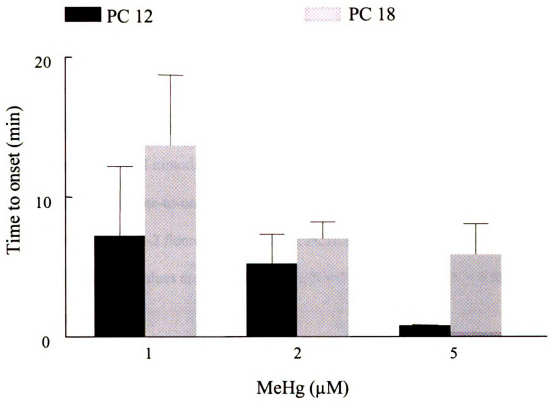

FIGURE 3.6

Figure 3.7 The L-type VGCC inhibitor nimodipine (1μM) caused a significant delay in time-to-onset of increases in fura-2 fluorescence when PC12 cells were perifused with 2μM MeHg. Significant differences were detected (two-way ANOVA, $P < 0.01$) between PC12 cells pre-treated with 1 μM nimodipine compared to non-nimodipine treated cells in both first and second phase time-to-onset. The (*) indicate significant differences in time-to-onset of increases in fura-2 fluorescence between PC12 nimodipine and non-nimodipine treatment groups. Values are mean ± SE min, N = 3 for control and N = 4 for nimodipine treatment groups.

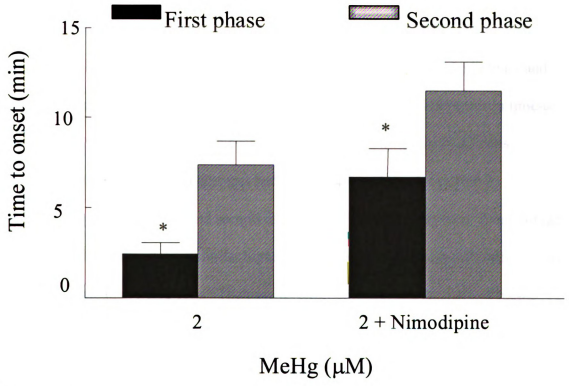
First phase
Second phase
Time to onset (min)
15
10
5
0
*
*
2
2 + Nimodipine
MeHg (μM)

FIGURE 3.7

in fura-2 fluorescence due to entry of Ca^{2+}_e. Other studies have shown that during the first phase, Ca^{2+} as well as non-Ca^{2+} divalent cations are released from intracellular sources (Marty and Atchison, 1997; Edwards and Atchison, 2001). In rat brain synaptosomes this non-Ca^{2+} divalent cation released during MeHg exposure has been shown to be Zn^{2+} (Denny and Atchison, 1994). In this study, no attempt was made to assess the non-Ca^{2+} contribution to fura-2 fluorescence during first phase.

MeHg-induced increase in fura-2 fluorescence from PC12 cells occurred in a time- and concentration-dependent manner (Fig. 3.4). Figure 3.5 shows the differences in time-to-onset of first phase MeHg-induced elevation of fura-2 fluorescence in PC12 cells compared to PC18 cells. Both cell types had similar rates of increase in fura-2 fluorescence in both the initial and second elevation of fura-2 fluorescence. Even though PC18 lack VGCCs they show a similar biphasic response to MeHg exposure, albeit on a longer time-scale than PC12 cells. The time-to-onset of first phase increase of fura-2 fluorescence was significantly delayed in PC18 cells compared to PC12 cells, (Fig. 3.5). This suggests that VGCCs are not required for MeHg-mediated elevation in $[Ca^{2+}]_i$. The second phase time-to-onset of increases of fura-2 fluorescence was not significantly different in PC18 cells as compared to PC12 in the 1, 2 and 5 μM MeHg-treatment groups (Fig. 3.6).

The amplitude of fura-2 fluorescence increase from PC12 cells following depolarization resulting from exposure to 40 mM KCl was significantly decreased (Student's t-test, $P <$

0.05) in presence of the L-type VGCC antagonist, nimodipine (1 μM). When VGCCs were inhibited in the presence of 1 μM nimodipine during MeHg application there was a significant delay in first phase (two-way ANOVA, $P < 0.05$) and second phase time-to-onset of increases of fura-2 fluorescence resulting from exposure to 2 μM MeHg (Fig. 3.7). Because nimodipine and other dihydropyridines may have effects other than inhibiting VGCCs, nimodipine control experiments were performed on PC18 cells. First- or second-phase time-to-onset of increases of fura-2 fluorescence were not significantly different (two-way ANOVA $P > 0.05$) in PC18 cells exposed to 2 μM MeHg in the presence of 1 μM nimodipine. The mean time-to-onset of first- and second-phase increases of fura-2 fluorescence in PC18 cells in the nimodipine control experiments of Figure 3.8 differ from the mean first and second phaste time-to-onset of increases in fura-2 fluorescence in Figures 3.5 and 3.6, respectively.

To test the role of VGCCs in MeHg-induced cytotoxicity, ethidium-homodimer and calcein-AM viability assays were performed 24.5 hr after cessation of MeHg exposure. MeHg caused significant decreases in the viability of PC12 but not PC18 cells. PC12 cell viability was significantly less (two-way ANOVA $P \leq 0.05$) at the 2 and 5 μM MeHg treatment groups compared to control values (Fig. 3.9). PC18 cell viability was not affected at any MeHg concentration tested (0.5-5 μM) (Fig. 3.9). When nimodipine (1 μM) was applied with MeHg (2 μM), there was no significant decrease in PC12 cell viability compared to control, HBS alone treatment group (Fig. 3.10). That inhibition of VGCCs by dihydropyridines, resulted in greater resistance to MeHg cytotoxicity, is in

agreement with MeHg cytotoxicity studies of cerebellar granule cells (Marty and Atchison, 1998). In comparison to PC12 cells, nimodipine had no significant effect on PC18 cell viability

Figure 3.8 The L-type VGCC antagonist nimodipine did not significantly alter time-to-onset of increases of fura-2 fluorescence from exposure to 2 μM MeHg in PC18 cells. PC18 cells were either pre-treated with nimodipine (1 μM) for 2 min prior to application of a MeHg/nimodipine solution or were exposed to MeHg-alone. Data are represented as mean ± SE, N = 6 for MeHg alone, N = 5 for MeHg/nimodipine treatment group. No significant differences were detected (two-way ANOVA, $P > 0.05$) between time-to-onset of first phase or second phase increase in fura-2 fluorescence in nimodipine treated or untreated PC18 cells.

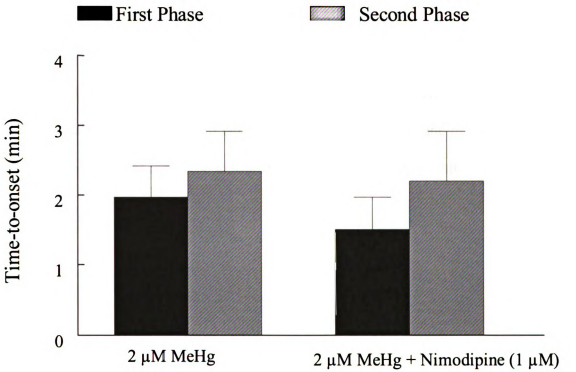
First Phase
Second Phase
Time-to-onset (min)
4
3
2
1
0
2 μM MeHg
2 μM MeHg + Nimodipine (1 μM)

FIGURE 3.8

Figure 3.9 Viability assay showing differences between the cytotoxic effects of MeHg on PC12 cells and PC18 cells. MeHg caused a significant (2-way ANOVA, $P < 0.05$) decrease in PC12 cell viability in the 2 μM MeHg treatment group when MeHg was applied for 2 hr and viability assayed 24.5 hr later. The (*) indicates significant differences in PC12 cell viability compared to MeHg-free control treatment group. Values are mean ± SE, $N \geq 5$.

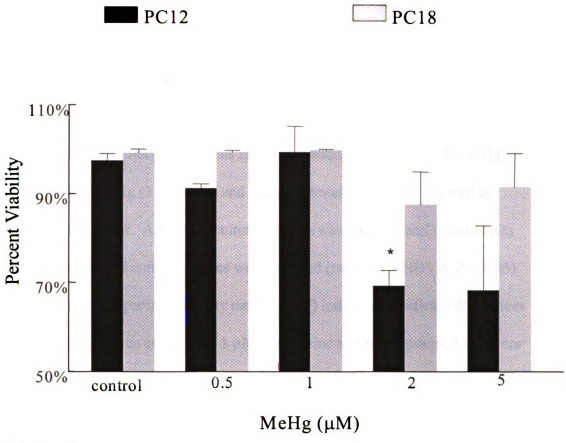
PC12
PC18
110%
90%
70%
50%
Percent Viability
*
control
0.5
1
2
5
MeHg (μM)

FIGURE 3.9

Figure 3.10 Nimodipine protects PC12 cells from cytotoxicity caused by 2 μM MeHg. Cells were exposed to MeHg (2 μM) with and without nimodipine (1 μM) as well as HBS alone (control) for 2 hr. After 2 hr, culture medium was replaced and viability was assessed 24 hr later. Significant differences were detected (two-way ANOVA, $P < 0.05$) in square root-transformed percent viability data. The (*) indicates significant differences between the PC12 MeHg-free control and 1 μM nimodipine treatment groups. Values are mean ± SE percent viability, $N = 4$.

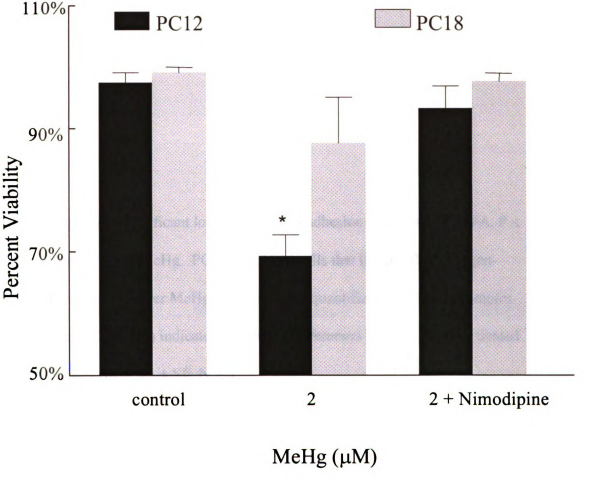
110%
90%
70%
50%
Percent Viability
PC12
PC18
*
control
2
2 + Nimodipine
MeHg (μM)

FIGURE 3.10

Figure 3.11 MeHg causes significant loss of PC12 cell adhesion (two-way ANOVA, $P \leq 0.05$) after exposure to 5 μM MeHg. PC12 and PC18 cells that lifted off of collagen-coated culture dish substrate after MeHg exposure were quantified from 100 μl samples of cell culture medium. The (*) indicates significant differences from non-MeHg treated control values. Values are mean ± SE, N = 3.

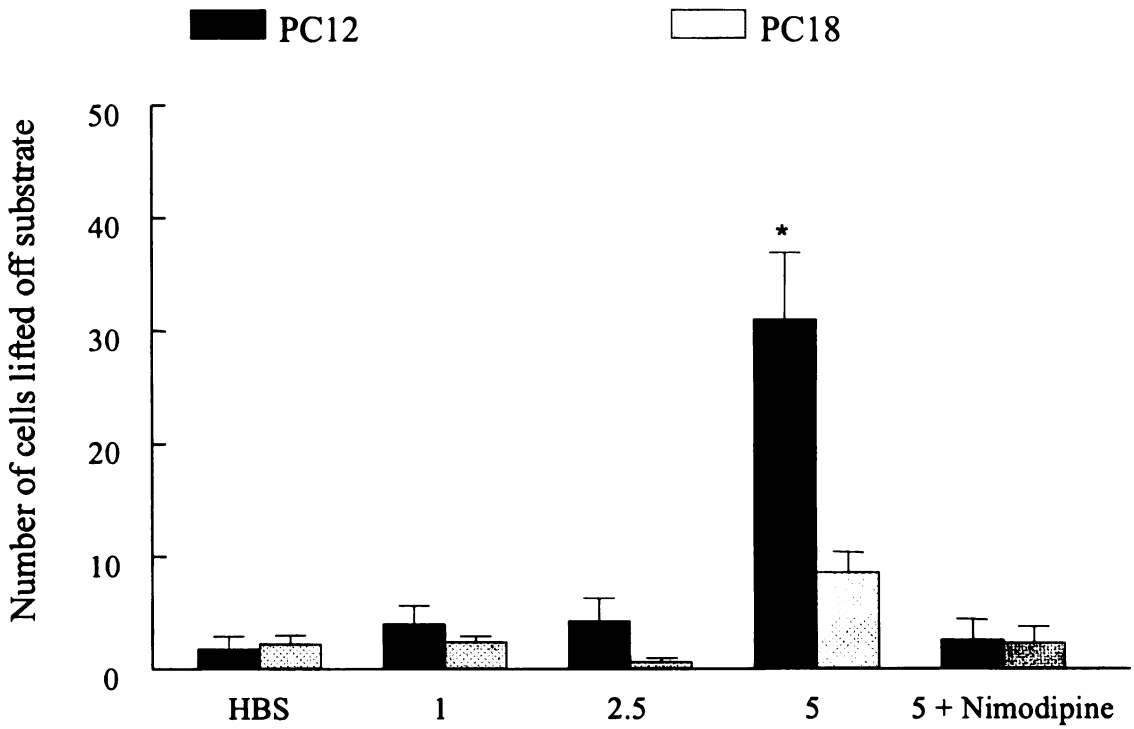
PC12
PC18
Number of cells lifted off substrate
50
40
30
20
10
0
*
HBS
1
2.5
5
5 + Nimodipine

FIGURE 3.11

Figure 3.12 MeHg causes differential loss of cell adhesion and viability in PC12 and PC18 cells. Of the PC12 cells that lost adhesion from the culture dish during MeHg exposure, a significant decrease of percent cell viability was found at the 5 μM MeHg treatment group (two-way ANOVA, $P \leq 0.05$). The (*) indicates significant differences between the 5 μM MeHg PC12 cell treatment group compared to 1 μM MeHg treatment group. Values are mean ± SE percent viability, N = 3; N = 2 for PC12 HBS control. No dead PC18 cells were found in the control, 1 and 2.5 μM MeHg treatment groups.

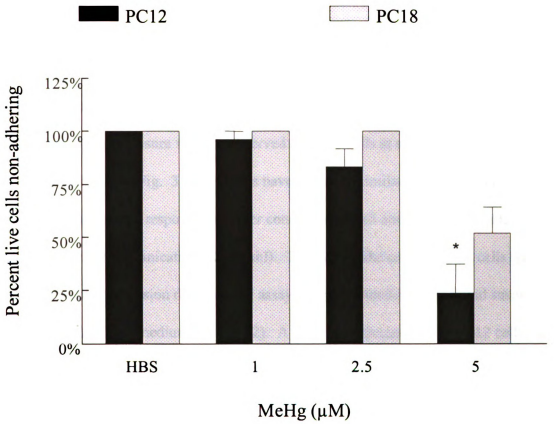
PC12
PC18
Percent live cells non-adhering
125%
100%
75%
50%
25%
0%
*
HBS
1
2.5
5
MeHg (μM)

FIGURE 3.12

during exposure to 2 μM MeHg (Fig. 3.10).

The number of PC12 cells adhering to the culture dish substrate in the trypan blue viability assays was found to decrease 24 hr after cessation of a 2 hr duration of MeHg exposure at 5μM MeHg treatment group (Fig. 3.11). Nimodipine (1 μM) prevented loss of PC12 cell adhesion from culture dish at the 5 μM MeHg treatment group. Loss of cell adhesion resulting from MeHg exposure was not observed in PC18 cells at any MeHg concentration tested (1, 2.5 and 5 μM) (Fig. 3.11). Others have observed similar loss of cell adhesion in cells grown in culture as a response to higher concentrations (5 and 7 μM) of MeHg exposure (personal communication, K. Reuhl). To assess if the non-adhering cells were viable, a trypan blue exclusion dye viability assay was performed on cells found suspended or floating in cell culture medium (Fig. 3.12). A significant percentage of PC12 cells were found to be non-viable at the 5 μM treatment group. In the control PC12 cell treatment group only two replicates had cells that lifted off the substrate in the 100 μl sample of cell culture medium. Thus there was a loss of cell adhesion when cells were treated with MeHg-free HBS, albeit fewer PC12 cells were found in control as compared to 5 μM MeHg treatment groups. Nimodipine did not significantly increase the viability of the non-adhering cells, although nimodipine did result in greater cell adhesion in PC12 cells.

DISCUSSION

The principal findings in this paper are that functional VGCCs play a role in MeHg-induced release of Ca^{2+} from intracellular stores and subsequent cytotoxicity. When VGCCs were inhibited by the selective L-type VGCC antagonist, nimodipine, in PC12 cells, or VGCCs were absent in PC18 cells, there was a resulting delay in MeHg-induced dysregulation of Ca^{2+} homeostasis and cytotoxicity, as compared to PC12 cells with normal VGCCs. Lastly, cell adhesion of PC12 cells to the collagen-coated substrate was less 24 hr after cessation of a 2 hr exposure duration of 5 μM MeHg. Application of the L-type VGCC antagonist, nimodipine (1μM) resulted in greater PC12 cell adhesion after MeHg exposure, but inhibition of VGCCs by nimodipine had no effect on PC18 cells.

The hypothesis that MeHg enters cells through VGCCs to cause dysregulation of Ca^{2+} homeostasis originated from studies using neuromuscular junction preparations. MeHg causes an increase in miniature end plate potential (MEPP) frequency then an irreversible decrease in MEPP frequency. In this way, MEPP frequency is a bioassay for MeHg exposure. MEPP frequency increased when MeHg was present in a Ca^{2+}-free buffer. Furthermore activation of VGCCs with either Bay K 8644 (Atchison, 1987) or depolarizing KCl solutions (Atchison, 1986) hastened time-to-onset of increases in MEPP frequency. Because MEPP frequency is a $[Ca^{2+}]_i$-dependent process this indicated that MeHg may use VGCCs as portals to cross phospho-lipid membranes into nerve terminals to cause release of Ca^{2+} from intracellular stores. Both the smooth endoplasmic reticulum (Hare and Atchison, 1995) and mitochondria (Levesque and Atchison, 1991; Limke and

Atchison 2002) have been identified as potential sources of Ca^{2+}_i release during MeHg exposure.

In this study I show that inhibition of L-type VGCC or lack of VGCCs resulted in enhanced resistance to MeHg-induced dysregulation of Ca^{2+} homeostasis and cytotoxicity. Other studies have shown that inhibition of VGCCs causes enhanced resistance to the ability of MeHg to alter Ca^{2+} homeostasis in NG108-15 cells and cerebellar granule cells (Marty and Atchison, 1997) as well as, enhanced resistance to MeHg-induced cytotoxicity (Marty and Atchison, 1998). It is likely that if MeHg enters cells through VGCCs, that normal VGCC functioning would be impeded. MeHg interacts with VGCCs in a non-competitive and irreversible manner to inhibit Ca^{2+} (Shafer, 1998) as well as Ba^{2+} (Sirois and Atchison, 2000) current in a variety of cell types and experimental preparations. The apparent affinity of MeHg for VGCCs is high due to the observation that MeHg causes disruption of VGCC functioning at very low MeHg concentrations. For example, 24 hr exposure to 30 nM MeHg caused a significant decrease in whole cell Ca^{2+} current in PC12 cells (Shafer *et al.*, 2002).

In this study PC18 cells, with non-functional VGCCs, responded to MeHg with release of Ca^{2+}_i and entry of Ca^{2+}_e. This would indicate that MeHg may enter PC18 cells through pathways other than VGCCs. It is likely that MeHg enters cells through passive diffusion, at least to a limited extent. However, the highly lipophilic mercury-containing compounds: dimethlymercury and ethylmercury, had similar effects as did MeHg on non-

depolarizing $^{45}Ca^{2+}$ uptake in rat brain synaptosomes (Hewett and Atchison, 1992). Thus, the lipophilic properties of MeHg do not account entirely for the disruptive effects of MeHg on Ca^{2+} homeostasis. If MeHg-induced dysregulation of Ca^{2+} homeostasis is dependent upon entry of MeHg into the cell, it is likely that MeHg enters PC18 cells through other specific receptor or surface protein-mediated pathways to cause dysregulation of Ca^{2+} homeostasis. Pathways other than VGCCs by which MeHg may enter PC18 cells are unknown at this time However, entry of MeHg into cells is probably not through NMDA or AMPA/kainate glutamate receptor pathways. For example pretreatment of cerebellar granule cells with the NMDA receptor antagonists AP-5 or MK801, or with the AMPA/kainate receptor antagonist DNQX resulted in no significant differences in time-to-onset of MeHg-induced dysregulation of Ca^{2+} homeostasis (Marty and Atchison, 1997).

In this study, nimodipine was applied to PC18 cells in the presence of MeHg to determine if nimodipine had any non-VGCC effects. The mean time-to-onset of first- and second-phase increase of fura-2 fluorescence in PC18 cells in the nimodipine control experiments differed from the mean time-to-onset values in the PC18 cell data from the PC12 cell comparison study. One possible explanation for this difference are that the nimodipine experiments were performed a year after the experiments comparing PC12 and PC18 cells were performed. As a result there were differences in PC18 cell passage number. In addition the PC18 cells used for the nimodipine experiments were not exposed to NGF where as the PC18 cells used in the PC12 cell comparison study were exposed to NGF.

Fura-2 fluorescence has been used as a direct indicator of entry of heavy metals through VGCCs. Both Cd^{2+} (Hinkle and Osborne, 1994) and Pb^{2+} (Tomsig and Suszkiw, 1991; Mazzolini *et al.*, 2001) may enter cells through VGCCs and bind with fura-2 to cause elevations in fluorescence. P-/Q-type VGCCs appeared to be the greatest contributor of Pb^{2+} entry in cerebellar granule cells (Mazzolini *et al.*, 2001), while inhibitors of L-type VGCCs nearly abolished shifts in fura-2 fluorescence due to Cd^{2+} entry in PC12 cells (Hinkle and Osborne, 1994). Nimodipine and BayK 8644 were ineffective at altering fura-2 fluorescence from PC18 cells, nor did PC18 cells respond to exposure to Cd^{2+} with greater fura-2 fluorescence (Hinkle and Osborne, 1994). Results presented in this study are in agreement with those of Hinkle and Osborne (1994) and Mazzolini *et al.*, (2001), although it is important to point out that unlike Cd^{2+} and Pb^{2+}, MeHg does not interact directly with fura-2 to cause changes in fluorescence (Hare *et al.*, 1993). The elevations of fura-2 fluorescence after MeHg exposure are due to release of $Ca^{2+}{}_i$ and entry of $Ca^{2+}{}_e$ and are not from MeHg binding to fura-2.

While this study supports the idea that MeHg might enter cells through VGCCs, it is important to consider that MeHg does not have to enter cells directly to cause elevations of $[Ca^{2+}]_i$. Inhibition of muscarinic receptors with atropine or desensitization of muscarinic receptors with chronic application of the muscarinic receptor agonist, bethanehcol resulted in attenuated elevations of fura-2 fluorescence as a result of MeHg exposure in cerebellar granule cells (Limke *et al.*, 2004). Furthermore, atropine delayed time-to-onset of MeHg-induced release of $Ca^{2+}{}_i$. Down regulation or inhibition of muscarinic receptors resulted in

greater cerebellar granule cell viability after MeHg exposure (Limke *et al.*, 2004). Granule cells express types II and III muscarinic receptors. The type III muscarinic receptor is coupled to phospholipase C, an enzyme that generates IP_3; furthermore, this receptor has been implicated as having a role in MeHg-induced cerebellar granule cell death (Limke *et al.*, 2004). A corollary to this is the MeHg-induced elevation in levels of IP_3 in cerebellar granule cells (Sarafian, 1991). Thus MeHg does not necessarily need to enter a cell to cause elevations of fura-2 fluorescence. However, if the only action of MeHg was to generate IP_3 through activation of type III muscarinic receptors, that effect alone would not explain how other, non-divalent cations are released from intracellular sources nor would it explain the mechanism by which MeHg causes entry of $Ca^{2+}{}_e$ (Hare *et al.*, 1994; Marty and Atchison, 1998; Edwards and Atchison, 2001; this study).

Future studies should focus on determining by what pathways MeHg enters PC18 cells. In addition, future studies should address the possible mechanism of MeHg-induced $Ca^{2+}{}_e$ entry into neurons. Because MeHg can cause elevations of $[Ca^{2+}]_i$ through mechanisms not dependent upon entry of MeHg into cells (Limke *et al.*, 2004), alternative methods could be employed to determine entry of MeHg into cells. Unfortunately MeHg, unlike Cd^{2+} and Pb^{2+}, does not bind directly with fura-2 to cause changes in fura-2 fluorescence. Therefore indirect methods for detecting MeHg should be employed. One possible and measurable cellular response to MeHg entry into cells could be the intracellular release of non-Ca^{2+} divalent cations that result from MeHg exposure to cerebellar granule (Marty and Atchison, 1997), Purkinje cells (Edwards and Atchison, 2001) rat brain synaptosomes

(Denny *et al.*, 1994).

CHAPTER FOUR

MYENTERIC PLEXUS NEURONS IMMUNOPOSITIVE FOR CALBINDIN-D28$_K$ ARE MORE RESISTANT TO THE NEUROTOXIC EFFECTS OF METHYLMERCURY COMPARED TO NON-CALBINDIN-D28$_K$ IMMUNOPOSITIVE NEURONS

ABSTRACT

MeHg is an environmental toxicant that causes elevations of $[Ca^{2+}]_i$. An early observation of MeHg intoxication is the loss of cerebellar granule neurons. Cerebellar granule neurons do not express the CaBP CB. This is in contrast to adjacent Purkinje neurons which do express CB. In addition, Purkinje neurons are one of the more resistant cell types to MeHg cytotoxicity. The presence of CB in neurons is thought to prevent cell death and buffer against elevations of $[Ca^{2+}]_i$. I hypothesized that neurons containing CB will have enhanced resistance to the cytotoxic effects of MeHg. To investigate this, I used myenteric plexus neurons isolated from the small intestine of the guinea pig and grown in culture. In general, two neuronal cell types were present in the myenteric plexus cultures; one type expressed CB and the other lacked CB, but expressed nitric oxide synthase (NOS). Myenteric plexus neurons were exposed to buffer control, 0.5, 1, 2 or 5 μM MeHg for 2 hr, then viability was assayed 24 hr later. A significant percent of cells died in the 2 and 5 μM MeHg treatment groups. Most of the neurons that remained in the 5 μM MeHg treatment group were the neurons which were immunopositive for CB. In addition, significant reductions of NOS immunopositive neurons occurred in the 5 μM MeHg treatment group. To explore further the potential role which CB has in attenuating MeHg-mediated elevations of $[Ca^{2+}]_i$ from myenteric plexus neurons, fura-2 fluorescence was monitored from neurons during acute exposure to MeHg. Acute application of 1 μM MeHg resulted in no significant difference (two-way ANOVA, $P = 0.132$) in time-to-onset of dysregulation of Ca^{2+} homeostasis in CB-immunopositive compared to NOS immunopositive (CB-immunonegative) myenteric plexus neurons. Thus CB may be an

important factor in determining if a particular cell type is sensitive to the neurotoxic effects of MeHg, but CB may not be a significant factor in determining how vulnerable a cell type is to MeHg-mediated dysregulation of Ca^{2+} homeostasis.

INTRODUCTION

MeHg and related alkylmercury compounds represent a class of potent environmental neurotoxicants (Chang, 1977). The most common route of exposure of MeHg is through the consumption of contaminated food (Takeuchi *et al.*, 1965, Bakir *et al.*, 1973; Frery *et al.*, 2001). Approximately 95% of ingested MeHg is absorbed rapidly across the intestinal wall of the gastrointestinal tract after ingestion in rat (Rowland *et al.*, 1980), mouse (Berlin and Ullberg, 1963) and humans (Bakir *et al.*, 1973). MeHg is lipophilic and presumably crosses the intestinal wall by passive diffusion. However there is evidence of the active transport of a MeHg-L-cysteine complex in the gut isolated from fish (Leaner and Mason, 2002). Thus, neurons located in the gastrointestinal tract, are likely to be one of the first neuronal cell types to be exposed to MeHg and at high concentrations of MeHg (Okabe and Takeuchi, 1980). Studies using small intestine segments isolated from guinea pighave shown muscle contraction mediated by the enteric nervous system is a potential target for Hg^{2+} and MeHg (Candura *et al.*, 1997).

There are two main classes of neurons found within the enteric nervous system based on morphology and electrophysiological properties that are responsible the peristaltic reflex (Hirst *et al.*, 1974; Brookes, 2001; Van den Berghe *et al.*, 2002; Denes and Gabriel, 2004; Wade and Cowen, 2004). One class of neuron is the after hyperpolarizing (AH) neuron that exhibit Dogiel type II morphology that is defined by a smooth cell body with several long processes (Furness *et al.*, 1998) and express CB (Kirchgessner and Liu, 1999; Zhou and Galligan, 2000). Based on electrophysiology experiments AH myenteric neurons

located in the small intestine of the guinea pig express a variety of VGCCs such as, L-, P-/Q- and N- (Hirning *et al.*, 1990; for review, Smith *et al.*, 2003), as well as R- type VGCCs (Bian *et al.*, 2004). Furthermore glutamate release from isolated guinea pig ileum was attenuated when L-, P/Q-, and N-type VGCCs were inhibited by selective VGCC antagonists (Reis *et al.*, 2000). Studies using immunohistochemistry techniques found that α-$_{1C}$, and α-$_{1B}$ VGCC subunits were co-localized with CB immunopositive cells in the myenteric plexus of the guinea pig small intestine, however α-$_{1D}$ or α-$_{1A}$ subunits were not co-localized with CB immunopositive neurons (Kirchgessner and Liu, 1999). The $[Ca^{2+}]_i$ increase in AH neurons resulting from action potential discharge is amplified further by Ca^{2+} release from ryanodine receptors (Hillsley *et al.*, 2000). AH neurons express Ca^{2+}-activated K^+ channels that are responsible for the pronounced hyperpolarizing effect following depolarization (Tatsumi *et al.*, 1988; Smith *et al.*, 2003). The after-hyperpolarization that follows an action potential in AH myenteric plexus neurons is due to K^+ efflux through Ca^{2+}-dependent K^+ channels (Hirst *et al.*, 1985; Vogalis *et al.*, 2002). Interestingly, the Ca^{2+}-dependent K^+ channels present within myenteric AH myenteric plexus neurons are unlike Ca^{2+}-dependent K^+ channels present elsewhere, in that AH neuron Ca^{2+}-dependent K^+ channels are less sensitive to charybdotoxin and clotrimazole than are other Ca^{2+}-dependent K^+ channels (Vogalis *et al.*, 2002). In contrast to AH neurons, the other main class of enteric neuron is the S-type neuron named because of the many fast, cholinergic synaptic inputs (Hirst *et al.*, 1974). S-type neurons exhibit Dogiel type I morphology that is characterized by short dendrites and a single axon (Furness *et al.*, 1988; Zhou and Galligan, 2000). Furthermore, S-type

neurons lack any electrical activity when depolarizing current is injected in the presence of the voltage-gated Na^+ channel inhibitor, tetrodotoxin (Hirst *et al.*, 1974). However, depolarization using intracellular current injection in S-type neurons causes an immediate elevation of $[Ca^{2+}]_i$ (Shuttleworth and Smith, 1999). This transient elevation of $[Ca^{2+}]_i$ during depolarization was completely inhibited when tetrodotoxin was present; in contrast, the N-type VGCC antagonist, ω-conotoxin GIVA did not completely abolish the current-induced elevation of $[Ca^{2+}]_i$. AH neurons act as primary afferent sensory neurons that can detect changes in pH and distention of the gut wall (Furness *et al.*, 1998), while S neurons are considered to be excitatory motor neurons or interneurons (Smith *et al.*, 1992).

MeHg causes dysregulation of Ca^{2+} homeostasis in a variety of neuronal cell types including rat brain synaptosomes (Komulainen and Bondy, 1987; Levesque *et al.*, 1992; Denny *et al.*, 1993), PC12 (Edwards and Atchison, 2003), cerebellar granule (Sarafian, 1993; Marty and Atchison, 1997; Limke and Atchison, 2002) and Purkinje neurons (Edwards and Atchison, 2001). Specifically, MeHg increases $[Ca^{2+}]_i$ in a multiphasic process including temporally and kinetically distinct phases associated with release of Ca^{2+} from intracellular stores followed by entry of $Ca^{2+}{}_e$ (Hare and Atchison 1995; Marty and Atchison 1997; Edwards and Atchison, 2001; Limke and Atchison, 2002). Extended elevations of $[Ca^{2+}]_i$ may initiate cell death. This could be a significant factor in the etiology of MeHg-induced neurotoxicity (Verity, 1992; Marty and Atchison 1998; Mori *et al.*, 2000).

One of the more resistant cell types to MeHg toxicity is the cerebellar Purkinje neuron. In contrast, adjacent cerebellar granule cells are one of the more sensitive cell types to MeHg cytotoxicity (Chang, 1977; Leyshon-Sorland *et al.*, 1994; Mori *et al.*, 2000). One potential contributing factor to the apparent differential neurotoxicity of MeHg in these two cell types is the selective expression of the CB. Purkinje neurons express CB in abundance while cerebellar granule cells do not (Celio, 1990). CB is a "buffer-type" of CaBP and is thought to act as a Ca^{2+} buffer to decrease cytotoxic concentrations of Ca^{2+}_i (Christakos *et al.*, 1989). Although the specific functional role of CB is unknown, the expression of this protein is tightly correlated with enhanced cell viability in a number of neurodegenerative disorders such as Parkinson's, Alzheimer's and Huntington's Diseases (Siesjo *et al.,* 1989; Iacopino and Christakos, 1990). In addition, cell lines transfected with CB have greater resistance to agonist evoked elevations of $[Ca^{2+}]_i$ and Ca^{2+}-mediated cell death (Chard *et al.*, 1992; McMahon *et al.*, 1998). CB is found in non-neuronal tissue such as, intestine (Arnold *et al.*, 1976; Feher, 1983; Shimura and Wasserman, 1984; Christakos *et al.*, 1989; Zhou and Galligan, 2000), kidney (Delorme *et al.*, 1983; Rhoten *et al.*, 1985) and bone (Balmain *et al.*, 1986). The expression of CB found in cells located outside the central nervous system (CNS) is highly induced by the hormonally active form of vitamin D, 1,25 dihydroxyvitamin D_3 (Norman *et al.*, 1982; Theofan *et al.*, 1987). CB expression in cells located within the CNS of the rat is not induced by 1,25 dihydroxyvitamin D_3 as measured by northern blot analysis (Christakos *et al.*, 1989). The difference between vitamin D expression of CB in neuronal and non-neuronal tissue is presumably due to the inability of 1,25 dihydroxyvitamin D_3 to cross

the blood-brain barrier.

Previous studies have shown that the cell viability of the CB-immunopositive cerebellar Purkinje neurons in rat was not significantly altered during chronic ingestion of MeHg (Kobayashi *et al.*, 1998). In addition, cerebellar granule neurons grown in culture were more sensitive to MeHg-induced neurotoxicity than Purkinje neurons in culture (Edwards *et al.*, in preparation). However, the culture conditions required for growth of adult Purkinje and granule neurons differed and could have been a complicating factor in previous MeHg viability studies. Other differences exist between Purkinje and granule cells such as: NMDA receptor expression (Gruol, 1983), IP_3 receptor sub-types, and cell size (Ito, 1984), that could contribute to the differential vulnerability to MeHg. As such, the goal of this study was to determine what potential cyto-protective role CB may have after MeHg exposure to neurons grown in the same primary cell culture conditions. To do this, we isolated neurons from the myenteric plexus of the guinea pig small intestine. Approximately 85% of AH neurons present within the myenteric plexus cell culture are CB immunopositive while S neurons are CB immunonegative, although they are nitric oxide synthase (NOS) immunopositive (Zhou and Galligan, 2000; Denes and Gabriel, 2004). We hypothesize that myenteric plexus neurons immunopositive for CB, will be more resistant to the cytotoxic effects of MeHg than are NOS immunopositive (CB immunonegative) myenteric plexus neurons. In addition, the ability of MeHg to disrupt Ca^{2+} homeostasis in both CB immunopositive and CB immunonegative myenteric plexus neurons was examined using the Ca^{2+} indicator fura-2.

METHODS

Materials. Trypsin (T-5266), Minimum Essential Medium (MEM) (M-0268), FBS (F-2442), mouse anti-Calbindin D-28K, poly-L-lysine (P-2636), penicillin/streptomycin, mouse anti-NOS and cytosine-β-arabinofuranoside (Ara-C) were purchased from Sigma Chemical Co. (St. Louis, MO). Collagenase was purchased from Calbiochem-Novabiochem, Corp. (La Jolla, CA).

Myenteric plexus cell culture. Myenteric plexus neurons from the guinea pig small intestine were isolated as previously described (Zhou and Galligan, 2000). Briefly, two new born guinea pigs (< 70g) were sacrificed by exsanguination following deep halothane anesthesia. The entire length of the small intestine was removed and placed in ice cold, sterile filtered Krebs' solution containing the following (mM): 117 NaCl, 4.7 KCl, 2.5 $CaCl_2$, 1.2 $MgCl_2$, 1.2 NaH_2PO_4, 25 $NaHCO_3$, 11 *d*-glucose with 100 units/ml penicillin and 50 μg/ml streptomycin. The small intestine was cut and lengths of small intestine 3 cm long were mounted on a glass rod and the longitudinal muscle myenteric plexus was stripped off with a cotton swab. The longitudinal muscle myenteric plexus from both animals was then minced and placed into four aliquots of 1 ml ice cold Krebs' solution containing 1.9 mg trypsin solution each (100 mg/ml stock) and incubated for 25 min at 37°C. Tissue was then triturated for approximately 4 min with fire-polished glass pipettes, then centrifuged for 5 min at 930*g*. Supernatant was discarded and tissue was resuspended in 1 ml Krebs' solution containing 2000 U collagenase and incubated for 25 min at 37°C. Tissue was then triturated again with fire polished glass pipettes and

centrifuged for 5 min at 920*g*. Supernatant was discarded and cells were resuspended in 1 ml MEM supplemented with 10% FBS, 100 units/ml penicillin and 50 μg/ml streptomycin and 10 μg/ml gentimycin. A volume of 200 μl of tissue homogenate was added to 35 mm poly-L-lysine coated cell culture dishes containing 3 ml of serum and penicillin/streptomycin antibiotic supplemented MEM. Cells for Ca^{2+} imaging experiments were plated on glass coverslips and cells for viability assays were plated without coverslips. Cells were maintained at 5% CO_2 at 37°C in a humidified environment and used between 10-14 days in culture.

Live/dead assay: The calcein-AM and ethidium homodimer viability assay is similar to that described in Chapter Two, with the exception that the length of MeHg exposure was 2 hr. To determine percentage of viable CB- or NOS-immunopositive cells, images resulting from the "live/dead" assay were compared to later images of the same cells, located in a previously demarcated (3.14 mm^2) area of the cell culture dish after cells were stained for the presence of CB or NOS.

Measurement of fura-2 fluorescence. The fura-2 loading and Ca^{2+} imaging protocol were similar to that of cerebellar Purkinje or granule neurons grown in culture and described in Chapter Two.

Immunocytochemistry. Following Ca^{2+}-imaging and viability assays, cells were stained for the presence of either CB or NOS. To fix cells for immunostaining, cells in culture

dishes were first rinsed with HBS then removed and 3 ml of Zamboni's fixative (2% v/v formaldehyde and 0.2% picric acid in 0.1 M sodium phosphate buffer pH 7.0) was added to the culture dishes and incubated overnight at 4°C. The next day Zamboni's fixative was removed by three washes of dimethylsulphoxide (DMSO) at 10 min intervals. Cells were then rinsed three times with Dulbecco's buffered phosphate solution (DBPS) which contained: (mM) 140 NaCl, 8.1 NaH_2PO_4, 0.49 $MgCl_2$, 1.47 KH_2PO_4, 2.68 KCl and 0.9 $CaCl_2$ (pH 7.3) at 10 min intervals and then incubated overnight with either mouse anti-CB antibody (1:100 dilution in DBPS) or mouse anti-NOS antibody (1:200 dilution in DBPS) in a humidified chamber at 4°C. After primary antibody incubation, cells were rinsed three times in DBPS and then incubated with goat anti-mouse IgG (1:50 dilution in DBPS) conjugated to TRITC in a humidified chamber for 1 hr.

Statistics. For data on the time-to-onset of $[Ca^{2+}]_i$ increases, one *n* value represents the average responses from 2 to 3 cells recorded simultaneously on a single coverslip. Comparisons for cell viability for each exposure group were made using a one-way or two-way analysis of variance (ANOVA) and/or students t-test. Percent data were square root transformed prior to statistical analysis. When multiple cell types and MeHg concentration were compared, a two-way ANOVA was used, if a single cell type with multiple MeHg concentrations was compared, a one-way ANOVA was used. If significant differences between sample means were detected, a *post-hoc* Tukey-Kramer test was performed to ascertain which mean values were significantly different. Values of $p < 0.05$ were considered to be statistically significant.

RESULTS

Myenteric plexus neurons did not exhibit neurite outgrowth or large, round soma until after 3 - 4 days in culture. Both neuronal and non-neuronal cell types were present in the myenteric plexus cell cultures, as determined by cell morphology and overall size. Despite the addition of 10 μM Ara-C to cell growth medium 3 days after isolation, neuron density was sparse as compared to non-neuronal cells, the ratio of non-neuronal : neuron cell types was approximately 7 : 1. MeHg caused a significant concentration-dependent decrease in myenteric plexus cell (neuron and non-neuronal) viability after exposure to 5 μM MeHg compared to HBS-alone control (Fig. 4.1). In addition, neuronal and non-neuronal myenteric plexus cells tended to show lack of cell adhesion by 24.5 hr after cessation of exposure to 5 μM MeHg (Fig. 4.2). No attempt was made to establish a time course for either myenteric plexus cell viability or loss of adhesion after MeHg exposure. Other cell types such as the PC12 cells have a similar loss of cell adhesion following exposure to higher concentrations of MeHg (see Chapter 3). AH neurons which were CB immunopositve, tended to grow in clusters of 4 - 5 cells (Fig. 4.3). The average number of myenteric plexus neurons that were CB immunopositive and located within the area demarcated by the circular marking objective (surface area = 3.14 mm^2) was 5 ± 0.8 in non-MeHg treated culture dishes. The percentage of viable neurons that were also CB-immunopositive was significantly increased in the 5 μM MeHg treatment group compared to HBS-alone control treated culture dishes (Fig. 4.6). The number of NOS immunopositive cells was 4.2 ± 1.2 within the area demarcated by the marking objective in MeHg-free culture dishes. The percent of NOS immunopositive myenteric plexus

neurons that were viable after MeHg exposure was significantly less following exposure to MeHg at 5 μM compared to HBS-alone control treatment group. Furthermore no NOS immunopositive cells were detected in the 5 μM MeHg treatment group (Fig. 4.8).

Intracellular [Ca^{2+}] was monitored as measured by changes in fura-2 fluorescence to examine further the mechanisms by which MeHg may cause cell death in CB immunopositive and NOS immunopositive (CB immunonegative) myenteric plexus neurons. CB does not change the isosbestic point of fura-2 fluorescence based on studies that monitored fura-2 excitation spectra derived in the presence of 370 μM CB, therefore CB does not interfere with fura-2 fluorescence (Chard *et al.*, 1992). Figure 4.9 is a representative tracing showing a biphasic increase in fura-2 fluorescence from a CB immunopositive myenteric neuron. All cells responded to brief (2 min) exposure to a 40 mM KCl depolarizing HBS solution with a transient increase in fura-2 fluorescence then returned to baseline fluorescence. Figure 4.10 is a fura-2 tracing demonstrating that the first phase elevation of fura-2 fluorescence from a CB immunopositive neuron was due to release of Ca^{2+} from intracellular stores and the second phase increase in fura-2 fluorescence was due to entry of Ca^{2+}_e. No second phase elevation of fura-2 fluorescence was observed when MeHg was applied in a Ca^{2+}-free, EGTA (20 μM) containing buffer. No attempt was made to determine the source of fura-2 fluorescence increase in NOS immunopositive myenteric plexus neurons. However, NOS immunopositive neurons did have a biphasic increase of fura-2 fluorescence. MeHg caused a biphasic increase in fura-2 fluorescence

Figure 4.1 Percent myenteric plexus cell viability (neuronal and non-neuronal) decreased significantly at 2 and 5 μM MeHg compared to control. Cells at 10 – 14 DIV were exposed to MeHg or HBS (control) for 2 hr; cell viability was assayed 24.5 hr later. No dead cells were observed after addition of HBS. After data were square root transformed, one-way ANOVA revealed significant differences ($P < 0.001$) from MeHg-free treated treatment group, as indicated by the asterisk (*). Data are represented as mean ± SE, N = 12, 6, 7, 10, 9 for control, 0.5, 1, 2, and 5 μM, respectively.

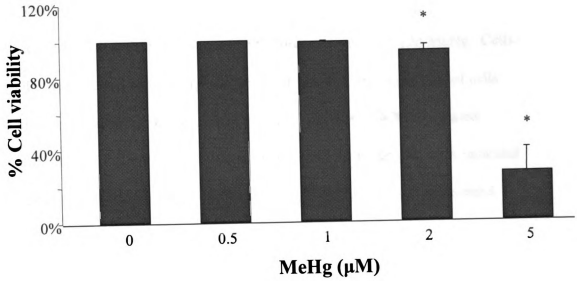

FIGURE 4.1

Figure 4.2 Number of myenteric plexus cells (neuronal and non-neuronal) per marked area on the cell culture dish decreased significantly after exposure to 5 μM MeHg. Cells at 10 – 14 DIV were treated with MeHg or HBS (control) for 2 hr; the number of cells remaining in a particular area was counted 24 hr later. One-way ANOVA revealed significant differences ($P < 0.001$) from MeHg-free control treatment group, as indicated by the asterisk (*). Data are represented as mean ± SE, N = 12, 6, 7, 10, 9 for control, 0.5, 1, 2, and 5 μM, respectively.

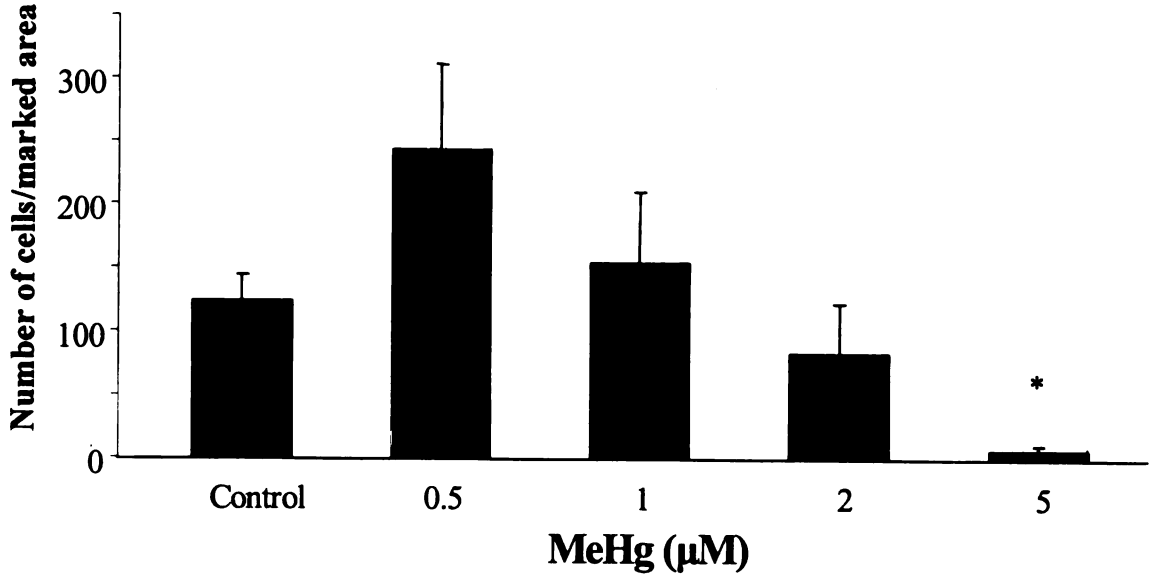
Number of cells/marked area
300
200
100
0
*
Control
0.5
1
2
5
MeHg (µM)

FIGURE 4.2

Figure 4.3 A-C Viability assay (HBS control) of myenteric plexus neurons grown in culture for 11 days. Panel A) light photomicrograph of myenteric plexus neurons. Panel B) photomicrograph after viability assay. Green fluorescent indicate that the cell is viable; red fluorescence indicate that the cell is dead. Panel C) photomicrograph of the same cells in A and B staining positive for the presence of CB. Figure 4.3 D-F Viability assay of myenteric plexus neurons 24 hr after 5 μM MeHg exposure. Panel D) light photomicrograph of myenteric plexus neurons at 12 days in culture. Panel E) Myenteric plexus neurons after exposure to 5 μM MeHg. Panel F) The same neurons in panels A and B stained for the presence of CB.

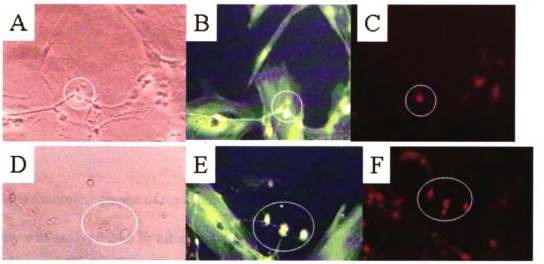

FIGURE 4.3

Figure 4.4 Photomicrographs of myenteric plexus cells treated with 5 μM MeHg for 2 hr; viability was assayed 24.5 hr after cessation of MeHg exposure. Panel A) Light-contrast photomicrograph of myenteric plexus cells after treatment with 5 μM MeHg. Panel B) Photomicrograph of the same cells in panel A after calcein-AM/ethidium-homodimer viability assay.

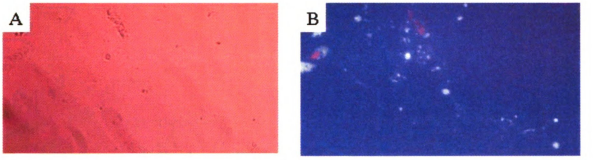

FIGURE 4.4

Figure 4.5 Panel A) Light-contrast photomicrograph of myenteric plexus cells. Panel B) photomicrograph of the same cells in panel A treated with TRITC conjugated secondary antibody alone (no primary antibody) and excited at 550 nm.

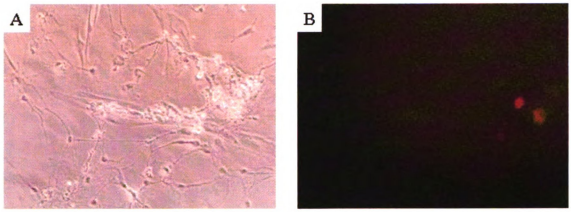

FIGURE 4.5

Figure 4.6 Percent of viable cells that were also CB immunopositive increased with MeHg exposure. A significant increase (*) was detected in percent live and calbindin CB immunopositive cells at the 5 μM MeHg treatment group compared to HBS-alone control (one-way ANOVA, P = 0.046) data are mean ± SE, N = 5, 3,3 for control, 2 and 5 μM MeHg, respectively.

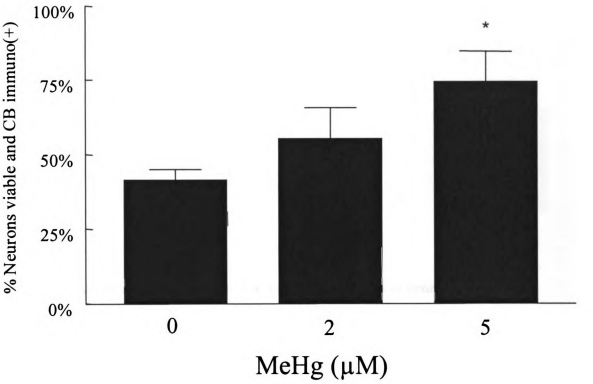

FIGURE 4.6

Figure 4.7 Viability assay of NOS immunopositive myenteric plexus neurons 24 hr after 2 μM MeHg exposure. Panel A) depicts a light photomicrograph of myenteric plexus neurons at 14 days in culture. Panel B) illustrates cytotoxicity induced in myenteric plexus neurons after exposure to 2 μM MeHg. Panel C) illustrates the same neurons in panels A and B stained for the presence of NOS.

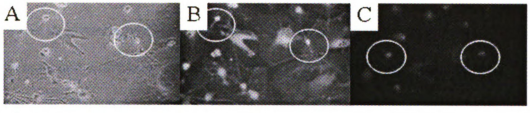

FIGURE 4.7

Figure 4.8 The percentage of viable myenteric plexus neurons that were also NOS immunopositive decreased significantly at 5 μM MeHg compared to control. Cells at 10 – 14 DIV were treated with MeHg or HBS (control) for 2 hr, then cell viability was assayed 24 hr later. Cells were then fixed and immunostained for the presence of NOS. No viable, NOS immunopositive cells were observed at the 5 μM MeHg treatment group. After data were square root transformed, one-way ANOVA revealed significant differences ($P < 0.001$) from control, MeHg-free treatment group, as indicated by the asterisk (*). Data are represented as mean ± SE, N = 10, 6, 7, 7, 7 for control, 0.5, 1, 2 and 5 μM MeHg, respectively.

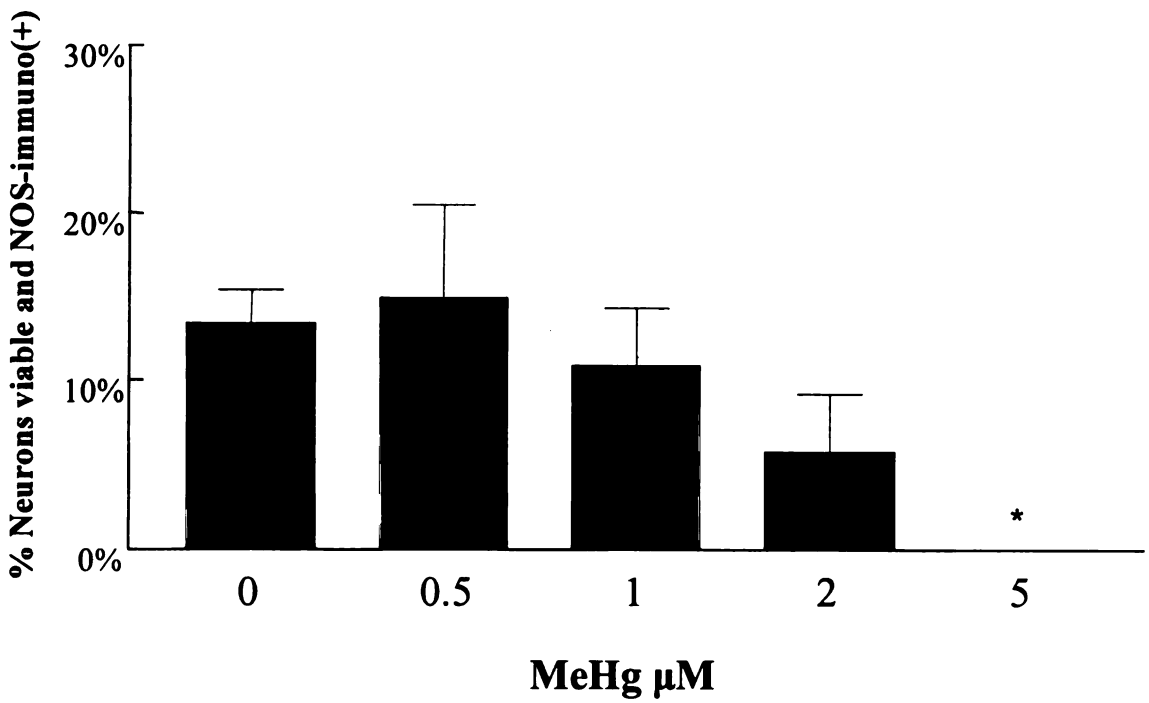

FIGURE 4.8

Figure 4.9 A representative tracing showing changes in fura-2 fluorescence in a CB immunopositive myenteric plexus neuron exposed to 1 μM MeHg. A biphasic increase in fura-2 fluorescence was observed after continuous perfusion with MeHg.

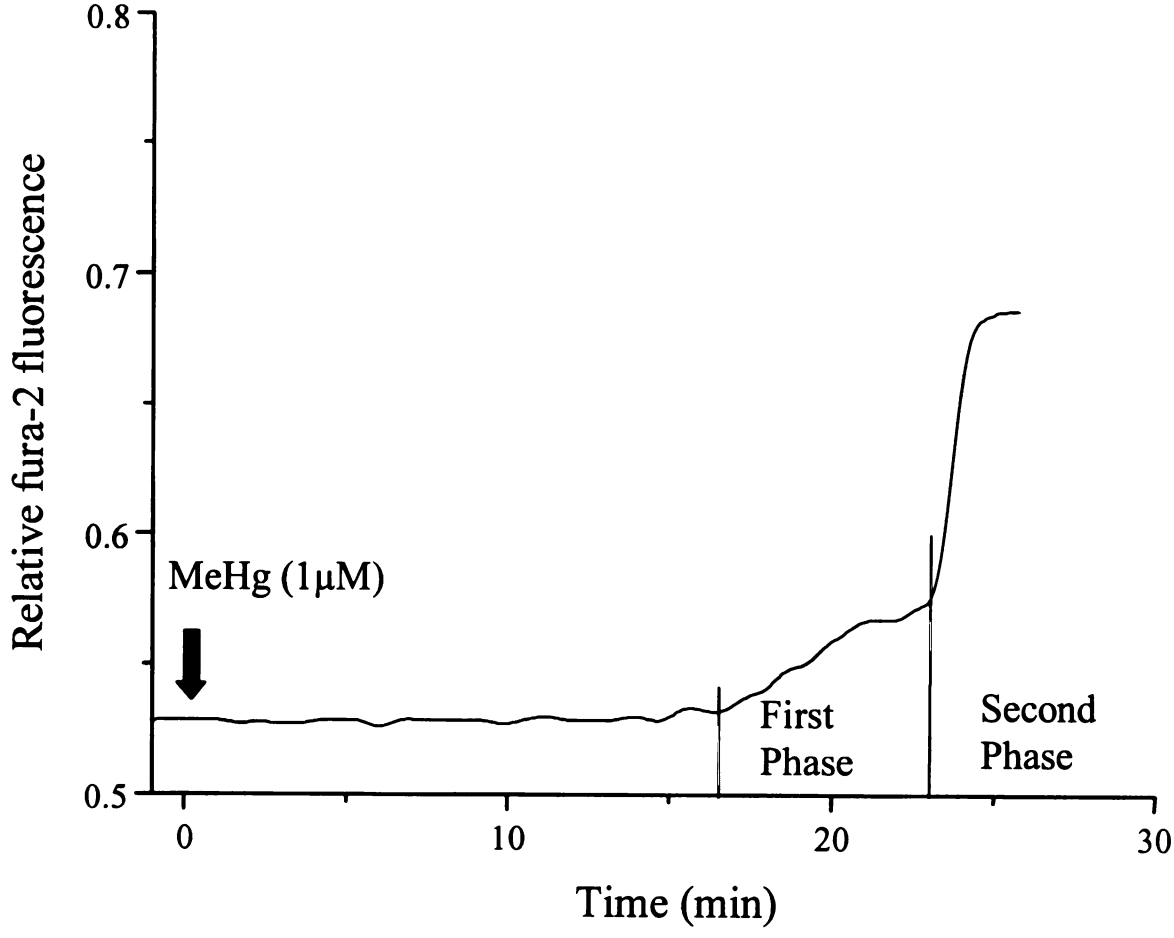
0.8
0.7
0.6
0.5
Relative fura-2 fluorescence
MeHg (1μM)
First
Phase
Second
Phase
0
10
20
30
Time (min)

FIGURE 4.9

Figure 4.10 This representative tracing depicts changes in fura-2 fluorescence from CB immunopositive myenteric plexus cell elicited during perfusion with 2 μM MeHg in Ca^{2+}-free, 20 μM EGTA-containing HBS.

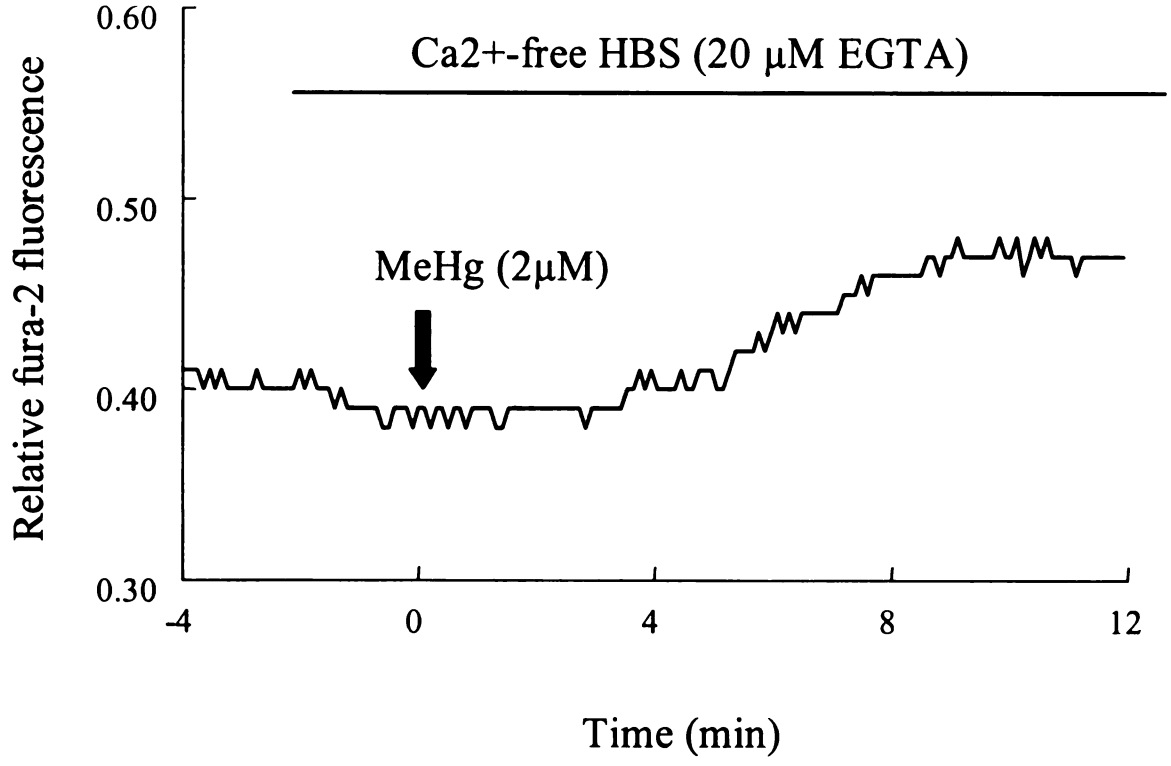
Ca2+-free HBS (20 μM EGTA)
MeHg (2μM)
Relative fura-2 fluorescence
0.60
0.50
0.40
0.30
-4
0
4
8
12
Time (min)

FIGURE 4.10

Figure 4.11 Time-to-onset of first and second phase increases of fura-2 fluorescence from CB immunopositive myenteric plexus neurons after application of MeHg. The asterisks (*) indicate significant differences within the time-to-onset first and second phase increases in fura-2 fluorescence in 0.5 and 5 μM MeHg treatment groups (two-way ANOVA, Tukey's test; $P < 0.05$). N = 3, 4, 3 and 4 for 0.5, 1, 2 and 5, respectively.

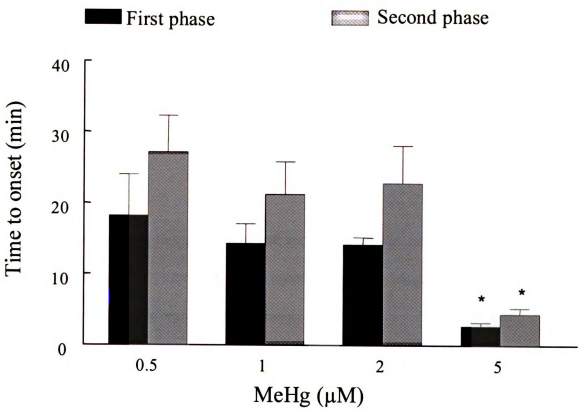
First phase
Second phase
Time to onset (min)
40
30
20
10
0
0.5
1
2
5
MeHg (μM)
*
*

FIGURE 4.11

Figure 4.12 Comparative time-to-onset of first and second phase increases of fura-2 fluorescence from CB and NOS immunopositive myenteric plexus cells during acute application of 1 μM MeHg. No significant differences in time-to-onset of elevations of fura-2 fluorescence were detected between CB and NOS immunopositive neurons (two-way ANOVA, $P = 0.132$). Data are presented as mean ± SE, $N = 4$ for CB immunopositive and $N = 3$ for NOS immunopositive neurons for the time-to-onset of both first and second phase increase in fura-2 fluorescence.

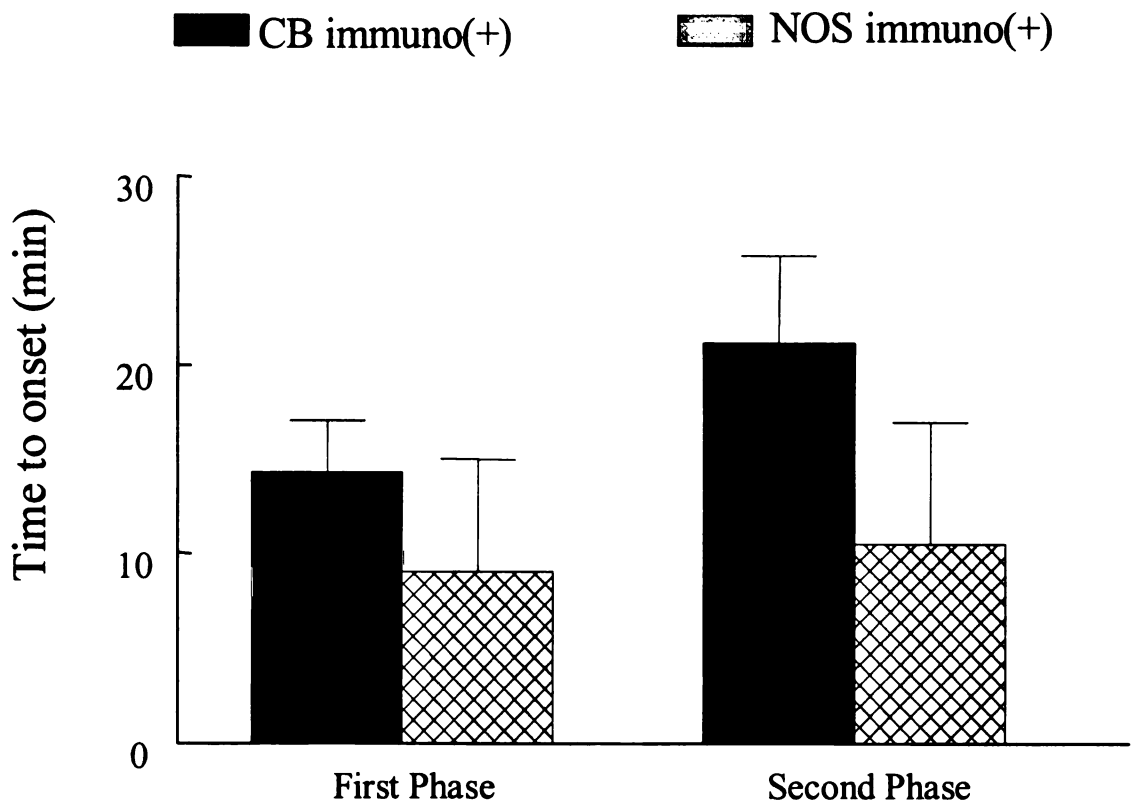
CB immuno(+)
NOS immuno(+)
Time to onset (min)
30
20
10
0
First Phase
Second Phase

FIGURE 4.12

in a concentration dependent manner in CB immunopositive myenteric plexus neurons (Fig. 4.11). There was no significant difference in the time-to-onset of elevations of fura-2 fluorescence of NOS immunopositive neurons compared to CB immunonegative neurons (Fig. 4.12, two-way ANOVA $P = 0.132$).

DISCUSSION

The main goal of this study was to examine the potential neuroprotective effects of the Ca^{2+} binding protein CB during acute exposure of MeHg to neurons. To do this, we used the myenteric plexus cell culture system isolated from the small intestine of the guinea pig. The myenteric plexus cell culture system represents a cell culture system with neurons that differentially express CB. The principal findings of this study indicate that myenteric plexus neurons that express CB are more resistant to the neurotoxic effects of MeHg than neurons that lack CB, as measured by calcein-AM and ethidium homodimer viability assay. However, at 1 μM MeHg, there was no significant difference in the time-to-onset of dysregulation of Ca^{2+} homeostasis in CB immunopositive myenteric plexus neurons and CB immunonegative neurons.

Myenteric plexus neurons that contain CB are more resistant to the neurotoxic effects of MeHg than are neurons that do not express CB. Other studies have shown that Purkinje cells, which express CB, are more resistant to MeHg-induced cytotoxicity *in vivo* (Kobyashi *et al.*, 1998; Mori *et al.*, 2000) as well as *in vitro* (Chapter 2) than are CB-negative granule cells. It is possible that the neuroprotective effects of CB during exposure to MeHg may relate to the ability of CB to chelate potentially cytotoxic $[Ca^{2+}]_i$ (Mattson *et al.*, 1991; Andressen *et al.*, 1993; McMahon *et al.*, 1998). Besides chelating $Ca^{2+}{}_i$, CB may have other cellular effects. For example, CB may modulate N-methyl-D-aspartate (NMDA) receptors (Rintoul *et al.*, 2001), or activate renal Ca^{2+},Mg-ATPase (Morgan *et al.*, 1986), CB also has high affinity for chick intestinal alkaline phosphatase

when CB is bound to Ca^{2+} (Norman and Leathers, 1982). CB alters both T- and L-type VGCC current (Lledo *et al.*, 1992), and reduces Ca^{2+} influx in dorsal root ganglion neurons (Chard *et al.*, 1993), In this study, CB-immunopositive AH neurons had a pronounced increase in fura-2 fluorescence resulting from acute application of depolarizing solutions of 40 mM KCl. Thus, endogenous CB present in AH neurons does not appear to alter VGCC activity, at least not to the same extent as in the fura-2 fluorescence studies in which CB was injected into dorsal root ganglion neurons (Chard *et al.*, 1993).

That CB may function to buffer elevated $[Ca^{2+}]_i$ in myeneric plexus neurons is important because MeHg causes dysregulation of Ca^{2+} homeostasis in a wide variety of cell types and in synaptosomal preparations (Komulainen and Bondy, 1987; Denny *et al.*, 1993; Hare and Atchison, 1995; Marty and Atchison, 1997; Edwards and Atchison, 2001; Limke and Atchison, 2002). During acute exposure to MeHg in cerebellar Purkinje neurons (Edwards and Atchison, 2001), granule cells (Marty and Atchison, 1997; Limke and Atchison, 2002), PC12 (Edwards *et al.*, 2002) and NG108-15 cells (Hare and Atchison, 1995), an initial increase in fura-2 fluorescence occurred as a result of release of Ca^{2+} from intracellular sources followed by a second increase in fura-2 fluorescence due to entry of Ca^{2+}_e through an, as yet, unidentified pathway. In AH neurons (this study) elevation of fura-2 fluorescence was from an initial release of Ca^{2+} from intracellular stores followed by entry of Ca^{2+}_e. Thus, similar cellular mechanisms may be responsible for MeHg-induced elevation of $[Ca^{2+}]_i$ in AH myenteric plexus neurons compared to the above-

mentioned studies. The source of MeHg-induced release of Ca^{2+}_i may be due to release of Ca^{2+} from mitochondria (Levesque and Atchison, 1991; Limke and Atchison, 2002) or endoplasmic reticulum (Sarafian, 1993; Hare and Atchison 1995; Limke *et al.*, 2004).

The expression of CB may be upregulated in response to elevated $[Ca^{2+}]_i$. Expression of CB is upregulated by exposure to excitatory amino acid receptor agonists in cerebellar Purkinje and hippocampal neurons (Lowenstein *et al.*, 1991; Batini *et al.*, 1997). Furthermore, exposure to the Ca^{2+} ionophore, A23187, resulted in greater CB levels in PC12 cells (Vyas *et al.*, 1994). Because MeHg causes elevation of $[Ca^{2+}]_i$ it is possible that MeHg ultimately causes the up-regulation of CB expression. However in this study, there was no apparent difference in the intensity of immunostaining for CB in MeHg-treated and non-treated myenteric plexus cells. Neither was the degree of CB immunostaining in MeHg-treated Purkinje neurons different as compared to non-MeHg treated Purkinje neurons.

There are inherent differences between AH and S type myenteric plexus neurons, other than the expression of CB, that may contribute to the differential neurotoxic effects of MeHg observed in the two cell types. During an action potential in AH neurons L- , P-/Q- , N- and R-type VGCCs open to allow Ca^{2+} entry (Bian *et al.*, 2004). This entry of Ca^{2+}_e is followed by release of Ca^{2+} from intracellular stores sensitive to ryanodine receptors in AH myenteric plexus neurons (Hillsley *et al.*, 2000,Vanden Berghe *et al.*, 2002; Vogalis *et al.*, 2003). That both AH- and S-type myenteric plexus neurons express VGCCs may be

significant because MeHg interacts with VGCCs with high specificity in a variety of cell types and preparations to block VGCC Ca^{2+} conductance (Shafer and Atchison, 1991; Shafer, 1998; Sirois and Atchison 2000; Hajela *et al.*, 2003). Furthermore, inhibition of N- and P/Q-type-VGCCs with ω-conotoxin MVIIC or L-type VGCCs with nifedipine, causes enhanced resistance to MeHg-induced cytotoxicity in cerebellar granule cells (Marty and Atchison, 1998). However the N-type VGCCs present within S-type myenteric plexus neurons appear to be very different than those expressed in AH neurons in that the N-type VGCCs are sensitive to tetrodotoxin in S-type neurons (Shuttleworth and Smith, 1999). It is unclear what these differences in N-type VGCCs in AH and S-type neurons have in MeHg-mediated neuroxicity.

In summary, this study demonstrates a correlation between expression of CB and resistance to MeHg-induced neurotoxicity in neurons grown in primary cell cultures. Additional studies are needed using neuronal-like cell lines transfected with CB expression plasmids to allow for the further elucidation of any potential and specific neuroprotective effects CB may have during MeHg exposure. Future studies demonstrating the up- or down-regulation of CB in cells following MeHg exposure would indicate a potential compensatory mechanism by which CB may be neuroprotective to MeHg-induced neurotoxicity. In addition, future studies of myenteric plexus neurons should focus on the effects of MeHg on Ca^{2+}-dependent K^+ channels in AH neurons and on what effect MeHg has on the apparent tetrodotoxin-sensitive, N-type VGCC present in S-type myenteric plexus neurons.

CHAPTER FIVE

DIFFERENTIAL EFFECTS OF METHYLMERCURY ON CALBINDIN-D28K-TRANSFECTED PHEOCHROMOCYTOMA (PC) 12 CELLS: DYSREGULATION OF Ca^{2+} HOMEOSTASIS AND CYTOTOXICITY

ABSTRACT

CB is a "buffer-type" CaBP that is associated with enhanced resistance to Ca^{2+}-mediated cell death. A prominent effect of exposure to the environmental neurotoxicant, MeHg is the elevation of $[Ca^{2+}]_i$ that is correlated with cell death. MeHg causes selective loss of cerebellar granule cells which do not express CB. In contrast, adjacent Purkinje neurons express CB and are more resistant to MeHg-mediated elevations of $[Ca^{2+}]_i$ and cell death. To examine the potential role of CB in MeHg-mediated dysregulation of Ca^{2+} homeostasis and cytotoxicity, I exposed PC12 and PC18 cells, a sub-clone of the PC12 cells lacking VGCC, to MeHg (0.5,1,2, and 5 μM) and recorded changes in fura-2 fluorescence as well as the release of lactate dehydrogenase (LDH) as a measure of cell viability. For both cell types, there was a biphasic increase in fura-2 fluorescence following acute exposure to MeHg. Mean time-to-onset values of 2 μM MeHg-mediated first phase increases in fura-2 fluorescence were greater in CB-transfected PC12 cells, 1.8 ± 0.4, (min ± SE) compared to non-transfected PC12 cells 5.5 ± 0.3 (min ± SE), however two-way ANOVA did not reveal significant differences when all (0.5, 1, 2 and 5 μM) MeHg concentrations were tested. The time-to-onset of increases in fura-2 fluorescence in CB-tansfected and non-transfected PC18 cells was not significantly different at 1 μM MeHg. Furthermore, the rate of increase of fura-2 fluorescence during 40 mM KCl-induced depolarization was significantly less ($P \leq 0.05$) in CB-transfected PC12 cells compared to non-transfected PC12 cells. Lastly, 24 hr after cessation of 2 hr exposure of 2.5 μM MeHg resulted in 76.9% ± 1.8 and 57.2% ± 3.4 percent LDH release from non-transfected and CB-transfected PC12 cells, respectively. Thus, a potential role of CB

may be to protect against MeHg-mediated elevation of $[Ca^{2+}]_i$ and subsequent cell death.

INTRODUCTION

CB is a "buffer-type" Ca^{2+}-binding protein with four functional Ca^{2+} binding domains and is expressed in specific populations of neurons (Persechini *et al.*, 1989; Celio, 1990). Although the specific functional role of CB is unknown, it is thought that CB functions to buffer cytosolic $[Ca^{2+}]_i$ (McMahon *et al.*, 1998; Meier *et al.*, 1998). Expression of CB is tightly correlated with enhanced cell viability in a number of neurodegenerative disorders such as Parkinson's, Alzheimer's and Huntington's Diseases (Siesjo *et al.*, 1989; Iacopino and Christakos, 1990). Minamata Disease is a neurological disorder resulting from exposure to the environmental neurotoxicant, MeHg (Chang, 1977; Takeuchi and Eto, 1999). A consistent pathological observation of Minamata Disease is the global loss of granule neurons from the granule cell layer of the cerebellum (Jacobs *et al.*, 1977). Both animal and human data demonstrate that cerebellar granule cells are one of the most sensitive neuronal cell types to the toxic effects of MeHg (Hunter and Russell, 1954; Leyshon-Sorland *et al.*, 1994; Mori *et al.*, 2000). In contrast, adjacent Purkinje cells are relatively unaffected despite accumulating equal or greater concentrations of MeHg as compared to cerebellar granule cells (Leyshon-Sorland *et al.*, 1994). Purkinje cells express CB at very high levels (0.1-0.2 mM), whereas cerebellar granule cells do not (Celio, 1990). The biological factors responsible for the apparent differential response to MeHg in cerebellar granule and Purkinje neurons are currently unknown. However, the presence of CB in Purkinje cells could be an important factor in their relative resistance to MeHg-induced neurotoxicity.

Various cell types demonstrate a biphasic elevation of $[Ca^{2+}]_i$ in response to acute exposure to low concentrations (0.2 - 2 μM) of MeHg (Marty and Atchison, 1997; Hare *et al.*, 1993). The first phase increase of $[Ca^{2+}]_i$ originates from intracellular sources and the second elevation results from entry of Ca^{2+}_e (Hare and Atchison, 1995b; Limke and Atchison, 2002). These effects occur at MeHg concentrations in the 1-5 μM range in the NG108-15 cell line (Hare *et al.*, 1993), but can occur at 0.1-0.5 μM MeHg in cerebellar granule cells (Marty and Atchison, 1997). Furthermore, elevations of $[Ca^{2+}]_i$ appear to be linked to cytotoxicity in cerebellar granule neurons in primary cell culture conditions. When granule cells were pre-treated with a cell-permeable form of the Ca^{2+} chelator BAPTA, the incidence of cytotoxicity was attenuated 3.5 hr after MeHg exposure (Marty and Atchison, 1998).

In addition to chelation of $[Ca^{2+}]_i$, CB may have other effects which could contribute to a protective role in MeHg neurotoxicity. One possibility is that CB may modulate VGCC functioning (Lledo *et al.*, 1992). When CB was either injected or transfected into neurons, there was a resulting decrease in whole cell Ca^{2+} current through VGCCs (Lledo *et al.*, 1992; Chard *et al.*, 1993). VGCCs have a role in MeHg-induced dysregulation of Ca^{2+} homeostasis and subsequent cell death. The exact role that VGCCs have in MeHg-induced neurotoxicity is unclear because acute exposure of cells to low μM concentrations of MeHg blocks current carried through VGCC (Shafer and Atchison, 1991; Sirois and Atchison, 2000; Peng *et al.*, 2002; Hajela *et al.*, 2003). However in fura-2 fluorescence experiments, VGCC antagonists delay the onset of MeHg-induced

increases in fura-2 fluorescence (Hare and Atchison, 1995a; Marty and Atchison, 1997). Additionally, inhibition of N- and P-/Q- type-VGCCs with ω-conotoxin MVIIC or L-type VGCCs with nifedipine, caused enhanced resistance to MeHg-induced neurotoxicity in cerebellar granule cells (Marty and Atchison, 1998). The apparent contradictory observations from electrophysiology and Ca^{2+} imaging studies can be reconciled if MeHg *itself* enters the cell through VGCCs. As such, it is possible that CB may not only act to buffer cytotoxic levels of Ca^{2+}_i, but also modulate VGCC functioning in providing protection against MeHg-induced dysregulation of $[Ca^{2+}]_i$ and subsequent cytotoxicity.

Neurons in mixed cell cultures that express CB are more resistant to cytotoxic effects of glutamate and Ca^{2+} ionophore exposure (Mattson *et al.*, 1991) as well as the toxic effects of MeHg as compared to neurons that do not express CB (Edwards and Atchison 2003). The purpose of this study was to determine if the presence of CB alone could alter MeHg-induced disruption of Ca^{2+} homeostasis and subsequent cytotoxicity. To do this, I transfected CB into a cell line which does not normally express this protein. The ratiometric Ca^{2+} indicator, fura-2, was used to subsequently monitor changes in $[Ca^{2+}]_i$ induced by MeHg in both CB-transfected and non-transfected PC12 cells. In addition, release of LDH was used as a measure of cell viability following MeHg treatment. PC18 cells, a sub-clone of PC12 cells, lack functional VGCCs and were used to examine potential interactions between CB and VGCCs. Therefore, the second goal of this study was to determine if the potential protective effects of CB on MeHg-induced dysregulation of Ca^{2+} homeostasis are associated with the expression of VGCCs.

METHODS

Materials. FuGENE (1814443) transfection reagent was purchased from Roche (Indianapolis, IN).

PC12 and PC18 cell culture conditions. Culture conditions for PC12 and PC18 cells are the same as described in Chapter Three with the exception that both cell types cells were undifferentiated and plated on 35mm culture dishes (plating density 1 X 10^5 cells per dish) with collagen-coated glass coverslips for fura-2 fluorescence experiments, and collagen-coated culture dishes without coverslips, for viability assays. Cells were not differentiated by adding NGF to cell culture medium because transfection efficiency is increased greatly in rapidly replicating cells as compared to slowly replicating cells. Differentiating agents, such as NGF, slow the rate of replication.

Measurement of fura-2 fluorescence changes. The ratio-metric Ca^{2+} fluorophore, fura-2 was used in experiments to monitor divalent cation flux from PC12 and PC18 cells as described in Chapter Three. To quantify the rate of increase in fura-2 fluorescence during application of depolarizing solutions of 40 mM KCl on CB-transfected and non-transfected PC12 cells, baseline and peak amplitude of fura-2 fluorescence (340/380) as a result of depolarization subsequent to exposure to 40 mM KCl were recorded. The difference in baseline and peak amplitude of fura-2 fluorescence was divided by the length of time required to achieve peak amplitude of fura-2 fluorescence during depolarization.

Transfection of CB. One day after cells were plated in culture dishes, PC12 and PC18 cells were transiently transfected using the FuGENE 6 transfection reagent. Briefly, expression plasmids (pcDNA3) containing a CB sequence (CB expression plasmids were a generous gift from Dr. Sylvia Christakos, University of Medicine and Dentistry of New Jersey) and plasmids containing a green fluorescence protein (GFP) sequence were co-transfected into PC12 and PC18 cells (4:1, CB:GFP, v:v). GFP fluorescence was verified and experiments completed 24-48 hrs after transfection. Only transfected cells that were GFP positive were used in the Ca^{2+} imaging experiments.

LDH assay: Cell culture medium was removed from cell culture dishes and then cells were rinsed 3X in 37°C sterile-filtered HBS prior to application of MeHg. HBS containing MeHg was applied to cells for 2 hr, after which, the cell culture medium was replaced. LDH activity was assayed 24 hr after replacement of medium. Our lab has observed significant loss of PC12 cell adhesion following exposure to high (5 μM) MeHg concentrations (see Chapter Three). To remove the potential live and non-adhering cells present in the medium, a 1ml sample of medium was taken from each cell culture dish and centrifuged (920*g* for 5 min) immediately prior to the LDH assay. A 0.3 ml sample of the centrifuged medium was removed from the top portion of the centrifuge tube and added to 2.8 ml of KH_2PO_4/K_2HPO_4 (0.1 M) (pH 7.5) with 11 mM Na-pyruvate and 12.5 mM NADH-K_2 and then assayed for LDH activity. The remaining medium in the cell culture dish was then removed and 0.3 ml of a 0.1% triton-X solution added to lyse the

adhering cells. Cell lysate was then measured for LDH activity. To quantify LDH activity, changes in absorbance at 340 nm were recorded over a 2 min period using a Beckman DU-600 spectrophotometer. LDH data are represented as the percent LDH release by recording the amount of LDH released (medium) divided by total LDH activity (lysate) multiplied by 100.

Statistics. For all fura-2 fluorescence data, one *n* value represents the average response from 2 to 6 PC12 or PC18 cell soma recorded simultaneously on a single coverslip. Data were analyzed using the Sigma Stat statistical program (Point Richmond, CA). Percent viability data were square root transformed prior to statistical analysis. Mean values were compared using a one-way or two-way analysis of variance (ANOVA) or students t-test, as appropriate. If significant differences between sample means were detected ($P \leq 0.05$), a *post-hoc* Tukey-Kramer test was performed to ascertain which mean values were significantly different.

RESULTS

PC12 cells that were GFP positive were CB-immunopositive as well (Fig. 5.1). Approximately 5-10% of non-differentiated PC12 and PC18 cells were GFP positive after transfection (Fig. 5.2). CB does not change the isosbestic point of fura-2 fluorescence based on studies that monitored fura-2 excitation spectra derived in the presence of 370 μM CB; therefore CB does not interfere with fura-2 fluorescence (Chard *et al.*, 1993). For Ca^{2+}-imaging experiments, an initial 40 mM KCl-induced depolarization was performed prior to acute application of MeHg to PC12 cells. The rate of increase of fura-2 fluorescence during depolarization was significantly less in CB-transfected as compared to non-transfected PC12 cells (Fig. 5.3). Similar actions of CB on the inhibition of Ca^{2+} influx and attenuated elevations of $[Ca^{2+}]_i$ during depolarization have been observed in various neuronal cell types using electrophysiology (Lledo *et al.*, 1992) as well as Ca^{2+}-imaging techniques (McMahon *et al.*, 1998; Chard *et al.*, 1993). In this study, there was no apparent difference in basal fura-2 fluorescence intensity in CB-transfected cells compared to that of non-tranfected or vector-transfected PC12 (Fig. 5.3) or PC18 cells. There was no apparent difference in the MeHg-induced rate of increase of fura-2 fluorescence for either first or second phase elevation of fura-2 fluorescence. Both CB-transfected (Fig. 5.4A) and non-CB-transfected PC12 (Fig. 5.4B) and PC18 cells responded to acute application of MeHg with a biphasic increase in fura-2 fluorescence. In this study, no experiments were performed to determine the source of the MeHg-mediated biphasic increase in fura-2 fluorescence. However, in other studies in our lab we have shown that the initial increase

Figure 5.1 Photomicrographs demonstrating successful transfection of CB plasmids in undifferentiated PC12 cells. Panel A is a light-contrast photomicrograph of the same PC12 cells shown in panels B and C. Panel B is a photomicrograph of PC12 cells demonstrating GFP fluorescence 48 hr after transfection. Panel C shows that the same PC12 cells in the other two panels are also immunopositive for CB.

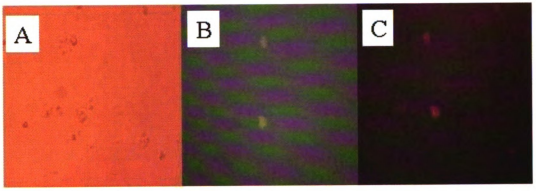

FIGURE 5.1

Figure 5.2 Photomicrographs demonstrating successful transfection of CB plasmids in undifferentiated PC18 cells. Panel A is a light-contrast photomicrograph of the same PC18 cells shown in panel B. Panel B is a photomicrograph of PC18 cells demonstrating GFP fluorescence 48 hr after transfection.

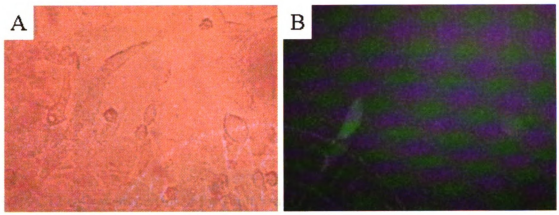

FIGURE 5.2

Figure 5.3 PC12 cells were perifused for 2 min with a solution of 40 mM KCl, and resulting changes in fura-2 fluorescence ($F_{340/380}$) were recorded. Representative $F_{340/380}$ tracings from CB-transfected and non-transfected PC12 cells are shown in panels B and C, respectively. Vector plasmid transfected control cells had similar fura-2 response compared to non-transfected cells (panel D). Significant differences were detected (panel A) in the rate of change of $F_{(340/380)}$ during depolarization in CB- transfected (diagonal) and non-transfected PC12 cells (solid), P = 0.002 (t-test), mean ± SE, N = 4.

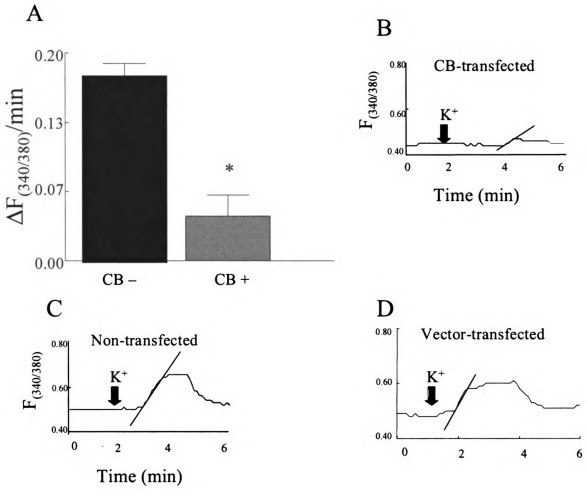
A
0.20
0.13
0.07
0.00
ΔF(340/380)/min
*
CB –
CB +
B
CB-transfected
0.80
0.60
0.40
F(340/380)
K+
0
2
4
6
Time (min)
C
Non-transfected
0.80
0.60
0.40
F(340/380)
K+
0
2
4
6
Time (min)
D
Vector-transfected
0.80
0.60
0.40
K+
0
2
4
6

FIGURE 5.3

Figure 5.4 Representative tracings showing changes in fura-2 fluorescence from CB-transfected (A) and non-transfected (B) PC12 cell during exposure to 2 μM MeHg. A typical biphasic response to MeHg exposure was observed in all experiments.

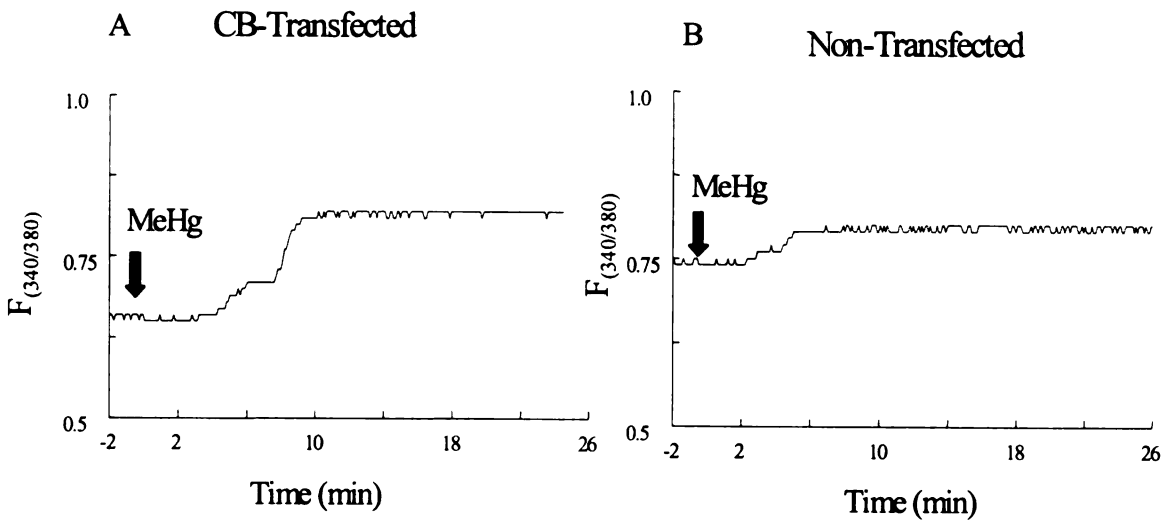
A
CB-Transfected
B
Non-Transfected
1.0
0.75
0.5
F(340/380)
MeHg
-2
2
10
18
26
Time (min)

FIGURE 5.4

Figure 5.5 Time-to-onset of first phase increases of fura-2 fluorescence from CB-transfected (diagonal) and non-transfected PC12 cells (solid) after application of MeHg. No significant differences in time-to-onset were detected for first phase (P = 0.054). Data are represented as mean ± SE, N = 5, 3, 5 and 3 for non-transfected PC12 cells at 0.5, 1, 2 and 5 μM MEHg treatment groups. Data are represented as mean ± SE, N = 5, 2, 3 and 4 for CB-transfected PC12 cells at 0.5, 1, 2 and 5 μM MeHg treatment groups.

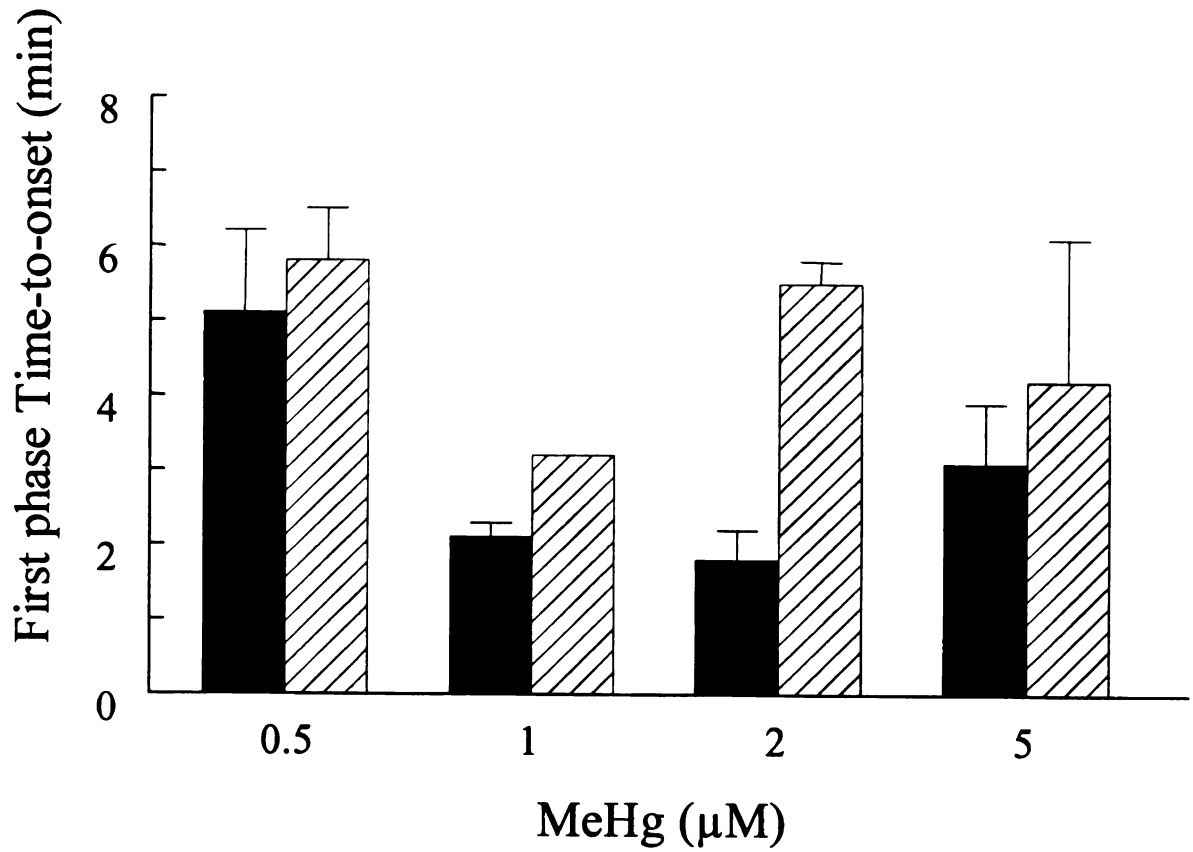

FIGURE 5.5

Figure 5.6 Time-to-onset of second phase increases of fura-2 fluorescence from CB-transfected (diagonal) and non-transfected PC12 cells (solid) after application of MeHg. No significant differences in time-to-onset were detected for second phase elevation of fura-2 fluorescence ($P > 0.05$). Data are represented as mean ± SE, N = 5, 3, 5 and 3 for non-transfected PC12 cells at 0.5, 1, 2 and 5 μM MeHg treatment groups. Data are represented as mean ± SE, N = 5, 2, 3 and 4 for CB-transfected PC12 cells at 0.5, 1, 2 and 5 μM MeHg treatment groups, respectively.

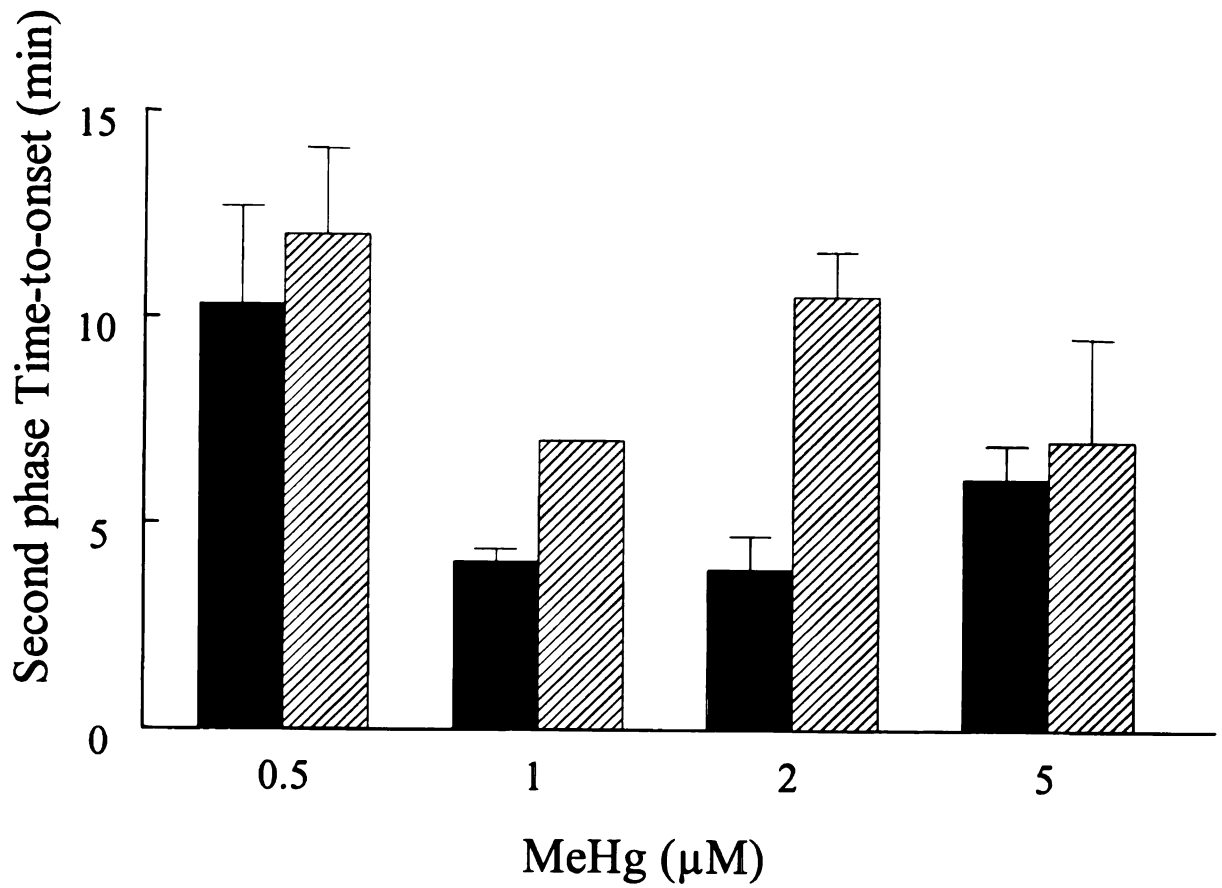

FIGURE 5.6

Figure 5.7 Time-to-onset of first and second phase increases of fura-2 fluorescence from CB-transfected PC18 cells (diagonal) and non-transfected PC18 cells (solid) resulting from acute application of 1 μM MeHg. No significant differences were detected between CB- or non-transfected PC18 cell time-to-onset of first phase (student's t-test, $P > 0.05$) or second phase ($P > 0.05$). Data are represented as mean ± SE, for both first and second phase time-to-onset, N = 3 and 4 for CB-transfected and non-transfected PC18 cells, respectively.

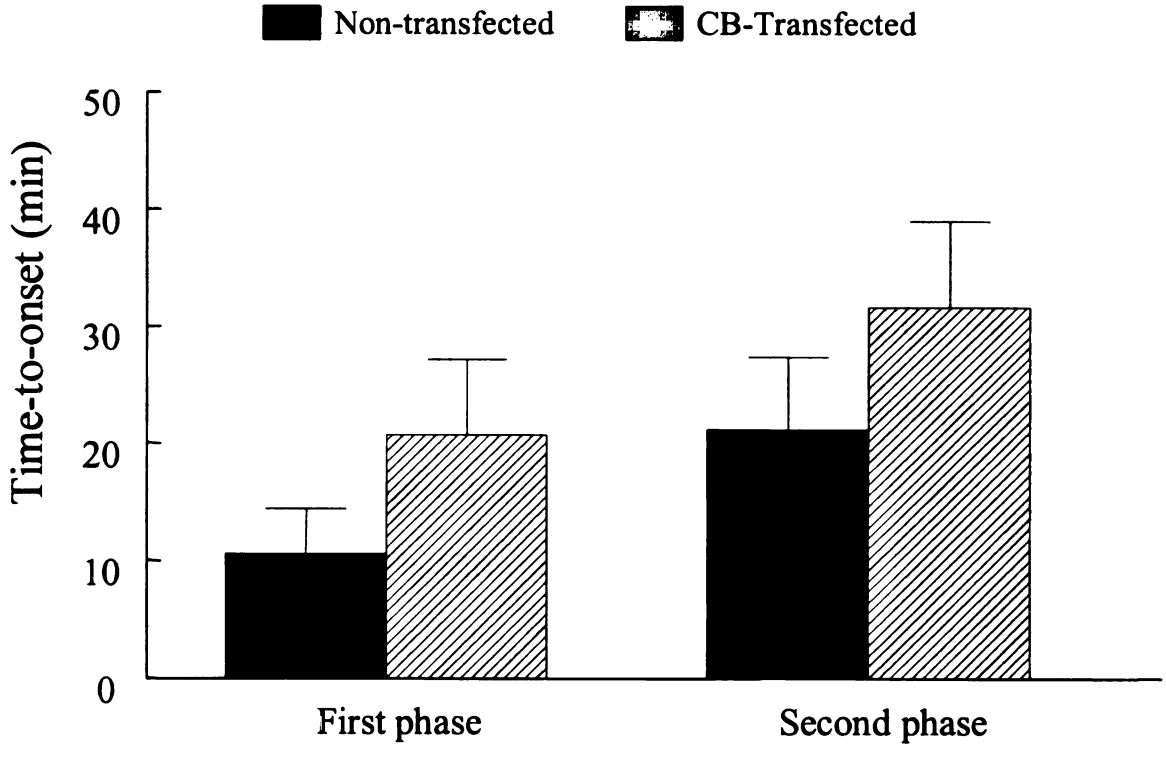
Non-transfected
CB-Transfected
Time-to-onset (min)
50
40
30
20
10
0
First phase
Second phase

FIGURE 5.7

Figure 5.8 Effects of CB on LDH release from MeHg treated PC12 cells. Release of LDH was significantly lower, as indicated by the asterisk (*) (two-way ANOVA, $P < 0.001$) in CB-transfected PC12 cells as compared to non-transfected control values, after exposure to MeHg N = 3 for each treatment group. Cells were treated for 2 hr with MeHg. LDH release was measured 24 hr after cessation of MeHg exposure.

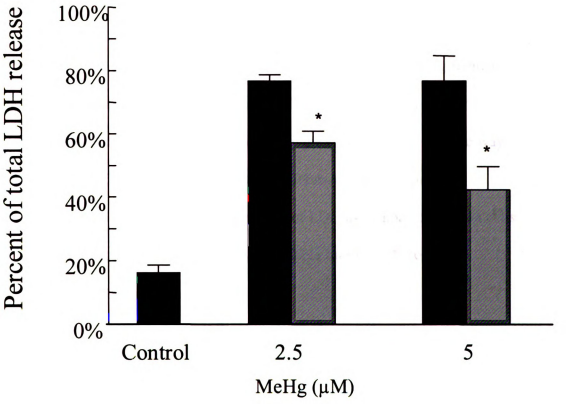
Percent of total LDH release
100%
80%
60%
40%
20%
0%
*
*
Control
2.5
5
MeHg (μM)

FIGURE 5.8

Figure 5.9 Effects of 10 μM BAPTA-AM on LDH release from 2 μM MeHg-treated PC18 cells 24 hr post-MeHg exposure. Release of LDH was significantly greater compared to DMSO control (0.1% v:v) as indicated by the single asterisk (*) (one-way ANOVA, $P < 0.001$). PC18 cells pre-treated with BAPTA-AM for 2 hr prior to application of MeHg had significantly greater release of LDH as compared to PC18 cells treated with 2 μM MeHg alone, as indicated by the double asterisk (**) (one-way ANOVA, ($P < 0.001$). Data are mean ± SE, N = 3.

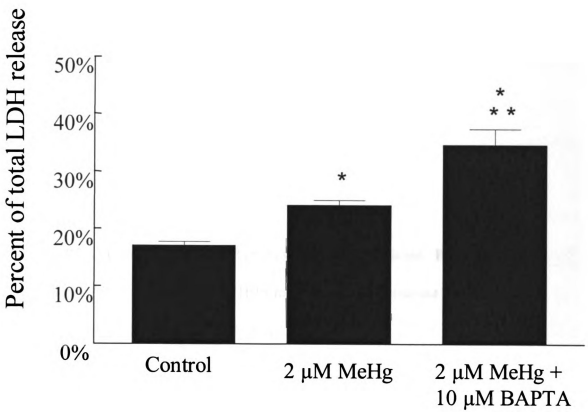
Percent of total LDH release
50%
40%
30%
20%
10%
0%
*
* *
Control
2 μM MeHg
2 μM MeHg +
10 μM BAPTA

FIGURE 5.9

Figure 5.10 BAPTA-AM (100 μM) caused an elevation in LDH release. PC12 cells were incubated in BAPTA-AM containing HBS for 2 hr then LDH release was measured 24 hr after cessation of exposure to BAPTA-AM.

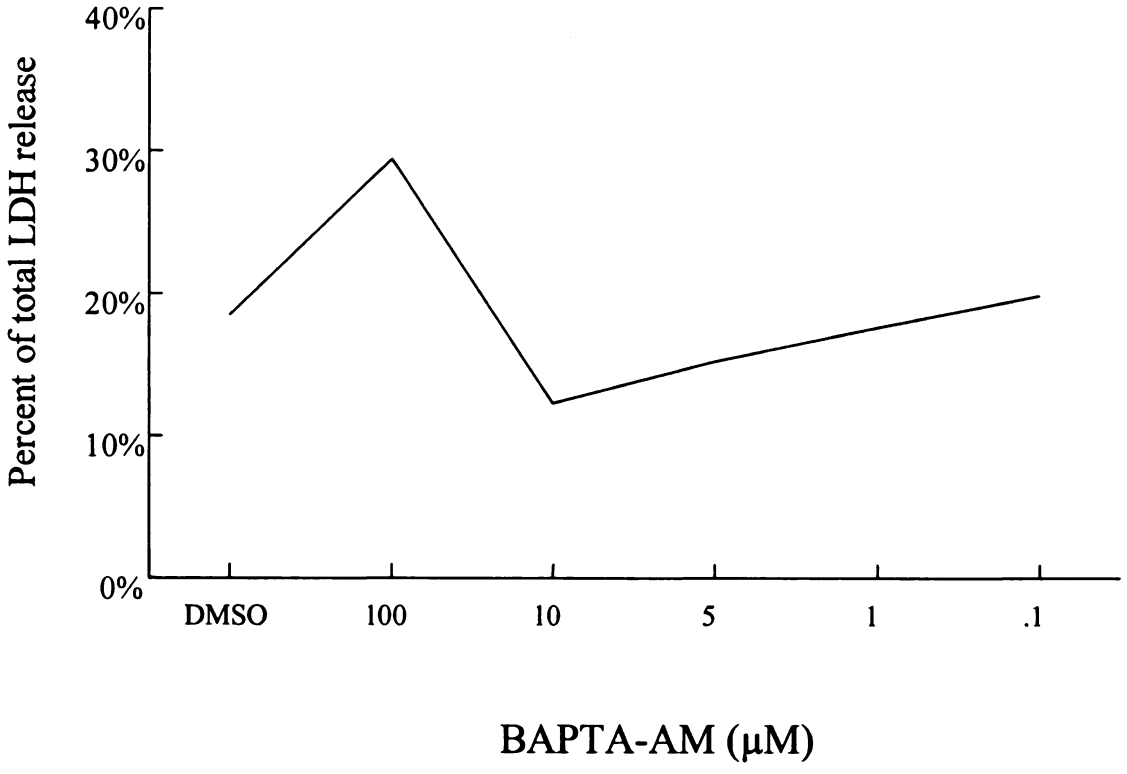
40%
30%
20%
10%
0%
Percent of total LDH release
DMSO
100
10
5
1
.1
BAPTA-AM (μM)

FIGURE 5.10

of fura-2 fluorescence was due to release of Ca^{2+} from intracellular stores while the second increase was due to entry of Ca^{2+}_e in both PC12 and PC18 cells (see chapter 3).

Mean time-to-onset values of first phase increase in fura-2 fluorescence in CB-transfected PC12 cells compared to non-transfected PC12 cells (Fig. 5.5) were not significantly different (two-way ANOVA, P = 0.054). However the mean time-to-onset increases of fura-2 fluorescence tended to be delayed in CB-transfected PC12 cells in the MeHg treatment groups (Fig. 5.5). Time-to-onset values were 5.1 ± 1.1 (min ± SE) and 5.8 ± 0.7 in non-transfected and transfected PC12 cells, respectively, when cells were exposed to 0.5 μM MeHg. Mean time-to-onset of the second phase increases in fura-2 fluorescence tended to be delayed in the CB-transfected compared to non-transfected PC12 cells with 10.3 ± 2.4 (min ± SE) and 12.0 ± 2.1 in non-transfected and transfected PC12 cells, respectively, during acute exposure to 0.5 μM MeHg (Fig. 5.6). However, no statistically significant differences in time-to-onset of second phase increase in fura-2 fluorescence in CB-transfected and non-transfected PC12 cells were detected (two-way ANOVA, P > 0.05). In PC18 cells, CB-transfected cells compared to non-transfected PC18 cells did not have significant differences in time-to-onset of first phase (student's t-test, P = 0.245) or second phase (student's t-test, P = 0.331) increase in fura-2 fluorescence as a result of acute application of 1 μM MeHg (Fig. 5.7).

Because CB-transfected PC12 cells displayed a trend of having a more delayed time-to-onset of dysregulation of Ca^{2+} homeostasis compared to non-transfected PC12 cells, I

wanted to examine what effects CB had on cell viability after MeHg exposure. Release of LDH was chosen as a measure of cell viability because LDH is commonly used to assay cell viability in clonal cell lines. Other cell viability assays such as the ethidium homodimer/calcein-AM cell viability assay would not be suitable due to potential complications arising from GFP and calcein-AM having similar emission spectra: 515 nm and 509 for calcein-AM and GFP, respectively. Figure 5.8 shows PC12 cell viability as measured by LDH release after 2.5 and 5 μM MeHg exposure was significantly less (two-way ANOVA, $P < 0.001$) in CB-transfected PC12 cells compared to non-transfected PC12 cells.

In PC18 cells, 2 hr pre-treatment with 10 μM BAPTA-AM prior to 2 μM MeHg significantly increased the release of LDH as compared to 2 μM MeHg treatment alone (one-way ANOVA, $P < 0.001$, Fig. 5.9). To determine if the apparent neuroprotective effects of CB are related solely to the Ca^{2+} buffering capacity of CB, PC12 cells were treated with the intracellular Ca^{2+} chelator, BAPTA-AM. Because previous studies have shown that BAPTA-AM may be harmful to neurons, a concentration-response experiment was performed to determine the highest BAPTA-AM concentration that does not result in elevated LDH release, (Fig. 5.10). 24 hr exposure to 100 μM BAPTA-AM resulted in elevated LDH release while, lower concentrations of 10, 5, 1 and 0.1 μM BAPTA-AM resulted in LDH release similar to application of the solvent, DMSO, alone ($N = 1$).

DISCUSSION

The primary findings of this study are as follows 1) The rate of increase of fura-2 fluorescence during exposure to depolarizing solutions of KCl was significantly less in CB-transfected PC12 cells compared to non-trasfected PC12 cells. 2) There was no statistically significant effect of CB to delay the time-to-onset of first or second phase MeHg-induced elevation of fura-2 fluorescence in PC12 cells. 3) CB-transfected PC18 cells, which lack functional VGCCs, exhibit no significant difference in time-to-onset of increases in fura-2 fluorescence resulting from exposure to 1 μM MeHg 4) LDH release was significantly less in CB-transfected PC12 cells as compared to non-transfected PC12 cells. 5) A cell permeable form of the Ca^{2+}_i chelator, BAPTA, did not save PC18 cells from the cytotoxic effects of 2 μM MeHg. Collectively, these results indicate that CB may be one determining factor in how susceptible a particular cell is to MeHg-induced cytotoxicity. Specifically, the selective expression of CB in Purkinje cells may contribute to the differential neurotoxic effects of MeHg observed in cerebellar Purkinje and granule cells (Leyshon-Sorland *et al.*; 1994; Mori *et al.*, 2001; Edwards and Atchison, 2001), however CB may not be an important factor in determining how sensitive a particular cell type is to MeHg-mediated dysregulation of Ca^{2+} homeostasis.

Although CB is classified as a "buffer-type" Ca^{2+}-binding protein and is thought to buffer elevated levels of $[Ca^{2+}]_i$, studies suggest that CB may have an additional function to regulate the activity of VGCCs. Both T- and L-type Ca^{2+} current densities were significantly less in the pituitary tumor cell line, GH_3 when transfected with CB (Lledo *et*

al., 1992) compared to vector-transfected GH_3 cells. By contrast, neither K^+ nor Na^+ current densities differed in CB-transfected GH_3 compared to wild-type GH_3 cells during depolarization. In addition, CB significantly decreased whole-cell Ca^{2+} influx as measured by whole-cell voltage clamp of dorsal root ganglion neurons (Chard *et al.*, 1993). In the same study, CB-injected dorsal root ganglion neurons had an apparent decreased rate of increase of fura-2 fluorescence as compared to non-injected control neurons, when cells were depolarized from a holding potential of -80 mV to 0 mV(Chard *et al.*, 1993). In this study, we found that CB-containing PC12 cells had a significantly decreased rate of increase in fura-2 fluorescence compared to non-transfected PC12 cells during brief exposure to depolarizing, 40 mM KCl-containing solutions. CB has a high affinity for Ca^{2+} (K_d = 0.5 μM). Therefore, it will likely compete with fura-2 (K_d = 135 nM) to bind free cytosolic Ca^{2+}. Thus, the decreased rate of increase of fura-2 fluorescence is most likely at least in part, due to the Ca^{2+}-binding ability of CB competing with the Ca^{2+}-binding ability of fura-2. However Ca^{2+} binding ability alone would not fully explain the actions of CB on VGCCs as indicated in the above mentioned electrophysiology studies (Lledo *et al.*, 1992; Chard *et al.*, 1993).

Cerebellar Purkinje neurons express CB at very high concentrations in comparison to any other neuronal cell type, with levels of 0.1 - 0.2 mM (Celio, 1990). However, the presence of CB does not appear to cause reductions in the amplitude in fura-2 fluorescence during 40 mM KCl-induced depolarization of Purkinje cells grown in culture or acutely dissociated (Edwards and Atchison, 2001). That CB does not impede

Ca^{2+} currents in Purkinje cells may reflect the differential expression of various sub-types of VGCCs, and the possible differential effects of CB on various sub-types of VGCCs. Purkinje neurons predominately express P-type VGCCs; approximately 90% of Ca^{2+} current during depolarization is due to Ca^{2+} current carried by P-type VGCCs (Mintz and Bean, 1993). Undifferentiated PC12 cells (Shafer and Atchison, 1990) used in this study as well as the GH_3 cell line and dorsal root ganglion neurons all predominately express the L-type VGCC (Harding *et al.*, 1999). Additionally, the expression of α_{1C} and α_{1D} VGCC subunits has been detected in undifferentiated PC12 cells determined by reverse transcription polymerase chain reaction (Colston *et al.*, 1998). CB may selectively act on the α_{1C} or α_{1D} subunits of the L-type VGCC to reduce or modulate Ca^{2+} current, but not act on the α_{1A} subunit of P-type VGCCs.

Other studies have shown that inhibition of VGCCs caused enhanced resistance to the MeHg-induced dysregulation of Ca^{2+} homeostasis in NG108-15 cells and cerebellar granule cells (Marty and Atchison, 1997) as well as, enhanced resistance to MeHg-induced cytotoxicity (Marty and Atchison, 1998). MeHg interacts with VGCCs in a non-competitive and irreversible manner to inhibit Ca^{2+} (Shafer, 1998) as well as Ba^{2+} (Sirois and Atchison, 2000) current in a variety of cell types and experimental preparations. Therefore MeHg acts to inhibit VGCC function despite the lack of Ca^{2+}-induced inhibition of VGCCs when Ba^{2+} current is measured as an indicator of VGCC activity. In addition, MeHg may share the same binding site on L-type VGCCs as that of dihydropyridines such as nifedipine. In rat forebrain synaptosomes, MeHg decreases the

affinity of binding of [^{3}H] nitrendipine to L-type VGCCs (Shafer *et al.*, 1990). However, human embryonic cells transiently transfected with the α_{1C-1}, α_{2b} and β_{3a} VGCC subunits exposed to 5 μM MeHg were still responsive to the L-type VGCC antagonist nimodipine and the agonist BayK 8644 (Peng *et al.*, 2002). Thus, there are contradictory results on the effects of MeHg on L-type VGCCs.

VGCCs could act as portals for MeHg to gain access inside cells and cause dysregulation of Ca^{2+} homeostasis (Atchison, 1986; Hare and Atchison 1995a). Other heavy metals have been found to enter cells through VGCCs. Using the Ca^{2+} fluorophore, fura-2, as a direct indicator of heavy metals, entry of Pb^{2+} (Mazzolini *et al.*, 2001) and Cd^{2+} (Hinkle and Osborne, 1994) into cells was dependent upon the presence of VGCCs. Thus if MeHg enters cells through VGCCs to cause ultimately cell death, any protein such as CB that modulates VGCC activity may contribute to determining how vulnerable a particular cell type is to the neurotoxic effects of MeHg.

In comparing Purkinje neurons with cerebellar granule neurons, there was a significant delay in time-to-onset of increases of fura-2 fluorescence at the 0.5, 1 and 2 μM MeHg treatment groups (see Chapter Two). The differences in Purkinje and granule cell time-to-onset increases in fura-2 fluorescence evoked by a given MeHg concentration were more apparent as compared to the data presented in this study comparing CB-transfected and non-transfected PC12 cells. The different results from the Purkinje/granule cell and this study could represent the greater concentrations of CB in Purkinje neurons as

compared to CB-transfected PC12 cells. Though we did not measure CB levels, the expression levels of CB induced by heterologous transfection are not likely to reach those present within Purkinje neurons. Alternatively, other differences between Purkinje and granule cells such as: NMDA receptor expression, IP_3 receptor subtype expression, cell size, and expression of other CaBP could also contribute to the differential effects of MeHg on these two cell types. Purkinje cells do not express functional NMDA receptors whereas granule cells do. However, this may not be very relevant in terms of MeHg-mediated cytotoxicity because the NMDA receptor antagonists; AP-5 or MK801 did not significantly attenuate or delay MeHg-induced dysregulation of Ca^{2+} homeostasis in cerebellar granule cells (Marty and Atchison, 1997). However, administration of the NMDA antagonist, MK801, ameliorated MeHg-induced neuronal cell death in the occipital cortex in rat pups (Miyamoto *et al.*, 2001).

The significantly increased release of LDH from PC18 cells during application of the $[Ca^{2+}]_i$ chelator BAPTA-AM with MeHg was surprising. One possible explanation is that after the acetomethoxy (-AM) group is cleaved by endogenous cellular esterase activity, it can be converted to either acetic acid or formaldehyde within the cell. This is significant because AM-conjugate compounds can "bioaccumulate" within cells to several hundred times greater concentration relative to the initial concentration in aqueous buffer (Tsien *et al.*, 1982). Pre-treatment of cerebellar granule cells with 10 μM BAPTA-AM did save cells 3.5 hr post-MeHg exposure but did not have any effect on cell viability 24.5 hour post-MeHg exposure (Marty and Atchison, 1998). Other studies have demonstrated

similar decreases in cell viability or functioning after BAPTA-AM treatment during exposure to MeHg. Chick forebrain neurons treated with 10 μM BAPTA-AM were saved from MeHg-mediated inhibition of neurite outgrowth within 2 hr of MeHg application. However, after one day of 10 μM BAPTA-AM treatment alone, neurite outgrowth was impaired and chick forebrain neurons appeared damaged with pyknotic cell bodies (Heidemann *et al.*, 2001). It is possible that in this study, the addition of formaldehyde and/or acetic acid resulting from BAPTA-AM exposure acted synergistically with MeHg to cause greater LDH release from PC18 cells than MeHg only treated PC18 cells.

Future studies should focus on the possible differential effects of MeHg on the α_{1C} and α_{1A} pore-forming subunits of VGCCs in the presence of CB. Also of interest would be what effect CB anti-sense oligonucleotides have on the Purkinje cell response to MeHg.

Summary and Discussion

A. Summary of research

The studies described in this thesis used cells isolated in primary culture to examine the differential effects of MeHg on cerebellar Purkinje and granule neurons. In addition I attempted to determine what effect CB and VGCCs may have on Ca^{2+} homeostasis and cell viability during acute exposure of MeHg (0.5 - 5 μM). I have shown that Purkinje neurons grown in culture are more resistant to MeHg-induced dysregulation of Ca^{2+} homeostasis as compared to cerebellar granule neurons. This enhanced resistance to MeHg in Purkinje cells is evident in the significantly delayed time-to-onset of sustained elevations of fura-2 fluorescence when compared to cerebellar granule cells, exposed to the same concentration of MeHg. Furthermore, Purkinje cells were more resistant to the cytotoxic effects of MeHg as compared to cerebellar granule cells as determined by the ethidium homodimer/calcein-AM viability assay. Presence of CB is associated with enhanced resistance to Ca^{2+}-mediated cell death; Purkinje cells express CB at very high levels and granule cells do not (Celio, 1990). Thus, the second goal of this research was to determine the potential contribution of CB in the differential neurotoxic effects of MeHg observed in these two cell types. To begin to address this issue, sub-populations of CB-containing neurons isolated from the small intestine of guinea pigs were studied and compared to non-CB-containing neurons in the same cell isolation. CB-immunopositive myenteric plexus neurons were more resistant to MeHg-induced cell death as compared to non-CB immunopositive cells. Additionally, CB-transfected PC12 cells had significantly less LDH release 24 hr post-exposure to 2.5 and 5 μM MeHg as compared to non-

transfected cells. Furthermore mean time-to-onset values of elevations of fura-2 fluorescence in CB-transfected PC12 cells were greater compared to non-transfected cells, (although not statistically significant, two-way ANOVA P = 0.054). Lastly, the rate of increase of fura-2 fluorescence was less in CB-transfected PC12 cells compared to non-transfected PC12 cells during exposure to depolarizing solutions containing 40 mM KCl. This decrease of Ca^{2+} binding to fura-2 during cell depolarization could be the result of CB competing for Ca^{2+} binding with fura-2. However other studies using electrophysiology techniques show the presence of CB has a modulatory effect on VGCCs (Lledo *et al.*, 1992). In the experiments above, where VGCCs were either inhibited or non-functional in the PC12 or PC18 cell lines respectively, there was a resulting enhanced resistance to MeHg-mediated dysregulation of Ca^{2+} homeostasis as well as cytotoxicity. This suggests that CB may have two functional roles in protecting cells from the neurotoxic effects of MeHg: 1) chelating cytotoxic elevations of $[Ca^{2+}]_i$ and 2) possibly modifying VGCC activity.

B. Relationship to previous work

MeHg inhibits VGCC activity resulting in reduced whole cell Ca^{2+} (Shafer and Atchison, 1991) and Ba^{2+} currents (Sirois and Atchison, 2000). The effects of MeHg on VGCCs are nearly irreversible and occur in all the major sub-types of high-voltage-activated channels (L-, R-, P/Q- and N-type) at low (0.5 μM) concentrations of MeHg (Sirois and Atchison, 2000). One possibility is that MeHg inhibits VGCCs when traversing the cell membrane through VGCCs to gain entry into neurons. Some of the first experiments to suggest that

MeHg may enter cells through VGCCs were electrophysiology recordings of MEPP frequency from isolated neuromuscular junction preparations. The time-to-onset of increases of MEPP frequency was hastened during activation of VGCCs with either Bay K 8644 (Atchison, 1987) or depolarizing KCl solutions (Atchison, 1986). MEPP frequency is dependent upon $[Ca^{2+}]_i$ but not specifically on Ca^{2+} influx as is action potential evoked release. Thus these results suggest that VGCCs may act as portals for MeHg to cross phospholipid membranes into nerve terminals to cause release of Ca^{2+} from intracellular stores. Other heavy metals have been found to enter cells through VGCCs. Using the Ca^{2+} fluorophore, fura-2, as an indicator of heavy metals, entry of Pb^{2+} (Mazzolini *et al.*, 2001) and Cd^{2+} (Hinkle and Osborne, 1994) into cells was dependent upon the presence of VGCCs. Data presented in this thesis support this hypothesis. When the L-type VGCCs were inhibited by the antagonist, nimodipine, or were absent in PC18 cells, in this thesis there was a delayed time-to-onset of increases in fura-2 fluorescence as well as enhanced resistance to MeHg-mediated neurotxicity. Furthermore, previous research has shown that the L-type VGCC antagonist, nifedipine attenuates or delays the disruptive effects of MeHg on Ca^{2+} homeostasis in NG108-15 cells (Hare and Atchison, 1995) and cerebellar granule cells (Marty and Atchison, 1997). Additionally, inhibition of N- and P/Q-type-VGCCs with ω-conotoxin MVIIC or L-type VGCCs with nifedipine, resulted in enhanced resistance to MeHg-induced cytotoxicity in cerebellar granule cells (Marty and Atchison, 1998). Furthermore, when the VGCC antagonists, nifedipine, nicardipine and verapamil were co-administered with MeHg in rats there was a decrease in MeHg-related symptoms of neuronal dysfunction and

mortality (Sakamoto *et al.*, 1996).

The data presented in this thesis support the idea that MeHg might enter cells through VGCCs. Thus it is important to consider that MeHg may not only act on VGCCs to cause elevations of $[Ca^{2+}]_i$. Inhibition or desensitization of muscarinic receptors resulted in delayed time-to-onset of MeHg-induced elevations of $[Ca^{2+}]_i$ and greater cerebellar granule cell viability (Limke *et al.*, 2004). The type III muscarinic receptor is coupled to phospholipase C, an enzyme that generates IP_3.

Figure 6.1 A cartoon drawing of proposed actions of MeHg entering cells through VGCCs as well as interacting with metallothionien to cause release of Zn^{2+}. The release of Zn^{2+} from metallothionien could be one potential source of Zn^{2+} and partly explain the drop in fura-2 fluorescence observed after acute application of the heavy-metal chelator, TPEN in Purkinje neurons.

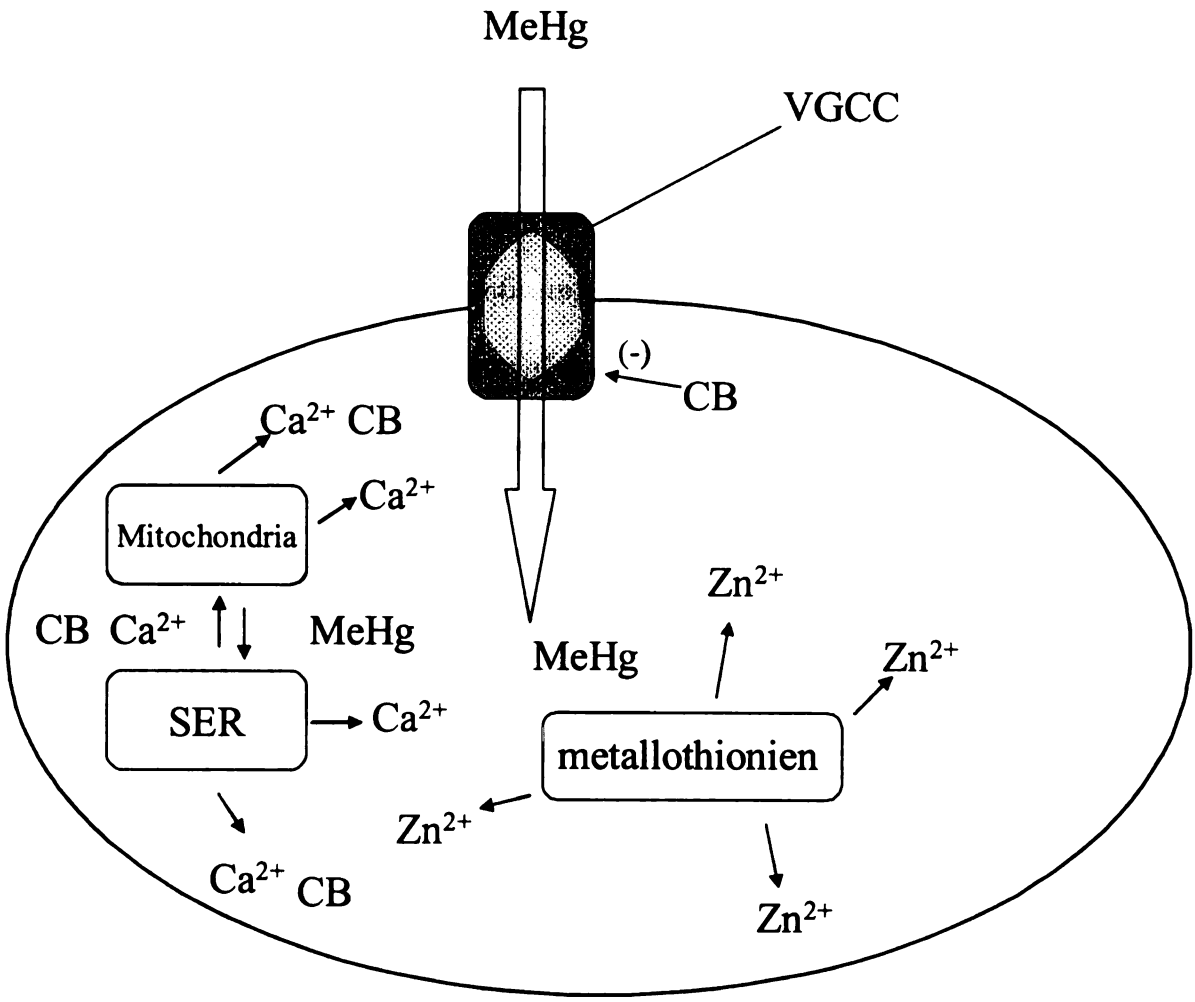
MeHg
VGCC
(-)
CB
Ca2+ CB
Mitochondria
Ca2+
CB Ca2+
MeHg
SER
Ca2+
Ca2+ CB
MeHg
Zn2+
Zn2+
metallothionien
Zn2+
Zn2+

FIGURE 6.1

Although CB is classified as a "buffer-type" CaBP and is thought to buffer elevated levels of cytotoxic $[Ca^{2+}]_i$, studies suggest that CB might have an additional function to regulate VGCCs. Both T- and L-type Ca^{2+} current densities were significantly less in the pituitary tumor cell line GH_3, transfected with CB (Lledo *et al.*, 1992). By contrast, neither K^+ nor Na^+ current densities differed in CB-transfected compared to wild-type GH_3 cells during depolarization. In addition, CB significantly decreased whole-cell Ca^{2+} influx as measured by whole-cell voltage clamp of dorsal root ganglion neurons (Chard *et al.*, 1993). Similarly, CB-injected dorsal root ganglion neurons had a significantly decreased rate of increase of fura-2 fluorescence when cells were depolarized from a holding potential of -80 mV to 0 mV (Chard *et al.*, 1993). In this thesis I found that CB-containing PC12 cells had a significantly decreased rate of increase of fura-2 fluorescence during brief exposure to depolarizing, 40 mM KCl-containing solutions. Thus, this study and the above-mentioned experimental preparations would suggest that CB may act to inhibit the activity of VGCCs. However, cerebellar Purkinje neurons express CB at very high concentrations in comparison to any other neuronal cell type, with levels of 0.1 - 0.2 mM (Celio, 1990). The presence of CB does not appear to cause reductions in the amplitude in fura-2 fluorescence during 40 mM KCl-induced depolarization of Purkinje cells (Edwards and Atchison, 2001). This may reflect the differential expression of various sub-types of VGCCs, and the possible differential effects of CB on various sub-types of VGCCs. Purkinje neurons predominately express P-type VGCCs with approximately 90% of Ca^{2+} conductance during depolarization being due to Ca^{2+} carried by P-type VGCCs (Mintz and Bean, 1993). Undifferentiated PC12 cells (Shafer and

Atchison, 1990) used in this study as well as the GH_3 cell line and dorsal root ganglion neurons, mentioned above all predominately express L-type VGCCs (Harding *et al.*, 1999). The GH_3 cell line preferentially expresses the α_{1D} VGCC subunit, however α_{1C} is also present as detected by reverse transcriptase polyclonal chain reaction (Safa *et al.*, 2001). Therefore, CB may selectively act on the α_{1C} or α_{1D} subunit of the L-type VGCC to reduce or modulate Ca^{2+} conductance.

C. Possible mechanisms underlying the comparative effects of MeHg on cerebellar Purkinje and granule cells

The cerebellar architecture may partially account for the apparent selective neurotoxic effects of MeHg-induced neurotoxicity. Golgi cells form an inhibitory feed-back loop that involves mossy fibers and cerebellar granule cells. In this pathway, excitatory mossy fibers first release glutamate on granule cell dendrites, which ultimately results in action potential propagation down the granule cell axon, or parallel fiber, to synapse with Purkinje as well as Golgi cells. The inhibitory Golgi cells release GABA on the mossy fiber/granule cell synapse upon Golgi cell activation via parallel fiber activity. This is significant because GABAergic synaptic transmission in isolated hippocampal slice preparations is more sensitive to MeHg disruption as compared to glutamatergic transmission (Yuan and Atchison, 1997). Therefore it is possible that MeHg disrupts the cerebellar granule-Golgi cell inhibitory feedback loop to cause ultimately excitotoxicity in cerebellar granule cells. Furthermore MeHg differentially affected cerebellar Purkinje and granule cells in a time- and concentration-dependent manner by first increasing then

decreasing both amplitude and frequency of spontaneous inhibitory post synaptic currents (Yuan and Atchison, 2003). Specifically, time-to-onset of block of spontaneous inhibitory post synaptic currents were significantly delayed in Purkinje cells compared to granule cells during exposure to 10, 20 and 100 μM MeHg in cerebellar slice preparations.

If the selective expression of CB was the only factor in determining the cellular sensitivity to the neurotoxic effects of MeHg, then the apparent differences in MeHg-induced time-to-onset of increases of fura-2 fluorescence from CB-transfected PC12 cells should have been greater in comparison to non-transfected PC12 cells. As such, the differences in time-to-onset of elevations of fura-2 fluorescence were much greater between Purkinje and granule cells. Thus, there are likely additional factors, other than CB, that may contribute to the differential neurotoxic effects of MeHg in Purkinje and granule cells. *In vivo* studies have shown that MeHg travels into and bioaccumulates within Purkinje neurons. Concentrations of Hg-containing compounds were co-localized with the metal-binding protein, metallothionein, in Purkinje neurons with the use of Tim's modified silver staining method (Leyshon-Sorland *et al.*, 1994). Thus, apparently MeHg accumulates within Purkinje cells by binding to metallothionien and therefore making MeHg innocuous. Furthermore, MeHg displaces Zn^{2+} from type I recombinant mouse metallothionein and binds to metallothionein with high affinity (Leiva-Presa *et al.*, 2004).

The differential neurotoxic effects of MeHg on cerebellar Purkinje and granule cells, *in vivo*, have been replicated *in vitro* and presented in this thesis. However relevant the

potential influence of the cerebellar architecture may be in the differential neurotoxic effects of MeHg *in vivo*, the cerebellar architecture alone does not account for the differential neurotoxic effects of MeHg on the dysregulation of Ca^{2+} homeostasis of Purkinje and granule cells grown in culture as reported in this thesis. Therefore other factors are likely involved in the cellular response to MeHg. Purkinje neurons express P-, N - and L-type Ca^{2+} channels with the P-type having the most Ca^{2+} current during depolarization (Mintz *et al.,* 1992). As noted above, while approximately 90% of Ca^{2+} current in Purkinje cells occurs through the P - type Ca^{2+} channel; in granule cells there are five Ca^{2+} channel types (L-, N-, P/Q-, and R-) with each sub-type contributing approximately 11-35% of the whole-cell current (Randall and Tsien 1995).

There is another potential mechanism by which CB may act to attenuate the neurotoxic effects of MeHg. Although CB lacks a nuclear localization sequence that most transcription factors have, CB may enter the nucleus to act as a transcription factor. For example, CB was found in the nucleus of nerve growth factor-differentiated PC12 cells (McMahon *et al.*, 1996) as well as in cerebellar Purkinje neurons (German *et al.*, 1997). In addition CB immunoreactivity was up-regulated during glutamate agonist exposure in cerebellar slice preparations (Batini *et al.*, 1997). Thus, another potential action of CB may be to up- or down-regulate the expression of a variety of proteins that may function to regulate Ca^{2+} homeostasis, including VGCCs or CB itself.

D. Potential mechanism of interaction between MeHg and CB

Although the cellular mechanisms of CB-VGCC interaction have not been elucidated, regulation of both NMDA receptors and VGCCs involve protein tyrosine kinase, an enzyme influenced by the action of calmodulin-dependent kinase (Guo *et al.*, 2004). When NMDA or L-type VGCCs are phosphorylated, there is a resulting increase in Ca^{2+} influx through NMDA receptors or L-type VGCCs (Liu *et al.*, 2001). It is thought that calmodulin-dependent kinase is activated by binding of Ca^{2+} which then activates protein tyrosine kinase and in turn, may phosphorylate subunits of NMDA receptors or VGCCs to cause greater influx of Ca^{2+} (Liu *et al.*, 2001). Because CB has high affinity (K_d = 0.5 μM) for Ca^{2+}, the activity of Ca^{2+} dependent calmodulin kinase may be decreased in the presence of CB. Therefore, CB may compete for Ca^{2+} binding with calmodulin and indirectly inhibit phosphorylation of both NMDA and L-type VGCCs resulting in less entry of Ca^{2+}_e and potentially less Ca^{2+} mediated cell death as a result of glutamate or MeHg exposure.

APPENDIX

A. Effects of MeHg-induced dysregulation of Ca^{2+} homeostasis on calbindin-D28k-transfected human embryonic kidney cells (HEK 293).

I have shown in previous chapters in this thesis that 1) the CB-expressing cerebellar Purkinje neurons are more resistant to MeHg-induced dysregulation of Ca^{2+} homeostasis and cytotoxicity as compared to granule neurons which do not express CB. 2) CB-containing PC12 cells are more resistant to MeHg-induced LDH release. 3) Myenteric plexus cells that express CB are more resistant to the cytotoxic effects of MeHg than are myenteric plexus cell that do not express CB. Based on the above observations of the probable cytoprotective role of CB in MeHg-mediated dysregulation of Ca^{2+} homeostasis and cytotoxicity, I hypothesized that human embyronic kidney (HEK 293) cells containing CB will be more resistant to MeHg-induced dysregulation of Ca^{2+} homeostasis than vector-transfected HEK293 cells. To test this hypothesis, I compared the fura-2 response in CB-transfected cells with vector-tranfected HEK293 cells. The HEK293 cell line represents a non-neuronal cell type of human origin. In addition, a wide variety of proteins have been expressed using HEK293 cells, making this cell line a useful tool for determining the biology of various proteins. Finally, the release of LDH, an indicator of cell viability, was recorded after MeHg exposure.

Cell culture conditions: HEK293 cells were purchased from American Type Culture Collection (ATCC) and cells were maintained in Dulbecco's Modified Eagle Medium (DMEM) (Gibco #12100-103) supplemented with 10% heat-inactivated horse serum, in a

humidified environment with 5% CO_2. During passage, cells were plated in 35mm, collagen-coated culture dishes at a density of 1 x 10^5 cells per dish. All experiments were performed on HEK293 cells from passage number 35 to 45 as determined from time of receipt of ATCC.

Calbindin transfection: Transfection of HEK293 cells is similar to the protocol presented in Chapter Five.

Figure A.1 Photomicrographs demonstrating successful transfection of CB plasmids in HEK293 cells. Panel A is a light photomicrograph of HEK293 cells. Panel B is a photomicrograph of the same cells in panel A showing immunopositivity for CB. Cells were transiently transfected with green fluorescence protein (GFP) and CB or non-CB vector expression plasmids (not shown). GFP was used as an indicator of successful transfection. Fura-2 fluorescence recordings and viability assays were conducted 24-48 hrs post-transfection. Only cells that were GFP(+) were used in fura-2 fluorescence experiments.

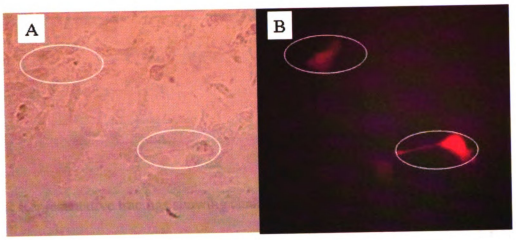

FIGURE A.1

Figure A.2 Representative tracings showing changes in fura-2 fluorescence in HEK293 cells during exposure to 1 μM MeHg. CB-transfected cells (top) lacked a pronounced increase in fura-2 fluorescence ($F_{(340/380)}$) after exposure to 1 μM MeHg as compared to vector-transfected (bottom) cells. There was little or no response to 40 mM KCl in any recording. Table showing frequency of response of increase in fura-2 fluorescence induced by MeHg in CB- and vector-transfected HEK cells. Fura-2 fluorescence was recorded from GFP(+) HEK cells 24-48 hr post-transfection. The majority of CB-transfected HEK cells did not show any sustained elevation of fura-2 fluorescence in response to 1 μM MeHg, whereas most vector transfected cells did show a response.

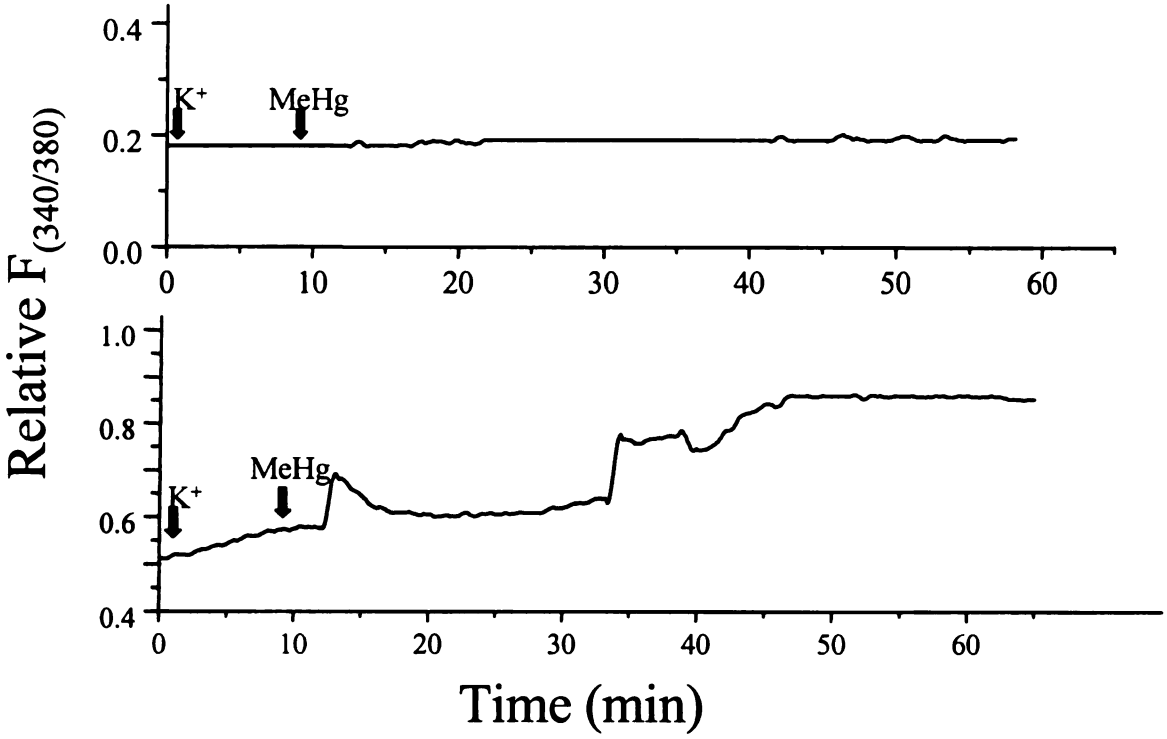

$F_{(340/380)}$ Response	Yes	No	Time-to-onset (min)
CB-transfected	1	10	49.7
Vector-transfected	10	3	51.5±2.9

FIGURE A.2

Figure A.3 Time-to-onset of increases in fura-2 fluorescence induced by 2.5 and 5 μM MeHg in HEK293 cells which were transfected with CB (diagonal) compared to vector-transfected cells (solid). No significant differences were detected between mean values (two-way ANOVA, $P = 0.108$) Data are represented as mean ± SE, $N = 3$ for each group.

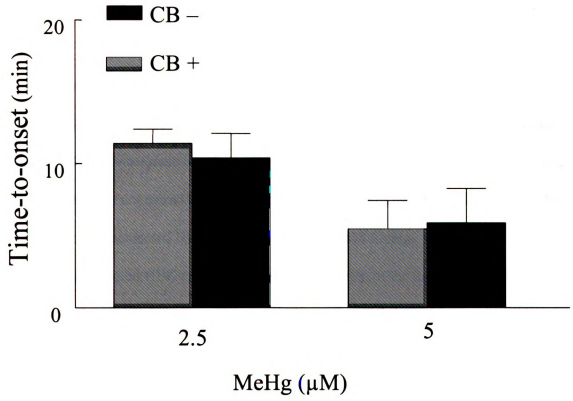

FIGURE A.3

CB plasmids were transfected successfully into approximately 7-10% of HEK293 cells. Furthermore, HEK cells were transfected more reliably as compared to the PC12 cell line. Many different combinations of FuGENE:plasmid DNA volume combinations were tested to find the best transfection efficiency in HEK293 cells. FuGENE transfection reagent was combined with CB plasmid DNA (following the FuGENE protocol) with 1 µl plasmid DNA (CB:GFP, 4:1) and 3µl FuGENE to 100 µl OptiMEM transfection medium for each 35 mm cell culture dish to be transfected.

CB-transfected and vector-transfected HEK cells responded to MeHg exposure with a brief increase in fura-2 fluorescence then a prolonged elevation of fluorescence. However at 1 µM MeHg, almost none of CB-tranfected HEK cells exhibited an elevation in fura-2 fluorescence when compared to vector-transfected HEK cells (see table figure A.2). All CB- and vector-transfected HEK cells responded to 5 µM MeHg. In comparison, only one vector-transfected HEK cell did not respond to MeHg in the 2.5 µM MeHg concentration. All CB-transfected HEK cells responded to 2.5 µM MeHg with a sustained increase in fura-2 fluorescence. Therefore, with increasing concentrations of MeHg the ability of CB transfection to prevent elevations of fura-2 fluorescence was diminished in HEK cells. Time-to-onset of fura-2 fluorescence elevations did not differ significantly within 2.5 or 5 µM MeHg treatment groups. This would indicate CB is able to protect HEK cells from MeHg-mediated dysregulation of Ca^{2+} homeostasis at low levels of MeHg but not at higher concentrations. Purkinje and granule cell data presented in chapter two show a similar delay in the time-to-onset of first and second phase

increases in fura-2 fluorescence at the lower MeHg concentrations tested (0.5 and 1 μM). At these lower MeHg concentrations, CB-containing Purkinje cells had significantly delayed time-to-onset compared to CB-negative granule cells. However at higher concentrations (5 μM) of MeHg there was no difference in time-to-onset of first or second phase increase in fura-2 fluroescence between Purkinje and granule cells.

B. Effects of MeHg-induced cytotoxicity on CB-transfected human embryonic stem cells (HEK 293).

Lactate dehydrogenase (LDH) assay: The ethidium homodimer/calcein-AM cell viability assay was not used because a portion of HEK cells were transfected, therefore it would be difficult to ascertain which cells were transfected and viable. GFP was used as an indicator for the successful transfection of CB. As an alternative, release of LDH was chosen as a measure of cell viability because LDH is a commonly used method to assay cell viability in clonal cell lines. In addition, others have used LDH to measure the potential cytoprotective effects of CB the PC12 cell line. Release of LDH from HEK293 cells was measured following the protocol described in Chapter Four.

Figure A.4 (line) CB- and (solid) vector-transfected HEK293 cells were exposed to MeHg for 2 hr; LDH activity was measured 24 hr after cessation of MeHg exposure. All data were square root transformed prior to statistical analysis. Release of LDH was significantly higher (two-way ANOVA, $P = 0.021$) in both the vector- and CB-transfected 5 μM MeHg treatment groups compared to HBS alone control, as indicated by asterisks (*). Data are represented as mean ± SE, $N = 4$ for each group.

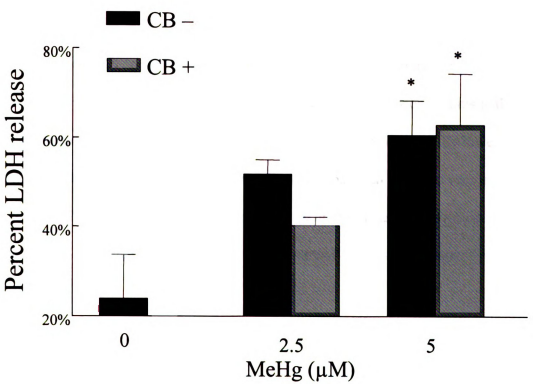

FIGURE A.4

Figure A.5 Effects of CB on LDH release from HEK cells treated with the Ca^{2+} ionophore A23187 (50 μM). All data were square root transformed prior to statistical analysis. Release of LDH after exposure to A23187 (50 μM) was significantly lower (ANOVA, P = 0.007) in CB-transfected HEK cells as compared to non- and vector-transfected control values (*). Cells were treated for 24 hr with A23187 present in growth medium. LDH release was subsequently measured N = 3 for all groups.

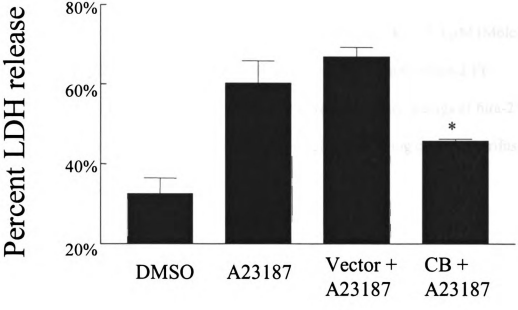
Percent LDH release
80%
60%
40%
20%
*
DMSO
A23187
Vector + A23187
CB + A23187

FIGURE A.5

C. MeHg-induced dysregulation of Ca^{2+} homeostasis using the low-affinity Ca^{2+} indicator, fura-2-FF.

CB is a Ca^{2+}-binding protein with high affinity for Ca^{2+}, K_d = 0.5 μM. However the Ca^{2+}-indicator fura-2 has even higher affinity for Ca^{2+} K_d = 135 nM. Thus, the fura-2 response from CB-containing neurons such as cerebellar Purkinje and myenteric plexus as well as CB-transfected PC12 and HEK cells may not truly represent $[Ca^{2+}]_i$. Fura-2 may mask the Ca^{2+}-binding action of endogenous proteins, such as CB, parvalbumin and calmodulin. I tested the low-affinity Ca^{2+} indicator, fura-2-FF, K_d = 5.4 μM (Molecular Probes, Eugene, OR) to determine if the MeHg-induced increases in fura-2-FF fluorescence would differ from those of fura-2 fluorescence. Recordings of fura-2 and fura-2-FF fluorescence were made from Purkinje cell soma during constant perifusion with 5 μM MeHg.

The Purkinje cell isolation procedure used to obtain these cell cultures was a modified organo-typic Purkinje cell culture system based on the protocol described by Gruol (1983). The Ca^{2+} imaging protocol follows that described for Purkinje cells in Chapter Two.

Figure A.6 Representative fura-2 fluorescence tracing from the soma of a Purkinje cell grown in culture 22-24 days. Fura-2 has higher affinity for Ca^{2+}, K_d = 135 nM than does CB, K_d = 0.5 μM. There was a biphasic increase in fura-2 fluorescence during constant perifusion with 5 μM MeHg in all Purkinje cells examined.

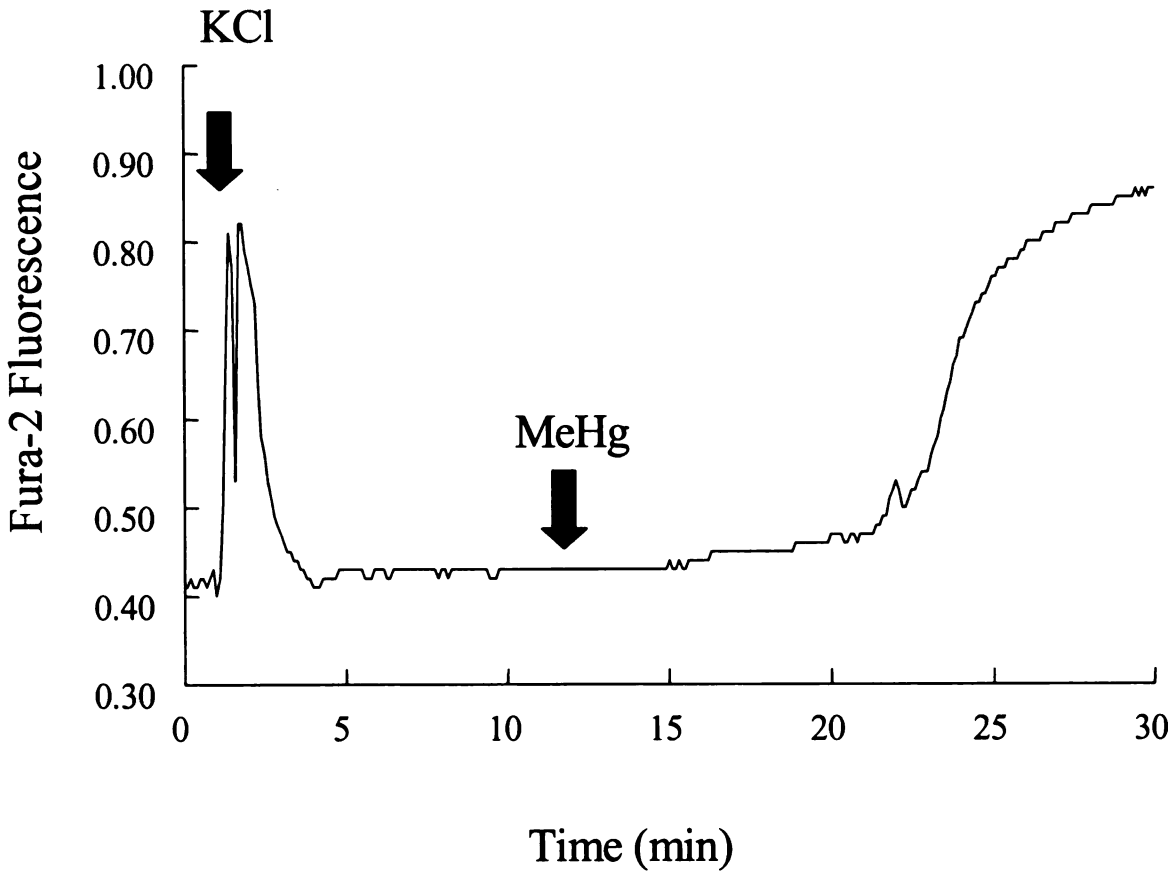
KCl
MeHg
Fura-2 Fluorescence
1.00
0.90
0.80
0.70
0.60
0.50
0.40
0.30
0
5
10
15
20
25
30
Time (min)

FIGURE A.6

Figure A.7 Representative fura-2-FF fluorescence tracing from a Purkinje cell soma grown in culture 22-24 days. Fura-2-FF (K_d = 5.4 μM) has lower affinity for Ca^{2+} than does fura-2 (K_d = 135 nM.). CB has a higher affinity for Ca^{2+} than does fura-2-FF (CB K_d = 0.5 μM). There was a biphasic increase in fura-2-FF fluorescence from Purkinje cells during constant perifusion with 5 μM MeHg.

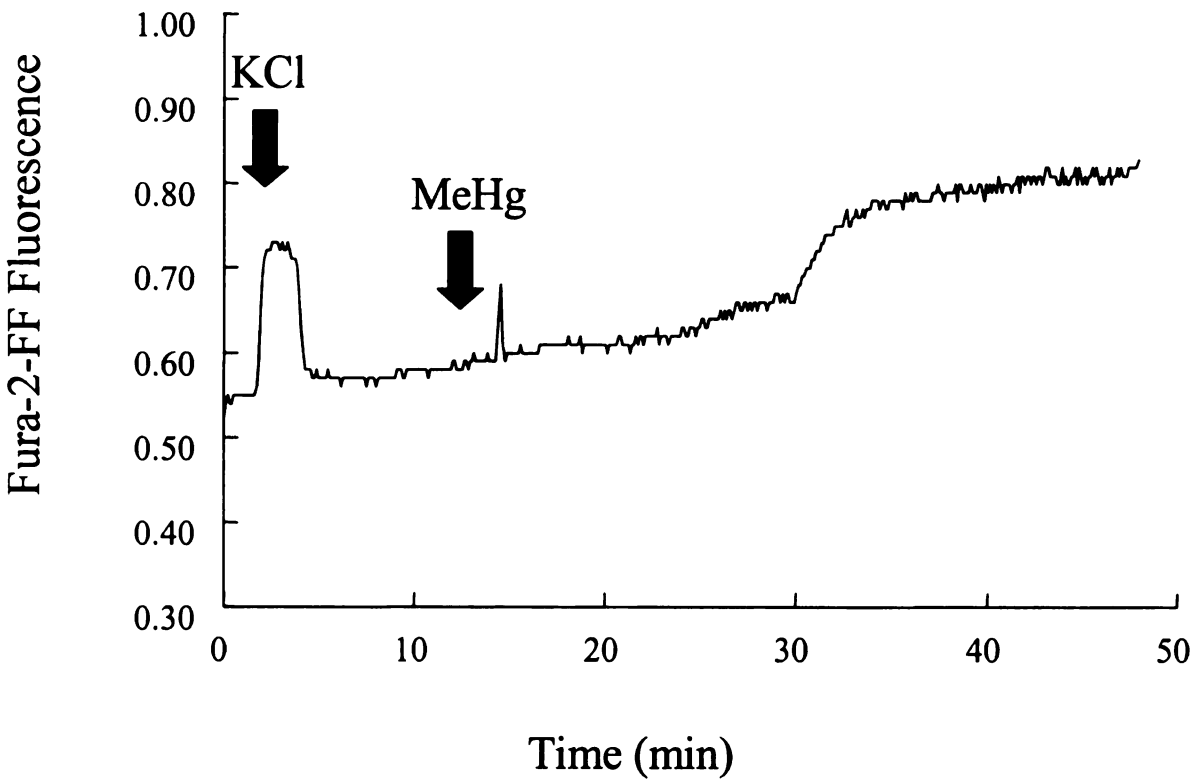
Fura-2-FF Fluorescence
1.00
0.90
0.80
0.70
0.60
0.50
0.40
0.30
KCl
MeHg
0
10
20
30
40
50
Time (min)

FIGURE A.7

There was no obvious difference between the fura-2 and fura-2-FF fluorescence response of Purkinje cells exposed to depolarizing solutions of 40 mM KCl or 5 μM MeHg. By the end of each recording, there was a sustained elevation in fluorescence in response to MeHg. Thus, fura-2 is apparently not acting to mask the Ca^{2+} binding ability of CB present within Purkinje cells and is an adequate Ca^{2+} indicator for use in these experiments. Alternatively, the MeHg-mediated influx of Ca^{2+} may be so great as to overwhelm the Ca^{2+} buffering capacity of CB and Ca^{2+}-binding of fura-2 simultaneously. No attempt was made to determine if Ca^{2+} was a component of the first phase increase in the fluorescence of fura-2-FF. It is possible that with a lower-affinity Ca^{2+} indicator, nearly all fura-2-FF fluorescence detected during first phase is due to the release of non-Ca^{2+} divalent cations that are known to interact with fura-2. More studies comparing fura-2-FF and fura-2 would need to be conducted to rule out the possibility of competing interactions of these Ca^{2+}-indicators and Ca^{2+}-binding proteins.

REFERENCES

Andressen, C., Blumcke, I. and Celio, M.R., 1993. Calcium-binding proteins: selective markers of nerve cells. Cell Tissue Res. **271**, 181-208.

Arnold, B.M., Kovacs, K. and Murray, T.M., 1976. Cellular localization of intestinal calcium-binding protein in pig duodenum. Digestion **1**, 77-84.

Arslan, P., Di Virgilio, F., Beltrame, M., Tsien, R.Y., and Pozzan, T., 1985. Cytosolic Ca^{2+} homeostasis in Ehrlich and Yoshida carcinomas. A new, membrane-permeant chelator of heavy metals reveals that these ascites tumor cell lines have normal cytosolic free Ca^{2+}. J. Biol. Chem. **260**, 2719-2727.

Aschner, M., Du Y.L., Gannon, M., and Kimelberg, H.K., 1993. Methylmercury-induced alterations in excitatory amino acid transport in rat primary astrocyte cultures. Brain Res. **602**, 181-186.

Aschner, M., 1997. Astrocyte metallothioneins (MTs) and their neuroprotective role. Ann. N.Y. Acad. Sci. **825**, 334-347.

Aschner, M., Vitarella, D., Allen, J.W., Conklin, D.R., and Cowan, K.S., 1998. Methylmercury-induced inhibition of regulatory volume decrease in astrocytes: characterization of osmoregulator efflux and its reversal by amiloride. Brain Res. **811**, 133-42.

Atchison, W.D., and Narahashi, T., 1982. Methylmercury-induced depression of neuromuscular transmission in the rat. Neurotoxicology. **3**, 37-50.

Atchison, W.D., 1986. Extracellular calcium-dependent and -independent effects of methylmercury on spontaneous and potassium-evoked release of acetylcholine at the neuromuscular junction. J. Pharmacol. Exp. Ther. **237**, 672-680.

Atchison, W.D., 1987. Effects of activation of sodium and calcium entry on spontaneous release of acetylcholine induced by methylmercury. J. Pharmacol. Exp. Ther. **241**, 131-139.

Atchison, W.D., 2003. Effects of toxic environmental contaminants on voltage-gated calcium channel function: from past to present. J. Bioenerg. Biomembr. **35**, 507-532.

Bakir, F., Damluji, S.F., Amin-Zaki, L., Murtadha, M., Khalidi, A., Al-Rawi, N.Y., Tikriti, S., Dahahir, H.I., Clarkson, T.W., Smith, J.C., and Dohert, R.A., 1973. Methylmercury poisoning in Iraq. Science. **181**, 230-241.

Balmain, N., Brehier, A., Cuisinier-Gleizes, P., and Mathieu, H., 1986. Evidence for the presence of calbindin-D 28K (CaBP-28K) in the tibial growth cartilages of rats. Cell Tissue Res. **245**, 331-335.

Bastianelli, E., 2003. Distribution of calcium-binding proteins in the cerebellum. Cerebellum. **2**, 242-262.

Batini, C., Palestini, M., Thomasset, M., and Vigot, R., 1993. Cytoplasmic calcium buffer, calbindin-D28k, is regulated by excitatory amino acids. Neuroreport. **4**, 927-930.

Berlin, M. and Ullberg, S. 1963. Accumulation and retention of mercury in the mouse. Arch. Environ. Hlth. **6**, 589-601.

Berthele, A., Laurie, D.J., Platzer S., Zieglgansberger, W., Tolle, T.R., and Sommer, B., 1998. Differential expression of rat and human type I metabotropic glutamate receptor splice variant messenger RNAs. Neuroscience. **85**, 733-749.

Bian, X., Zhou, X. and Galligan, J.J., 2004. R-type calcium channels in myenteric neurons of guinea pig small intestine. Am. J. Physiol. Gastrointest. Liver Physiol. **287**, G134-142.

Black, J.L., 2003. The voltage-gated calcium channel [gamma] subunits: A review of the literature. J. Bioenerg. Biomembr.**35**, 649-660

Brorson, J.R., Zhang, Z., and Vandenberghe, W., 1999. Ca^{2+} permeation of AMPA receptors in cerebellar neurons expressing glu receptor 2. J. Neurosci. **19**, 9149-9159.

Brookes, S.J., 2001. Classes of enteric nerve cells in the guinea-pig small intestine. Anat. Rec. **262**, 58-70.

Candura, S.M., D'Agostino, G., Castoldi, A.F., Messori, E., Liuzzi, M., Manzo, L. and Tonini, M., 1997. Effects of mercuric chloride and methyl mercury on cholinergic neuromuscular transmission in the guinea-pig ileum. Pharmacol. Toxicol. **80**, 218-224.

Catterall, W.A., 1991. Functional subunit structure of voltage-gated calcium channels. Science. **253**, 1499-1500.

Celio, M.R., 1990. Calbindin D-28k and parvalbumin in the rat nervous system. Neuroscience. **35**, 375-475.

Chang, L.W., 1977. Neurotoxic effects of mercury--a review. Environ. Res. **14**, 329-373.

Chang, L.W., Reuhl, K.R., and Lee G.W., 1977. Degenerative changes in the developing

nervous system as a result of *in utero* exposure to methylmercury. Environ. Res. **14**, 414-423.

Chard, P.S., Bleakman, B., Christakos, S., Fullmer, C.S., and Miller, R.J., 1992. Calcium buffering properties of calbindin-$D28_K$ and parvalbumin in rat sensory neurons. J. Physiol. (Lond.) **472**, 341-357.

Choi, D.W., and Koh, J.Y., 1998. Zinc and brain injury. Annu. Rev. Neurosci. **21**, 347-375.

Christakos, S., Gabrielides, C., and Rhoten, W.B., 1989. Vitamin D-dependent calcium binding proteins: chemistry, distribution, functional considerations, and molecular biology. Endocr. Rev. **10**, 3-26.

Christakos, S., Gill, R., Lee, S., and Li, H., 1992. Molecular aspects of the calbindins. J. Nutr. **122**, 678-682.

Clarkson, T.W., 1972. The pharmacology of mercury compounds. Annu. Rev. Pharmacol. **12**, 375-406.

Clementi, E., and Meldolesi, J., 1996. Pharmacological and functional properties of voltage-independent Ca^{2+} channels. Cell Calcium. **19**, 269-279.

Danbolt, N.C., 2001. Glutamate uptake. Prog. Neurobiol. **65**, 1-105.

Delorme, A.C., Danan, J.L., and Mathieu, H., 1983. Biochemical evidence for the presence of two vitamin D-dependent calcium-binding proteins in mouse kidney. J. Biol. Chem. **258**, 1878-1884.

Denes, V., and Gabriel, R., 2004. Calbindin-immunopositive cells are cholinergic interneurons in the myenteric plexus of rabbit ileum. Cell Tissue Res. **318**, 465-472.

Denny, M.F., Hare, M.F., and Atchison, W.D., 1993. Methylmercury alters intrasynaptosomal concentrations of endogenous polyvalent cations. Toxicol. Appl. Pharmacol. **122**, 222-232.

Denny, M.F., and Atchison, W.D., 1994. Methylmercury-induced elevations in intrasynaptosomal zinc concentrations: an ^{19}F-NMR study. J. Neurochem. **63**, 383-386.

Denny, M.F., and Atchison, W.D., 1996. Mercurial-induced alterations in neuronal divalent cation homeostasis. Neurotoxicology. **17**, 47-61.

Didier, M., Xu, M., Berman, S.A., Saido, T.C., and Bursztajn, S., 1997. Involvement of

three glutamate receptor epsilon subunits in the formation of N-methyl-D-aspartate receptors mediating excitotoxicity in primary cultures of mouse cerebellar granule cells. Neuroscience. **78**, 1129-1146.

Doering, C.J., and Zamponi, G.W., 2003. Molecular pharmacology of high voltage-activated calcium channels. J. Bioenerg. Biomembr.. **35**, 491-505.

Dolphin, A.C., 2003. β Subunits of voltage-gated calcium channels. J. Bioenerg. Biomembr.. **35**, 599-620

Dubinsky, J.M., and Rothman, S.M., 1991. Intracellular calcium concentrations during "chemical hypoxia" and excitotoxic neuronal injury. J. Neurosci. **11**, 2545-2551.

Dubinsky, J.M., 1993. Examination of the role of calcium in neuronal death. Ann. N. Y. Acad. Sci. **679**, 34-42.

Edwards, J.R., and Atchison W.D., 2001. Methylmercury causes prominent elevations in both Ca^{2+} and non-Ca^{2+} divalent cations in Purkinje cells in culture. Soc. Neurosci. Abstr. 27, 383.3, San Diego, CA.

Edwards, J., Cobbett, P., and Atchison, W., 2002. Comparative disruption of intracellular calcium regulation by methylmercury in PC12 and PC18 cells. Program No. 833.5. 2002 Abstract Viewer/Itinerary Planner. Washington, DC: Society for Neuroscience, 2002. Online.

Edwards, J., and Atchison, W., 2003. Expression of calbindin D-28K correlates with decreased methylmercury (MeHg) cytotoxicity in myenteric plexus neurons. Abstract, Annual Society of Toxicology meeting Salt Lake City, UT.

Eimerl, S., and Schramm, M., 1994. The quantity of calcium that appears to induce neuronal death. J. Neurochem. **62**,1223-6.

Feher, J.J., 1983. Facilitated calcium diffusion by intestinal calcium-binding protein. Am. J. Physiol. (Lond.) **244**, C303-307.

Feil, R., Hartmann, J., Luo, C., Wolfsgruber, W., Schilling, K., Feil, S., Barski, J.J., Meyer, M., Konnerth, A., De Zeeuw, C.I., and Hofmann, F., 2003. Impairment of LTD and cerebellar learning by Purkinje cell-specific ablation of cGMP-dependent protein kinase I. J. Cell Biol. **163**, 295-302.

Fox, J.H., Patel-Mandlik, K., and Cohen, M.M., 1975. Comparative effects of organic and inorganic mercury on brain slice respiration and metabolism. J. Neurochem. **24**, 757-762.

Frery, N., Maury-Brachet, R., Maillot, E., Deheeger, M., de Merona, B., and Boudou, A., 2001. Gold-mining activities and mercury contamination of native amerindian communities in French Guiana: key role of fish in dietary uptake. Environ. Health. Perspect. **109**, 449-456.

Furness, J.B., Kunze, W.A., Bertrand, P.P., Clerc, N. and Bornstein, J.C., 1998. Intrinsic primary afferent neurons of the intestine. Prog. Neurobiol. **54**, 1-18.

Furuya, S., Makino A., and Hirabayashi, Y., 1998. An improved method for culturing cerebellar Purkinje cells with differentiated dendrites under a mixed monolayer setting. Brain Res. Brain Res. Protoc. **3**, 192-198.

German, D.C., and Liang, C.L., 1993. Neuroactive peptides exist in the midbrain dopaminergic neurons that contain calbindin-D28k. Neuroreport. **4**, 491-494.

Gerstner, H.B., and Huff, J.E., 1977. Selected case histories and epidemiologic examples of human mercury poisoning. Clin. Toxicol. **11**, 131-150.

Greene, L.A., and Tischler, A.S., 1976. Establishment of a noradrenergic clonal line of rat adrenal pheochromocytoma cells which respond to nerve growth factor. Proc. Natl. Acad. Sci. U.S.A. **73**, 2424-2428.

Gruol, D.L., 1983. Cultured cerebellar neurons: endogenous and exogenous components of Purkinje cell activity and membrane response to putative transmitters. Brain Res. **263**, 223-241.

Gruol, D.L., and Crimi, C.P., 1988. Morphological and physiological properties of rat cerebellar neurons in mature and developing cultures. Brain Res. **469**, 135-146.

Gruol, D.L., Netzeband, J.G., and Parsons, K.L., 1996. Ca^{2+} signaling pathways linked to glutamate receptor activation in the somatic and dendritic regions of cultured cerebellar purkinje neurons. J. Neurophysiol. **76**, 3325-3340.

Grynkiewicz, G., Poenie, M., and Tsien, R.Y., 1985. A new generation of Ca^{2+} indicators with greatly improved fluorescence properties. J. Biol. Chem. **260**, 3440-3450.

Hajela, R.K., Peng, S.Q., and Atchison, W.D., 2003. Comparative effects of methylmercury and Hg^{2+} on human neuronal N- and R-type high-voltage activated calcium channels transiently expressed in human embryonic kidney 293 cells. J. Pharmacol. Exp. Ther. **306**,1129-1136.

Harding, M., Beadle, L.M., and Bermudez, D.J., 1999. Voltage-dependent calcium channel subtypes controlling somatic substance P release in the peripheral nervous

system. Prog. Neuropsychopharmacol. Biol. Psych. **23,** 1103-1112.

Hare, M.F., McGinnis, K.M., and Atchison, W.D., 1993. Methylmercury increases intracellular concentrations of Ca^{2+} and heavy metals in NG108-15 cells. J. Pharmacol. Exp. Ther. **266**, 1626-1635.

Hare, M.F., and Atchison W.D., 1995a. Nifedipine and tetrodotoxin delay the onset of methylmercury-induced increase in $[Ca^{2+}]_i$ in NG108-15 cells. J. Pharmacol. Exp. Ther. **135**, 299-307.

Hare, M.F. and Atchison, W.D., 1995b. Methylmercury mobilizes Ca^{2+} from intracellular stores sensitive to inositol 1,4,5-trisphosphate in NG108-15 cells. J. Pharmacol. Exp. Ther. **272**, 1016-1023.

Heidemann, S.R., Lamoureux, P. and Atchison, W.D., 2001. Inhibition of axonal morphogenesis by nonlethal, submicromolar concentrations of methylmercury. Toxicol. Appl. Pharmacol. **174**, 49-59.

Hewett, S.J., and Atchison, W.D., 1992. Effects of charge and lipophilicity on mercurial-induced reduction of $^{45}Ca^{2+}$ uptake in isolated nerve terminals of the rat. Toxicol. Appl. Pharmacol. **113**, 267-273.

Hillsley, K., Kenyon, J.L., and Smith, T.K., 2000. Ryanodine-sensitive stores regulate the excitability of AH neurons in the myenteric plexus of guinea-pig ileum. J. Neurophysiol. **84**, 2777-2785.

Himi, T., Ikeda, M., Sato, I., Yuasa, T., and Murota, S., 1996. Purkinje cells express neuronal nitric oxide synthase after methylmercury administration. Brain Res. **718,** 189-192.

Hinkle, P.M., and Osborne M.E., 1994. Cadmium toxicity in rat pheochromocytoma cells: studies on the mechanism of uptake. Toxicol. Appl. Pharmacol. **124**, 91-98.

Hirning, L.D., Fox, A.P. and Miller, R.J., 1990. Inhibition of calcium currents in cultured myenteric neurons by neuropeptide Y: evidence for direct receptor/channel coupling. Brain Res. **532**, 120-130.

Hirst, G.D., Holman, M.E., and Spence, I., 1974. Two types of neurons in the myenteric plexus of duodenum in the guinea-pig. J. Physiol. (Lond.) **236**, 303-326.

Hirst, G.D., Johnson, S.M. and van Helden, D.F., 1985. The calcium current in a myenteric neurone of the guinea-pig ileum. J. Physiol. (Lond.) **361,** 297-314.

Hook, S.S., and Means, A.R., 2001. Ca^{2+}/CaM-dependent kinases: from activation to function. Annu. Rev. Pharmacol. Toxicol. **41**, 471-505.

Hunter, D., and Russell, D., 1954. Focal cerebral and cerebellar atrophy in a human subject due to organic mercury compounds. Neurol. Neurosurg. Psychiat. **17**, 235-241.

Hughes, W.L., 1957. A physicochemical rationale for the biological activity of mercury and its compounds. Ann. N. Y. Acad. Sci. **65**, 454-460.

Iacopino, A.M., and Christakos, S., 1990. Specific reduction of calcium-binding protein (28-kilodalton calbindin-D) gene expression in aging and neurodegenerative diseases. Proc. Natl. Acad. Sci. U.S.A. **87**, 4078-4082.

Jacobs, J.M., Carmichael, N., and Cavanagh, J.B., 1977. Ultrastructural changes in the nervous system of rabbits poisoned with methyl mercury. Toxicol. Appl. Pharmacol. **39**, 249-261.

Juang, M.S., 1976. An electrophysiological study of the action of methylmercuric chloride and mercuric chloride on the sciatic nerve-sartorius muscle preparation of the frog. Toxicol. Appl. Pharmacol. **37**, 339-348.

Ito, M., 2000. Mechanisms of motor learning in the cerebellum. Brain Res. **886**, 237-245.

Ito, M., 1984. The cerebellum and neural control. Raven Press, New York.

Kandel, E., Schwartz, J., and Jessell, T., 2000. Principles of Neural Science 4^{th} ed. McGraw-Hill, New York.

Kass, G.E., and Orrenius, S., 1999. Calcium signaling and cytotoxicity. Environ. Health Perspect. **107**, 25-35.

Keinanen, K., Wisden, W., Sommer, B., Werner, P., Herb, A., Verdoorn, T.A., Sakmann, B., and Seeburg, P.H., 1990. A family of AMPA-selective glutamate receptors. Science. **249**, 556-560.

Khodakhah, K., and Armstrong, C.M., 1997. Inositol trisphosphate and ryanodine receptors share a common functional Ca^{2+} pool in cerebellar Purkinje neurons. Biophys. J. **73**, 3349-3357.

Kirchgessner, A.L., and Liu, M.T., 1999. Differential localization of Ca^{2+} channel alpha1 subunits in the enteric nervous system: presence of α_{1B} channel-like immunoreactivity in intrinsic primary afferent neurons. J. Comp. Neurol. **409**, 85-104.

Klugbauer, N., Welling, A., Specht, V., Seisenberger, C., and Hofmann, F., 2002. L-type Ca^{2+} channels of the embryonic mouse heart. Eur. J. Pharmacol. **447**, 279-284.

Kobayashi, Y., Sawa, H., Watanabe, M., Furoka, H., Matsui, T. and Nagashima, K., 1998. Calbindin D immunoreactivity and chronic lesions of rat cerebella in methylmercury chloride intoxication. Neuropathology. **18**, 402-407.

Komulainen, H., and Bondy, S.C., 1987. Increased free intrasynaptosomal Ca^{2+} by neurotoxic organometals: distinctive mechanisms. Toxicol. Appl. Pharmacol. **88**, 77-86.

Kumagai, H., Nishida, E., Kotani, S., and Sakai, H., 1986. On the mechanism of calmodulin-induced inhibition of microtubule assembly *in vitro*. J. Biochem. **99**, 521-525.

Kumar, P.P., Stotz, S.C., Paramashivappa, R., Beedle, A.M., Zamponi, G.W., and Rao, A.S., 2002. Synthesis and evaluation of a new class of nifedipine analogs with T-type calcium channel blocking activity. Mol. Pharmacol. **61**, 649-658.

Kunimoto, M., and Suzuki, T., 1997. Migration of granule neurons in cerebellar organotypic cultures is impaired by methylmercury. Neurosci Lett. **226**, 183-186.

Kuwajima, G., Futatsugi, A., Niinobe, M., Nakanishi, S., and Mikoshiba. K., 1992. Two types of ryanodine receptors in mouse brain: skeletal muscle type exclusively in Purkinje cells and cardiac muscle type in various neurons. Neuron. **9**, 1133-1142.

Leaner, J.J. and Mason, R.P., 2002. Methylmercury accumulation and fluxes across the intestine of channel catfish, *Ictalurus punctatus*. Comp. Biochem. Physiol. C Toxicol. Pharmacol. **132**, 247-259.

Lerma, J., Paternain, A.V., Rodriguez-Moreno, A., and Lopez-Garcia, J.C., 2001. Molecular physiology of kainate receptors. Physiol. Rev. **81**, 971-998.

Levesque, P.C., and Atchison, W.D., 1991. Disruption of brain mitochondrial calcium sequestration by methylmercury. J. Pharmacol. Exp. Ther. **256**, 236-242.

Levesque, P.C., Hare, M.F. and Atchison, W.D., 1992. Inhibition of mitochondrial Ca^{2+} release diminishes the effectiveness of methylmercury to release acetylcholine from synaptosomes. Toxicol. Appl. Pharmacol. **115**, 11-20.

Leiva-Presa, A., Capdevila, M., Cols, N., Atrian, S., and Gonzalez-Duarte, P., 2004. Chemical foundation of the attenuation of methylmercury(II) cytotoxicity by metallothioneins. Eur. J. Biochem. **271**, 1323-1328.

Leyshon, K., Morgan, A.J., 1991. An integrated study of the morphological and

gross-elemental consequences of methyl mercury intoxication in rats, with particular attention on the cerebellum. Scanning Microsc. **3**, 895-904.

Leyshon-Sorland, K., Jasani, B., Morgan, A. J., 1994. The localization of mercury and metallothionein in the cerebellum of rats experimentally exposed to methylmercury. Histochem. J. **26**, 161-169.

Limke, T.L., and Atchison, W.D., 2002. Acute exposure to methylmercury opens the mitochondrial permeability transition pore in rat cerebellar granule cells. Toxicol. Appl. Pharmacol. **178**, 52-61.

Limke, T.L., Bearss, J.J., and Atchison, W.D., 2004. Methylmercury causes Ca^{2+} dysregulation and neuronal death in rat cerebellar granule cells through an M3 muscarinic receptor-linked pathway. Toxicol. Sci. **80**, 60-68.

Lledo, P.M., Somasundaram, B., Morton, A.J., Emson, P.C. and Mason, W.T., 1992. Stable transfection of calbindin-D28k into the GH_3 cell line alters calcium currents and intracellular calcium homeostasis. Neuron. **9**, 943-954.

Lowenstein, D.H., Miles, M.F., Hatam, F., and McCabe, T., 1991. Up regulation of calbindin-D28K mRNA in the rat hippocampus following focal stimulation of the perforant path. Neuron. **6**, 627-633.

Ludwig, A., Flockerzi, V., and Hofmann, F., 1997. Regional expression and cellular localization of the $\alpha 1$ and β subunit of high voltage-activated calcium channels in rat brain. J. Neurosci. **17**, 1339-1349.

Magos, L., Peristianis, G.C., and Snowden, R.T., 1978. Postexposure preventive treatment of methylmercury intoxication in rats with dimercaptosuccinic acid. Toxicol. Appl. Pharmacol. **45**, 463-475.

Manev, H., Kharlamov, E., Uz, T., Mason, R.P., and Cagnoli, C.M., 1997. Characterization of zinc-induced neuronal death in primary cultures of rat cerebellar granule cells. Exp. Neurol. **146**, 171-178.

Marty, M.S., and Atchison, W.D., 1997. Pathways mediating Ca^{2+} entry in rat cerebellar granule cells following *in vitro* exposure to methyl mercury. Toxicol. Appl. Pharmacol. **147**, 319-330.

Marty, M.S., and Atchison, W.D., 1998. Elevations of intracellular Ca^{2+} as a probable contributor to decreased viability in cerebellar granule cells following acute exposure to methylmercury. Toxicol. Appl. Pharmacol. **150**, 98-105.

Mattson, M.P., Rychlik, B., Chu, C., and Christakos, S., 1991. Evidence for calcium-reducing and excito-protective roles for the calcium-binding protein calbindin-D28$_K$ in cultured hippocampal neurons. Neuron. **6**, 41-51.

Mazzolini, M., Traverso, S., and Marchetti, C., 2001. Multiple pathways of Pb^{2+} permeation in rat cerebellar granule neurones. J. Neurochem. **79**, 407-416.

McKeown-Eyssen, G.E., and Ruedy, J., 1983. Methyl mercury exposure in northern Quebec. I. Neurologic findings in adults. Am. J. Epidemiol. **118**, 461-469.

McMahon, A., Wong, A., Iacopino, B.S., Ng, A.M., Chi, S., and German, D.C., 1998. Calbindin-D28k buffers intracellular calcium and promotes resistance to degeneration in PC12 cells. Brain Res. Mol. Brain Res. **54**, 56-63.

Meier, T.J., Ho, D.Y., Park, T.S., and Sapolsky, R.M., 1998. Gene transfer of calbindin D28k cDNA via herpes simplex virus amplicon vector decreases cytoplasmic calcium ion response and enhances neuronal survival following glutamatergic challenge but not following cyanide. J. Neurochem. **71**, 1013-1023.

Minghetti, P.P., Cancela, L., Fujisawa, Y., Theofan, G., and Norman, AW., 1988. Molecular structure of the chicken vitamin D-induced calbindin-D28K gene reveals eleven exons, six Ca^{2+}-binding domains, and numerous promoter regulatory elements. Mol. Endocrinol. **2**, 355-367.

Mintz, I.M., Adams, M.E., and Bean, B.P., 1992. P-type calcium channels in rat central and peripheral neurons. Neuron. **9**, 85-95.

Mintz, I.M., and Bean B.P., 1993 Block of calcium channels in rat neurons by synthetic ω-Aga-IVA. Neuropharmacology. **32**, 1161-1169.

Morel, F.M., Kraepiel, A.M., and Amyot, M., 1998. The chemical cycle and bioaccumulation of mercury. Ann. Rev. Ecol. Syst. **29**, 543-566.

Mori, F., Tanji, K., and Wakabayashi, K., 2000. Widespread calcium deposits, as detected using the alizarin red S technique, in the nervous system of rats treated with dimethyl mercury. Neuropathology. **20**, 210-215.

Morgan, D.W., Welton, A.F., Heick, A.E., and Christakos, S., 1996. Specific in vitro activation of Ca,Mg-ATPase by vitamin D-dependent rat renal calcium binding protein (calbindin D28K). Biochem. Biophys. Res. Commun. **138**, 547-553.

Mundy, W.M., Parran, D., and Barone, S.Jr., 2000. Gestational exposure to methylmercury alters neurotrophin- and carbachol-stimulated phosphatidylinositide

hydrolysis in cerebral cortex of neonatal rats. Neurotox. Res. **1**, 271-283.

Myers, G.J., and Davidson, P.W., 1998. Prenatal methylmercury exposure and children: neurologic, developmental, and behavioral research. Environ. Health Perspect. **106**, 841-847.

Nicotera, P., and Orrenius, S., 1992. Ca^{2+} and cell death. Ann. N. Y. Acad. Sci. **648**, 17-27.

Nicotera, P., Bellomo, G., and Orrenius, S., 1992. Calcium-mediated mechanisms in chemically induced cell death. Annu. Rev. Pharmacol. Toxicol. **32**, 449-470.

Norman, A.W., and Leathers, V., 1982. Preparation of a photoaffinity probe for the vitamin D-dependent intestinal calcium binding protein: evidence for a calcium dependent, specific interaction with intestinal alkaline phosphatase. Biochem. Biophys. Res. Commun. **108**, 220-226.

Okabe, M., and Takeuchi, T., 1980. Distribution and fate of mercury in tissues of human organs in Minamata disease. Neurotoxicology. **1**, 607-624.

O'Kusky, J.R., and McGeer, E.G., 1989. Methylmercury-induced movement and postural disorders in developing rat: high-affinity uptake of choline, glutamate, and γ-aminobutyric acid in the cerebral cortex and caudate-putamen. J. Neurochem. **53**, 999-1006.

Orrenius, S., Zhivotovsky, B., and Nicotera, P., 2003. Regulation of cell death: the calcium-apoptosis link. Nat. Rev. Mol. Cell Biol. **4**, 552-565.

Ozawa, S., Kamiya, H., and Tsuzuki, K., 1998. Glutamate receptors in the mammalian central nervous system. Prog. Neurobiol. **54**, 581-618.

Park, S.T., Lim, K.T., Chung, Y.T., and Kim, S.U., 1996. Methylmercury-induced neurotoxicity in cerebral neuron culture is blocked by antioxidants and NMDA receptor antagonists. Neurotoxicology. **17**, 37-45.

Patel, S., Joseph, S.K., and Thomas, A.P., 1999. Molecular properties of inositol 1,4,5-trisphosphate receptors. Cell Calcium. **25**, 247-264.

Peng, S.Q., Hajela, R.K., and Atchison, W.D., 2002. Effects of methylmercury on human neuronal L-type calcium channels transiently expressed in human embryonic kidney cells (HEK-293). J. Pharmacol. Exp. Ther. **302**, 424-432.

Perkel, D.J., Hestrin, S., Sah, P., and Nicoll, R.A., 1990. Excitatory synaptic currents in

Purkinje cells. Proc. R. Soc. Lond. B. Biol. Sci. **241**, 116-121.

Persechini, A., Moncrief, N.D., and Kretsinger, R.H., 1989. The EF-hand family of calcium-modulated proteins. Trends Neurosci. **12**, 462-467.

Randall, A., and Tsien, RW., 1995. Pharmacological dissection of multiple types of Ca^{2+} channel currents in rat cerebellar granule neurons. J. Neurosci. **15**, :2995-3012.

Reis, H.J., Massensini, A.R., Prado, M.A., Gomez, R.S., Gomez, M.V. and Romano-Silva, M.A., 2000. Calcium channels coupled to depolarization-evoked glutamate release in the myenteric plexus of guinea-pig ileum. Neuroscience. **101**, 237-242.

Rhoten, W.B., Bruns, M.E., and Christakos, S., 1985. Presence and localization of two vitamin D-dependent calcium binding proteins in kidneys of higher vertebrates. Endocrinology. **117**, 674-683.

Rintoul, G.L., Raymond, L.A., and Baimbridge, K.G., 2001. Calcium buffering and protection from excitotoxic cell death by exogenous calbindin-D28k in HEK 293 cells. Cell Calcium. **29**, 277-287.

Rowland, I.R., Davies, M.J., and Evans, J.G., 1980. The effect of the gastrointestinal flora on tissue content of mercury and organomercurial neurotoxicity in rats given methylmercuric chloride. Dev. Toxicol. Environ. Sci. **8**, 79-82.

Sarafian, T.A., 1993. Methyl mercury increases intracellular Ca^{2+} and inositol phosphate levels in cultured cerebellar granule neurons. J. Neurochem. **61**, 648-657.

Shafer, T.J., Contreras M.L., and Atchison, W.D., 1990. Characterization of interactions of methylmercury with Ca^{2+} channels in synaptosomes and pheochromocytoma cells: radiotracer flux and binding studies. Mol. Pharmacol. **38**, 102-113.

Shafer, T.J., and Atchison, W.D., 1991. Transmitter, ion channel and receptor properties of pheochromocytoma (PC12) cells: a model for neurotoxicological studies. Neurotoxicology. **12**, 473-492.

Shafer, T.J., and Atchison, W.D., 1992. Effects of methylmercury on perineurial Na^{+} and Ca^{2+}-dependent potentials at neuromuscular junctions of the mouse. Brain Res. **595**, 215-219.

Shafer, T.J., 1998. Effects of Cd^{2+}, Pb^{2+} and CH_3Hg^{+} on high voltage-activated calcium currents in pheochromocytoma (PC12) cells: potency, reversibility, interactions with extracellular Ca^{2+} and mechanisms of block. Toxicol. Lett. **99**, 207-221.

Shafer, T.J., Meacham, C.A., and Barone, S, Jr., 2002. Effects of prolonged exposure to nanomolar concentrations of methylmercury on voltage-sensitive sodium and calcium currents in PC12 cells. Brain Res. Dev. Brain Res. **136**, 151-164.

Shaw, P.J., and Eggett, C.J., 2000. Molecular factors underlying selective vulnerability of motor neurons to neurodegeneration in amyotrophic lateral sclerosis. J. Neurol. **247**, 17-27.

Sherlock, J.C., Lindsay, D.G., Hislop, J.E., Evans, W.H., and Collier, T.R., 1982. Duplication diet study on mercury intake by fish consumers in the United Kingdom. Arch. Environ. Health. **37**, 271-278.

Sherlock, J., Hislop, J., Newton, D., Topping, G., and Whittle, K., 1984. Elevation of mercury in human blood from controlled chronic ingestion of methylmercury in fish. Hum. Toxicol. **3**, 117-131.

Shimizu, T., Suzuki, N., Takao, M., Koto, A., and Fukuuchi, Y., 2000. Calbindin-D28k in cerebrovascular extrinsic innervation system of the rat. Auton. Neurosci. **84**, 130-139.

Shimura, F., and Wasserman, R.H., 1984. Membrane-associated vitamin D-induced calcium-binding protein (CaBP): quantification by a radioimmunoassay and evidence for a specific CaBP in purified intestinal brush borders. Endocrinology. **115**, 1964-1972

Shuttleworth, C.W., and Smith, T.K., 1999. Action potential-dependent calcium transients in myenteric S neurons of the guinea-pig ileum. Neuroscience. **92**, 751-762.

Siesjo, B.K., Bengtsson, F., Grampp, W., and Theander, S., 1989. Calcium, excitotoxins, and neuronal death in the brain. Ann. N. Y. Acad. Sci. **568**, 234-251.

Sirois, J.E., and Atchison, W.D., 2000. Methylmercury affects multiple subtypes of calcium channels in rat cerebellar granule cells. Toxicol. Appl. Pharmacol. **167**, 1-11.

Smith, T.K., Bornstein, J.C., and Furness, JB., 1992. Convergence of reflex pathways excited by distension and mechanical stimulation of the mucosa onto the same myenteric neurons of the guinea pig small intestine. J. Neurosci. **4**, 1502-1510.

Smith, T.K., Kang, S.H., and Vanden Berghe, P., 2003. Calcium channels in enteric neurons. Curr. Opin. Pharmacol. **6**, 588-593.

Syversen, T.L., Totland, G., and Flood, P.R., 1981. Early morphological changes in rat cerebellum caused by a single dose of methylmercury. Arch. Toxicol. **47**, 101-111.

Takano, H., Sugimura, M., Kanazawa, Y., Uchida, T., Morishima, Y., and Shirasaki, Y.,

2003. Protective effect of DY-9760e, a calmodulin antagonist, against neuronal cell death. Biol. Pharm. Bull. **27**, 1788-1791.

Takayama, C., and Inoue, Y., 2004. GABAergic signaling in the developing cerebellum. Anat. Sci. Int. **79**, 124-36.

Takeuchi, T., and Eto, K., 1999. The pathology of Minamata Disease: a tragic story of water pollution. Kyushu University Press, INC. Okinawa, Japan.

Tanaka, O., and Kondo, H., 1994. Localization of mRNAs for three novel members (beta 3, beta 4 and gamma 2) of phospholipase C family in mature rat brain. Neurosci. Lett. **182**, 17-20.

Tatsumi, H., Hirai, K., and Katayama, Y., 1988. Measurement of the intracellular calcium concentration in guinea-pig myenteric neurons by using fura-2. Brain Res. **451**, 371-375.

Tayebati, S.K., Vitali, D., Scordella, S., and Amenta, F., 2001. Muscarinic cholinergic receptors subtypes in rat cerebellar cortex: light microscope autoradiography of age-related changes. Brain Res. **889**, 256-259.

Taylor, L.L., and DiStefano, V., 1976. Effects of methylmercury on brain biogenic amines in the developing rat pup. Toxicol. Appl. Pharmacol. **38**, 489-497.

Theofan, G., King, M.W., Hall, A.K., and Norman, A.W., 1987. Expression of calbindin-D28K mRNA as a function of altered serum calcium and phosphorus levels in vitamin D-replete chick intestine. Mol. Cell Endocrinol. **54**, 135-140.

Tomsig, J.L., and Suszkiw, J.B., 1991. Permeation of Pb^{2+} through calcium channels: fura-2 measurements of voltage- and dihydropyridine-sensitive Pb^{2+} entry in isolated bovine chromaffin cells. Biochim. Biophys. Acta. **1069**, 197-200.

Traxinger, D.L., and Atchison, W.D., 1987. Reversal of methylmercury-induced block of nerve-evoked release of acetylcholine at the neuromuscular junction. Toxicol. Appl. Pharmacol. **90**, 23-33.

Tsien, R.Y. Pozzan, T., and Rink, T.J., 1982. Calcium homeostasis in intact lymphocytes: cytoplasmic free calcium monitored with a new, intracellularly trapped fluorescent indicator. J. Cell Biol. **94**, 325-334.

Vahter, M., Mottet, N.K., Friberg, L., Lind, B., Shen, D.D., and Burbacher, T., 1994. Speciation of mercury in the primate blood and brain following long-term exposure to methyl mercury. Toxicol. Appl. Pharmacol. **124**, 221-229.

Vanden Berghe P., Kenyon J.L., and Smith T.K., 2002. Mitochondrial Ca^{2+} uptake regulates the excitability of myenteric neurons. J. Neurosci. **22**, 6962-6971.

Verity, M.A. 1992. Ca^{2+}-dependent processes as mediators of neurotoxicity. *Neurotoxicology* **13**, 139-147.

Verity, M.A., Brown, W.J., Cheung, M., and Czer, G., 1977. Methyl mercury inhibition of synaptosome and brain slice protein synthesis: *in vivo* and *in vitro* studies. J. Neurochem. **29**, 673-679.

Vig, P.J., McDaniel, D.O., Subramony, S.H., and Qin, Z., 1999. The effects of calbindin D-28K and parvalbumin antisense oligonucleotides on the survival of cultured Purkinje cells. Res. Commun. Mol. Pathol. Pharmacol. 103, 249-259.

Vogalis, F., Harvey, J.R., Lohman, R.J. and Furness, J.B., 2002. Action potential afterdepolarization mediated by a Ca^{2+}-activated cation conductance in myenteric AH neurons. Neuroscience. **115**, 375-393.

Vogalis, F., Harvey, J.R., and Furness, J.B., 2003. PKA-mediated inhibition of a novel K^+ channel underlies the slow after-hyperpolarization in enteric AH neurons. J. Physiol. (Lond.) **548**, 801-814.

Vyas, S., Michel, P.P., Copin, M.C., Biguet, N.F., Thomasset, M. and Agid, Y., 1994. Induction of calbindin-D 28K gene and protein expression by physiological stimuli but not in calcium-mediated degeneration in rat PC12 pheochromocytoma cells. FEBS Lett. **351**, 53-57.

Wade, P.R., and Cowen, T., 2004. Neurodegeneration: a key factor in the aging gut. Neurogastroenterol. Motil. **16**, 19-23.

Wassef, M., and Sotelo, C., 1984. Asynchrony in the expression of guanosine 3':5'-phosphate-dependent protein kinase by clusters of Purkinje cells during the perinatal development of rat cerebellum. Neuroscience. **13**, 1217-1241.

Watanabe, C., 2002. Modification of mercury toxicity by selenium: practical importance? Tohoku. J. Exp. Med. **196**, 71-77.

WHO, 1990. Methylmercury. Geneva : World Health Organization.

WHO, 1989. Mercury : environmental aspects. Geneva : World Health Organization.

Williams, R.J., 1992. Calcium and calmodulin. Cell Calcium. **13**, 355-362.

Womack, M.D., Walker, J.W., and Khodakhah K., 2000. Impaired calcium release in cerebellar Purkinje neurons maintained in culture. J. Gen. Physiol. **115**, 339-346.

Worley, P.F., Baraban, J.M., and Snyder, S.H., 1989. Inositol 1,4,5-trisphosphate receptor binding: autoradiographic localization in rat brain. J. Neurosci. **9**, 339-346.

Yamada, T., McGeer, P.L., Baimbridge, K.G., and McGeer, E.G., 1990. Relative sparing in Parkinson's disease of *substantia nigra* dopamine neurons containing calbindin-D28K. Brain Res. **526**, 303-307.

Yool, A.J., Krieger, R.M., and Gruol, D.L., 1992. Multiple ionic mechanisms are activated by the potent agonist quisqualate in cultured cerebellar Purkinje neurons. Brain Res. **573**, 83-94.

Yuan, Y., and Atchison, W.D., 1997. Action of methylmercury on $GABA_A$ receptor-mediated inhibitory synaptic transmission is primarily responsible for its early stimulatory effects on hippocampal CA1 excitatory synaptic transmission. J. Pharmacol. Exp. Ther. **282**, 64-73.

Yuan, Y., and Atchison, W.D., 1999. Comparative effects of methylmercury on parallel-fiber and climbing-fiber responses of rat cerebellar slices. J. Pharmacol. Exp. Ther. **288**, 1015-1025.

Yuan, Y. and Atchison, W.D., 2003. Methylmercury differentially affects $GABA_A$ receptor-mediated spontaneous IPSCs in Purkinje and granule cells of rat cerebellar slices. J. Physiol. (Lond.) **550**, 191-204.

Zhang, N., Ottersen, O.P., 1992. Differential cellular distribution of two sulphur-containing amino acids in rat cerebellum. An immunocytochemical investigation using antisera to taurine and homocysteic acid. Exp. Brain Res. **90**, 11-20.

Zhou, X., and Galligan, J.J., 2000. $GABA_A$ receptors on calbindin-immunoreactive myenteric neurons of guinea pig intestine. J. Auton. Nerv. Syst. **78**, 122-135.